

Skylab System Compatibility Analysis

Earth Resources Experiments

MLS/Bellcomm
March 31, 1970

BELLCOMM. INC.

INTRODUCTION*

The system capability of Skylab I for the support of a proposed set of earth resources experiments has been summarized for the Program Director and others (1, 2).

The memoranda collated here report the technical work on which the summary reports were based. An additional reference (3) supports summary (2).

REFERENCES

1. System Compatibility Analysis, Earth Resources Experiments Proposal, Case 620, Memorandum for File, G. M. Anderson, et al, February 11, 1970, B70 02032.
2. Earth Resource Experiment Package (EREP) Impact on AAP Missions, Case 610, Memorandum for File, D. R. Hagner, February 25, 1970, B070 02067.
3. Photography of Ground Sites from AAP Orbit - Case 610, D. A. DeGraaf and E. W. Radany, Memorandum for File, February 12, 1970, B70 02023.

*The memoranda in this compendium were prepared and partially typed before the change of the Program name. It was decided to maintain the previous Apollo Applications designation to avoid retyping and for uniformity.

BELLCOMM, INC.

955 L'ENFANT PLAZA NORTH, S.W., WASHINGTON, D.C. 20024

COVER SHEET FOR TECHNICAL MEMORANDUM

TITLE- A Study of Some Attitude and Control Options Compatible with the Performance of Earth-Pointing Experiments by the AAP Cluster TM- 70-1022-2
DATE- February 3, 1970
FILING CASE NO(S)- 620 AUTHOR(S)- J. J. Fearnside
FILING SUBJECT(S) Apollo Applications Program,
(ASSIGNED BY AUTHOR(S))- Satellite Attitude Control,
Control Moment Gyroscopes

ABSTRACT

This paper is concerned with the impact on the Saturn V Workshop attitude control systems of acquiring and holding an Earth-pointing attitude. Three different methods of acquiring this attitude from the solar inertial attitude are discussed. The primary practical results are:

1. The CMGs have the capability to stabilize the Workshop in the XIOP/Z-LV mode (X-axis in the orbital plane, Z-axis along the local vertical).
2. The maneuvers required to acquire this Earth-pointing attitude can be performed by the CMGs only if the RCS¹ is used to desaturate (or dump) the bias momentum which accumulates in the CMGs.

These results (which are based on the variation of the resultant CMG angular momentum vector) lead to the conclusion that the CMGs could be the primary control system in XIOP/Z-LV with the RCS used only for dumping. This control option can perform Earth-pointing attitude control of the Workshop for less than 20% of the propellant which would be required if attitude control were performed by RCS alone.

There is, in addition, the important technical result that an accumulation of bias momentum in the CMGs as a result of a constant external torque can occur only about the spin axis (in this case, the axis which is perpendicular to the orbital plane). It is shown that a constant torque applied about a spacecraft axis which is in the plane perpendicular to the spin axis

¹RCS denotes here a generic reaction control system which on the AAP Cluster can be either the TACS on the SVWS or the RCS on the CSM.

will produce a periodic momentum change in the CMGs. This result is especially important for the example which is considered in this paper since the important disturbance torques acting on an Earth-pointing satellite are constant relative to the spacecraft.

Finally, it is shown that the momentum which does accumulate in the CMGs due to the torque about the spin axis can be dumped either with an RCS or by performing vehicle maneuvers on the dark side of the orbit.

DISTRIBUTION

COMPLETE MEMORANDUM TO

CORRESPONDENCE FILES:

OFFICIAL FILE COPY
plus one white copy for each
additional case referenced

TECHNICAL LIBRARY (4)

NASA Headquarters

H. Cohen/MLR
J. H. Disher/MLD
W. B. Evans/MLO
L. K. Fero/MLV
J. P. Field, Jr./MLP
W. H. Hamby/MLO
T. E. Hanes/MLA
T. A. Keegan/MA-2
M. Savage/MLT
W. C. Schneider/ML

Goddard Space Flight Center

J. T. Skladany/713

Langley Research Center

P. R. Kurzhals/AMPD

MSC

R. G. Brown/ES-16
C. N. Crews/KS
W. R. Cunningham/CB
R. E. Durkee/ES-5
R. L. Frost/KS
O. K. Garriott/CB
F. C. Littleton/KM
R. M. Machell/KF
P. S. Miglicco/KS
O. G. Smith/KF
H. E. Whitacre/KM

MSFC

R. M. Aden/S&E-ASTR-E
W. B. Chubb/S&E-ASTR-SGD
J. C. Cody/S&E-ASTR-MA
C. B. Graff/S&E-ASTR-EP

COMPLETE MEMORANDUM TO

MSFC (continued)

G. B. Hardy/PM-AA-EI
G. D. Hopson/S&E-ASTN-PL
E. H. Hyde/S&E-ASTN-PF
H. F. Kennel/S&E-ASTR-A
G. F. McDonough/S&E-CSE-A
E. F. Noel/S&E-ASTR-SI
W. C. Patterson/S&E-ASTN-PLA
J. W. Sims/S&E-ASTN-PTA
J. D. Stroud/S&E-ASTR-SE
J. W. Thomas/PM-AA
H. F. Trucks/S&E-ASTN-PTA
J. L. Vaniman/S&E-ASTN-PT
R. D. Wegrich/S&E-CSE-AA
A. P. Woosley/S&E-ASTR-SEC
H. E. Worley/S&E-AERO-DOI

Martin-Marietta

H. S. Nassen/Denver
E. F. Bjoro/Washington
M. S. Imamura/Denver
R. W. Wilson/Denver

McDonnell-Douglas

G. Weber/Eastern Division

Bellcomm

A. P. Boysen
D. R. Hagner
W. G. Heffron
B. T. Howard
J. Z. Menard
J. M. Nervik
I. M. Ross
P. F. Sennewald
J. W. Timko
R. L. Wagner
M. P. Wilson
Departments 2031, 2034 Supervision
Department 1024 File
Division 102
Central Files

SUBJECT: A Study of Some Attitude and Control
Options Compatible with the Performance
of Earth-Pointing Experiments by the
AAP Cluster

DATE: February 3, 1970

FROM: J. J. Fearnside

TM-70-1022-2

TECHNICAL MEMORANDUM

I. INTRODUCTION

This paper is concerned with the impact on the Saturn V Workshop (SVWS) attitude control systems of acquiring and holding an Earth-pointing attitude. Three different methods of acquiring this attitude from the solar inertial (SI) attitude are discussed. These attitude (or acquisition) options are:

- A01. Noon acquisition of orbital rate,
- A02. Midnight acquisition of orbital rate with preceding roll maneuver, and
- A03. Earth-pointing acquisition immediately preceding experiment zone.

In addition, four different control options (CO) are considered. They are:

- C01. Control moment gyros (CMGs) for acquisition, stabilization and momentum dumping.
- C02. Reaction control system (RCS)¹ for acquisition and stabilization.
- C03. CMGs for acquisition and stabilization; RCS for momentum dumping.
- C04. CMGs for stabilization; RCS for acquisition and momentum dumping.

The primary practical results are the following:

- 1. If the CMGs have the capability to stabilize a given inertial attitude, then, with proper initialization, they have the capability to stabilize the corresponding

¹In this paper RCS will be used to denote both the TACS and the reaction control system of the CSM.

Earth-pointing attitude.¹

2. The maneuvers required to acquire an Earth-pointing attitude can be performed by the CMGs only if some assistance is provided by the RCS for dumping the bias momentum accumulated by the CMGs.

These results are based on an analysis of the variation of the components of the total CMG angular momentum vector, not on the details of gimbal angle motion.

There is, in addition, the important technical result that an accumulation of bias momentum in the CMGs as a result of a constant external torque can occur only about an axis perpendicular to the orbital plane. It is shown that a constant torque applied about a spacecraft axis which lies in the orbital plane produces an oscillating momentum change. Some bias accumulation is possible due to the diurnal bulge effect in the atmosphere but this is shown to be quite small.

The organization of this material is as follows: In Section II a detailed analysis of the capability of the CMGs to stabilize an Earth-pointing attitude is presented; Section III contains an evaluation of the various attitude and control options; and Section IV is reserved for some concluding comments.

II. ATTITUDE HOLD OF AN EARTH-POINTING ORIENTATION WITH CMGS

The equations of motion relative to a set of coordinates which are fixed in a spacecraft containing CMGs is given by

$$(1) \quad \dot{\underline{I}}\underline{\omega} + \tilde{\omega}\underline{I}\underline{\omega} + \underline{\dot{H}} + \tilde{\omega}\underline{H} = \underline{N}$$

where: \underline{I} = the 3×3 inertia tensor,

$\underline{\omega}$ = a 3×1 matrix representing the angular velocity of the spacecraft relative to a set of inertial coordinates,

$\tilde{\omega}$ = the 3×3 skew-symmetric matrix which is isomorphic to the vector cross-product operator,

¹An Earth-pointing coordinate system is defined to correspond to an inertial coordinate system if they differ only by an angular displacement about an axis which is perpendicular to the orbital plane. This displacement is given by $\omega_0 t$ where ω_0 equals the orbital rate and t is the variable representing time.

\underline{N} = a 3×1 matrix representing the total external torque vector acting on the spacecraft, and

\underline{H} = a 3×1 matrix which represents the vector sum of the individual spin angular momenta contributed by each CMG. That is, for a system containing n CMGs with the spin angular momentum of the i^{th} CMG given by \underline{h}_i ,

$$(2) \quad \underline{H} = \sum_{i=1}^n \underline{h}_i .$$

The dots over $\underline{\omega}$ and \underline{H} in (1) denote the time rate of change of those vectors as measured in a set of coordinates fixed in the spacecraft.

For the purpose of investigating the attitude-hold momentum requirements on the CMGs of an Earth-pointing spacecraft in a circular orbit, let

$$(3) \quad \underline{\omega} = \underline{\omega}_0 + \underline{\Delta\omega}$$

where $\underline{\omega}_0$ is the constant orbital rate about the axis which is perpendicular to the orbital plane (and which will be called the POP axis). Substitution of (3) into (1) yields

$$(4) \quad I \underline{\Delta\dot{\omega}} + (\tilde{\omega}_0 + \Delta\tilde{\omega}) I (\underline{\omega}_0 + \underline{\Delta\omega}) + \dot{\underline{H}} + (\tilde{\omega}_0 + \Delta\tilde{\omega}) \underline{H} = \underline{N} .$$

The assumption is now made that the CMG control system is capable of maintaining the actual state of the system identically equal to the desired state. Then, $\underline{\Delta\omega} = \underline{0}$ and (4) becomes

$$(5) \quad \dot{\underline{H}} + \tilde{\omega}_0 \underline{H} = \underline{N} - \tilde{\omega}_0 I \underline{\omega}_0 \stackrel{\Delta}{=} \underline{T} .$$

This assumption is certainly justified for the determination of the CMG momentum capacity which will be required to stabilize a particular attitude. The neglected terms are merely perturbations [1] from the solution of (5).

Since $\underline{\omega}_0$ is constant, (5) is a linear, time-invariant, vector differential equation which can be solved (e.g. by Laplace transform) once the external torques are defined. Before this is done, however, two coordinate systems will be defined.

The orbit-referenced coordinate system (ORS) is specified by axes X_0 , Y_0 , and Z_0 which are defined as follows:

- Y_0 - perpendicular to the orbital plane (POP);
positively directed to make an acute angle
with the ecliptic North Pole,
- Z_0 - along the local vertical; positively directed
towards the geocenter,
- X_0 - completes the orthogonal right triad.

The geometric coordinate system (GS) is defined in Figure 1. Note that when the GS is aligned with the ORS the spacecraft is in the XIOP/Z-LV¹ attitude mode.

Equation (5) will be solved in the ORS. For the case where the GS is aligned with the ORS, the solutions will yield the required CMG momentum variation relative to spacecraft coordinates. When these systems are not aligned, e.g. if they differ by a constant X-axis transformation, the solution of (5) must be transformed into the GS.

Relative to the ORS then, the transpose of $\underline{\omega}_0$ is given by $\underline{\omega}_0' = [0 \quad \omega_0 \quad 0]$ and the expanded and transformed version of (5) for arbitrary $\underline{T}(t)$ is given by

$$\begin{aligned} sH_X(s) + \omega_0 H_Z(s) &= T_X(s) + H_X(0+) \\ (6) \quad sH_Y(s) &= T_Y(s) + H_Y(0+) \\ -\omega_0 H_X(s) + sH_Z(s) &= T_Z(s) + H_Z(0+) \end{aligned}$$

¹X-axis in the orbital plane, Z-axis along local vertical.

where t is the time variable and the initial time, t_0 , is taken equal to zero. Notice that the Y-axis equation exhibits the behavior that is expected when the CMGs hold an inertial attitude. That is, the momentum change about a given axis is equal to the integral over time of the torque which is acting about that axis. This is because the Y-axis is the axis of rotation and is fixed relative to a set of inertial coordinates. On the other hand, the equations for the momentum variation about the axes which lie in the orbital plane are coupled. The simultaneous solution of these equations leads to the characteristic equation $s^2 + \omega_0^2 = 0$ which implies that the natural response of this system is an undamped oscillation of angular frequency ω_0 .

These general principles are now applied to the problem of holding the SVWS in XIOP/Z-LV and acted upon by gravity-gradient torques.¹ The problem is made non-trivial by assuming a non-diagonal inertia tensor for the Workshop. That is, the geometric axes will be kept XIOP/Z-LV instead of the principal axes. The gravity-gradient torque for this problem is constant under the assumptions made above as are the effects of the $\omega_0 I_{\omega_0}$ term. A time domain solution of (5) under these circumstances is given by

$$\begin{aligned}
 H_x(t) &= \{-T_z/\omega_0 + [H_x(0+) + T_z/\omega_0] \cos \omega_0 t \\
 &\quad - [H_z(0+) - T_x/\omega_0] \sin \omega_0 t\} \\
 (7) \quad H_y(t) &= H_y(0+) + \int_0^t T_y dt \\
 H_z(t) &= \{T_x/\omega_0 + [H_z(0+) - T_x/\omega_0] \cos \omega_0 t \\
 &\quad + [H_x(0+) + T_z/\omega_0] \sin \omega_0 t\}
 \end{aligned}$$

¹Since the CMGs can hold the spacecraft's attitude very close to the nominal XIOP/Z-LV, the end of the cylinder is pointed into the "wind" as are the edges of the solar panels. Using the mass properties given in [2], the bias momentum accumulation in the CMGs due to aerodynamic effects is conservatively estimated to be 35 ft-lb-sec/orbit.

where $T_x = -4\omega_o^2 I_{yz},$

$$T_y = 3\omega_o^2 I_{xz},$$

$$T_z = \omega_o^2 I_{xy}, \text{ and}$$

$I_{ij}; i, j = x, y, z$ are the appropriate elements of the inertia tensor.

Note that the oscillatory terms in the equations for H_x and H_z can be eliminated by a proper choice of $H_x(0+)$ and $H_z(0+)$.^{1,2} Further, note that the initial time t_o could have been chosen arbitrarily, that is the $0+$ reference in this problem is not related to any orbital time. Therefore, for example, the time of firing of a set of thrusters which produce an almost impulsive torque would be an appropriate choice for t_o .

Some representative numbers for equation (7) as it represents the SVWS in the XIOP/Z-LV orientation and in a 235 nautical mile circular orbit are [2]

$$T_x/\omega_o \approx 86 \text{ ft-lb-sec}$$

$$T_z/\omega_o \approx 1.5 \text{ ft-lb-sec}$$

$$\int_0^{2\pi/\omega_o} T_y dt \approx 4,645 \text{ ft-lb-sec}$$

Unfortunately, the effect of an unusually large I_{xz} term appears about the axis of rotation which means that 4,645 ft-lb-sec of momentum must be dumped per orbit. It is shown in Appendix A that this dumping can be achieved by the gravity-gradient torque if a single-axis maneuver is permitted on the dark side of the orbit. For the AAP Earth-pointing modes, however, there are good arguments for using RCS thrust for dumping (See Table 1 in §2).

¹This is not used, however, in the example presented in this paper.

²Also, note that, since the position of \underline{H} relative to spacecraft coordinates can be varied to produce a specified torque, the solution of (5) when $\underline{T} = \underline{0}$ must be $\underline{H} = \underline{0}$ to avoid needless gimbal motion.

An alternate method of reducing the large, Y-axis bias momentum accumulation is to hold an attitude which differs only by a small, Y-axis rotation, θ , from XIOP/Z-LV. The gravity-gradient torque for this condition is given by

$$(8) \quad \underline{N}_{gg} = 1.5\omega_o^2 \begin{bmatrix} I_{xy} \sin 2\theta - I_{yz}(1+\cos 2\theta) \\ (I_{zz}-I_{xx}) \sin 2\theta + 2I_{xz} \cos 2\theta \\ I_{xy}(1-\cos 2\theta) - I_{yz} \sin 2\theta \end{bmatrix}$$

The Y component of this expression is nulled when $\theta = -4.4$ degrees for the SVWS. This is the angle which removes the X-axis component (in the ORS) of the vector $I\mathbf{a}_{zo}^1$ where \mathbf{a}_{zo} is a unit vector along the local vertical (the $-Z_o$ axis in the ORS). No significant increase in the momentum requirement about the X and Z axes of the GS is caused by this rotation.

III. AAP APPLICATIONS

The establishment of the mathematical model for the momentum requirements of the CMGs of the SVWS for holding a local vertical attitude enables an evaluation of various possible options for performing Earth resources experiments. As mentioned in §I, three attitude options and four control options were studied. The results are presented in matrix form in Table 1 and presented in more detail in the sequel.

The first attitude option (A01), the noon acquisition of the local vertical attitude, is considered because it is easiest to perform from a control system standpoint. If it were found that the thermal and power systems could withstand two or more consecutive orbits of the XIOP/Z-LV attitude, then this option would be worthy of consideration. The principal results are:

1. A01 could be accomplished by three CMGs without any RCS assist (C01). This includes the gravity-gradient dump maneuver described in Appendix A which is performed on the dark side of the orbit. This is illustrated in Figure 2. The peak-to-peak (PTP) variation in $|\underline{H}|$ is 7550 ft-lb-sec when only the gravity-gradient

¹Recall that, using this notation, the gravity-gradient torque is given by $\underline{N}_{gg} = 3\omega_o^2 \mathbf{a}_{zo} \mathbf{I} \mathbf{a}_{zo}$.

TABLE 1

A MATRIX OF ATTITUDE AND CONTROL OPTIONS
FOR PERFORMING EARTH-POINTING EXPERIMENTS

	Control Option 1 CMGs Alone	Control Option 2 RCS Alone	Control Option 3 CMG/RCS Dump	Control Option 4 CMG/RCS Dump, Acq.
Attitude Option 1 (Noon)	Peak-to-peak $\Delta H $ = 7550 ft-lb-sec Includes gravity gradient dump.	1,000 lb-sec impulse required per orbit for non- consecutive orbits.	200 lb-sec impulse per orbit for dump- ing. Peak-to-peak $\Delta H \approx 4,800$ ft-lb- sec.	800 lb-sec impulse required per orbit for non-consecutive orbits.
Attitude Option 2 (Midnight)	Exceeds CMG capa- bility unless 4.4 deg.Y-axis offset is controlled.	1,160 lb-sec impulse required per orbit for non- consecutive orbits.	185 lb-sec impulse per orbit could re- duce peak-to-peak $\Delta H $ to $\approx 4,800$ ft- lb-sec.	960 lb-sec impulse required per orbit for non-consecutive orbits.
Attitude Option 3 (Over target)	$\pm 8,000$ ft-lb-sec maneuvering re- quirement exceeds CMG capability.	1,310 lb-sec impulse for 60 deg. exp. pass. Approx. 2,000 lb- sec for 120 deg. exp. pass.	Not applicable	Not applicable

¹All RCS impulse estimates are based on a 32.5 foot moment arm about the Y and Z axes.

torque is considered. Hence, this control option would be impossible if one of the CMGs were disabled.

2. The propellant consumption estimate for A01 if RCS control is used exclusively (C02) is approximately 1,000 lb-sec/orbit for one orbit. This includes an extra 80 lb-sec to account for the effects of the aerodynamic torque and other contingencies.
3. If, instead of the gravity-gradient dump maneuver in C01, the dumping is done by the RCS (C03), then the rest of A01 could be performed with 2 CMGs. The propellant requirement estimate for C03 is 200 lb-sec orbit. This includes an estimate for initializing the momentum vector such that the total change in $|\underline{H}|$ is minimized. If this is done the PTP change in $|\underline{H}|$ is approximately 4,800 ft-lb-sec.
4. Since most of the RCS propellant in C02 is required for maneuvering, C04 is relatively unattractive. About 200 lb-sec/orbit of propellant could be saved by holding attitude with CMGs but 800# sec/orbit would still be required.

Attitude option 2 (A02) is illustrated in Figure 3. The local vertical attitude is acquired sequentially. First, a roll maneuver is initiated at the sunset terminator to align the experiment window with the local vertical at midnight where the roll rate is removed and the orbital rate is initiated about the pitch (Y) axis. Then, the spacecraft stays in a local vertical attitude for one full orbit or until the midnight following acquisition at which time the orbital rate is removed and the return roll maneuver rate initiated. Finally, the roll rate is removed at the sunrise terminator. This attitude requires more control effort but allows a longer experiment interval for the same duration in the local vertical attitude. The results obtained by considering the cost of A02 with each of the control options are as follows:

1. Figure 4 illustrates the variation of the x, y and z components of \underline{H} measured in spacecraft coordinates over the solar inertial attitude and through all the steps of A02. Since the dark side roll maneuver does not include a gravity-gradient dump maneuver, the Y axis accumulates momentum because of the bias gravity-gradient torque mentioned in §II. This produces a

large transient effect¹ in the Y and Z axes during the return roll maneuver. The combination of these two effects results in a momentum requirement that exceeds the capacity of the CMGs ($\pm 6,000$ ft-lb-sec). Thus, without any RCS assist, this combination of options is not considered feasible unless the nominal attitude includes the 4.4 degree offset mentioned in §II.

2. If the same 80 lb-sec estimate for aerodynamic torque and other contingencies is included for the A02-C02 combination as it was for A01-C02, then the propellant consumption is 1,160 lb-sec/orbit for one orbit.
3. Figure 5 illustrates the variation of the x, y and z components of \underline{H} relative to spacecraft coordinates if 3,891 ft-lb-sec of Y-axis momentum is dumped immediately after acquisition of the orbital rate. This profile costs 120 lb-sec of propellant/orbit. Another 65 lb-sec of propellant could, if judiciously applied, reduce the variation of the x and z components of \underline{H} to an insignificant level.
4. As in the A01-C04 combination, A02-C04 saves 200 lb-sec relative to their corresponding control option, i.e. C02. Since the CMGs are capable of performing A01 and A02 with less RCS assist it is inefficient to use them only for attitude hold.

The third attitude option (A03) is illustrated in Figure 6. This is the best option for the thermal and power systems but has the most severe impact on the attitude control systems. The numbers given below for the various control options associated with A03 correspond to a 60 degree experiment interval. If this interval is increased to 120 degrees, the impact on the controller² increases by a factor of 1.6 and the roll maneuver must be initiated at the terminator instead of orbital 6 a.m. Further, since the time in local vertical is relatively small, only control options C01 and C02 are considered.

If 80 lb-sec is added for contingencies, the propellant consumption estimate for A03-C02 is 1310 lb-sec/orbit.

¹The principles which were outlined in §II can be generalized to provide a mathematical model for the roll maneuver since it involves spinning at a constant rate about a spacecraft axis. Since the X axis is now the spin axis, there is coupling between the Y and Z axis motions.

²That is, the fuel consumption of the RCS or the momentum variation of the CMGs.

This is only 150 lb-sec more than the cost of A02-C02. Therefore, if a 60 degree experiment interval is satisfactory, the requirements imposed by the thermal and power systems might dictate the choice of A03-C02 rather than A02-C02.

Finally, it is easy to show that A03 cannot be performed using only CMG control (i.e. C01). The primary problem is that, even though the required rate for the maneuver from

② to ③ in Figure 6 is only the negative of the orbital rate (.062 deg/sec), the required change in momentum to remove this rate and initiate the orbital rate, ω_o , for local vertical acquisition (a rate change equal to $2\omega_o$) is approximately 8,000 ft-lb-sec. Since the reverse maneuver must be performed at ④ in Figure 6 (i.e. a $\Delta H_y = -8,000$ ft-lb-sec), the total required change is seen to exceed the $\pm 6,000$ ft-lb-sec capacity of the SVWS CMGs.

IV. SUMMARY AND CONCLUSIONS

It is concluded from the results summarized in Table 1 that the CMGs may be used to good advantage to minimize the amount of RCS propellant required to perform the Earth-pointing experiments. In fact, the CMGs could be the primary system which requires only an occasional assist from the RCS.

Another point which should be made here is that the momentum profile illustrated in Figure 5 can be achieved in such a way that the gimbals of the CMGs remain away from their stops. Further, this momentum profile can be achieved with either two or three CMGs as long as some form of momentum dumping strategy is available. The question of whether or not the control law which is selected for controlling the SVWS in the solar inertial mode will also be acceptable for control in an Earth-pointing mode is presently being studied.

There is another reason for preferring C03 to C02 with either A01 or A02. That is, the CMGs can control the spacecraft attitude much more accurately than an RCS whose control law requires (at present) a 0.5 degree deadband. This means, in turn, that the Earth Resources Experiments can be pointed with better accuracy.

Finally, some important technical results are presented in §2. Chief among these is the demonstration of the fact that

bias momentum accumulation is primarily about the axis which is perpendicular to the orbit plane. A detailed study of §2 will also reveal a fundamental difference in the way CMGs oppose external torques acting on the vehicle if the desired attitude is spinning relative to a set of inertial coordinates.

ACKNOWLEDGEMENT

The excellent assistance in programming and computation provided by Mrs. P. R. Dowling is appreciatively acknowledged.

J. J. Fearnside

J. J. Fearnside

1022-JJF-cf

Attachment
Appendix A

REFERENCES

1. Kranton, J., "Application of Optimal Control Theory to Attitude Control with Control Moment Gyros," D.Sc. Dissertation, George Washington University, February, 1970.
2. Hough, W. W., "AAP Cluster Mass Properties and CMG Control Capability," Memorandum for File, B69-11054, Bellcomm, Inc., Washington, D.C., November 20, 1969.

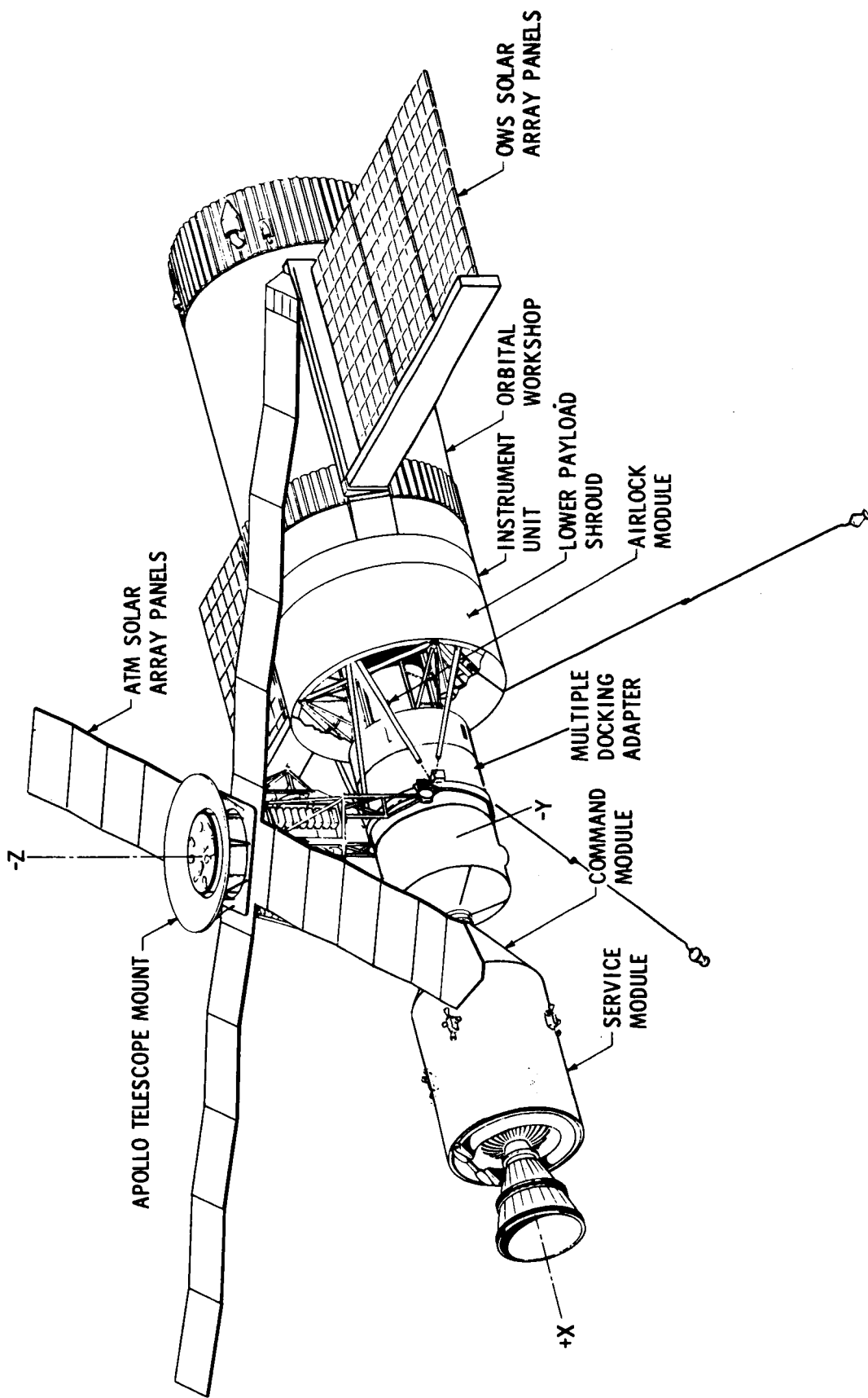
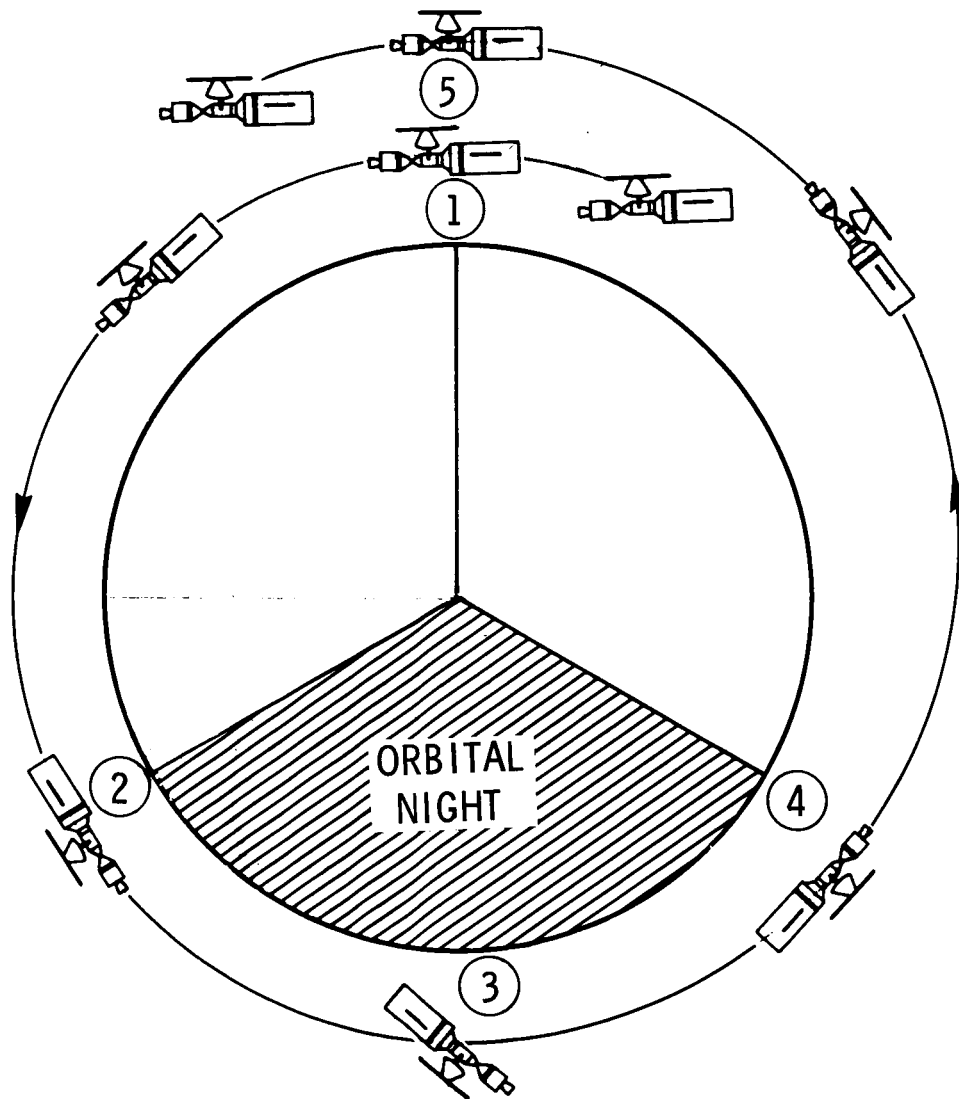


FIGURE 1 - SATURN V WORKSHOP

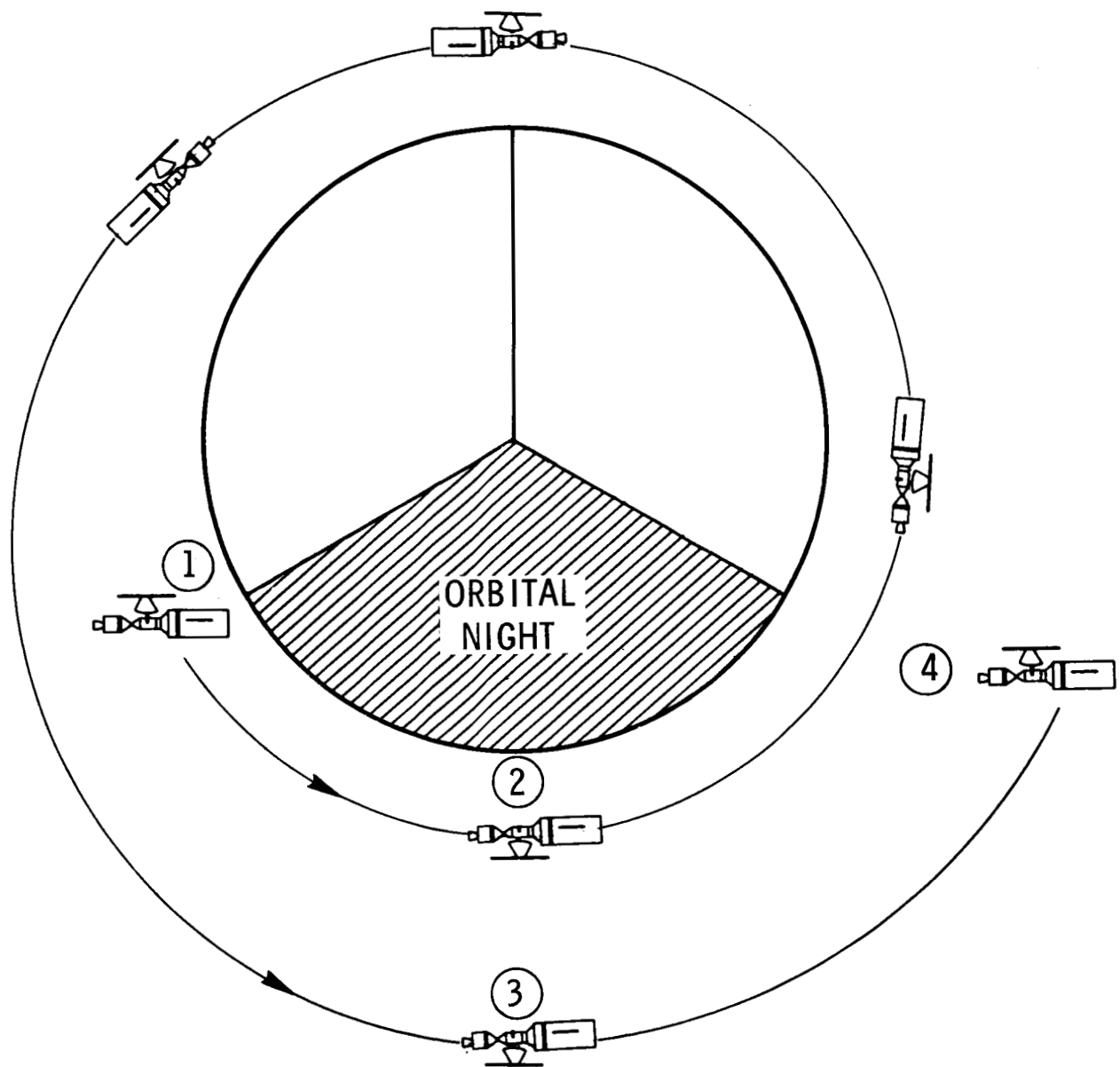
ATTITUDE OPTION 1



- ① ACQUIRE LOCAL VERTICAL FROM SOLAR INERTIAL.
- ② INITIATE GRAVITY-GRADIENT DUMP MANEUVER.
- ③ REVERSE PITCH RATE AND CONTINUE DUMPING.
- ④ REACQUIRE LOCAL VERTICAL BY REMOVING PITCH RATE.
- ⑤ REACQUIRE SOLAR INERTIAL.

FIGURE 2

ATTITUDE OPTION 2



- ① INITIATE ROLL MANEUVER TO ALIGN EXP. AXIS WITH THE LOCAL VERTICAL AT ORBIT MIDNIGHT.
- ② REMOVE ROLL RATE, INITIATE PITCH ORBITAL RATE.
- ③ REMOVE PITCH ORBITAL RATE, INITIATE RETURN ROLL RATE.
- ④ REMOVE ROLL RATE, SOLAR INERTIAL REACQUIRED.

FIGURE 3

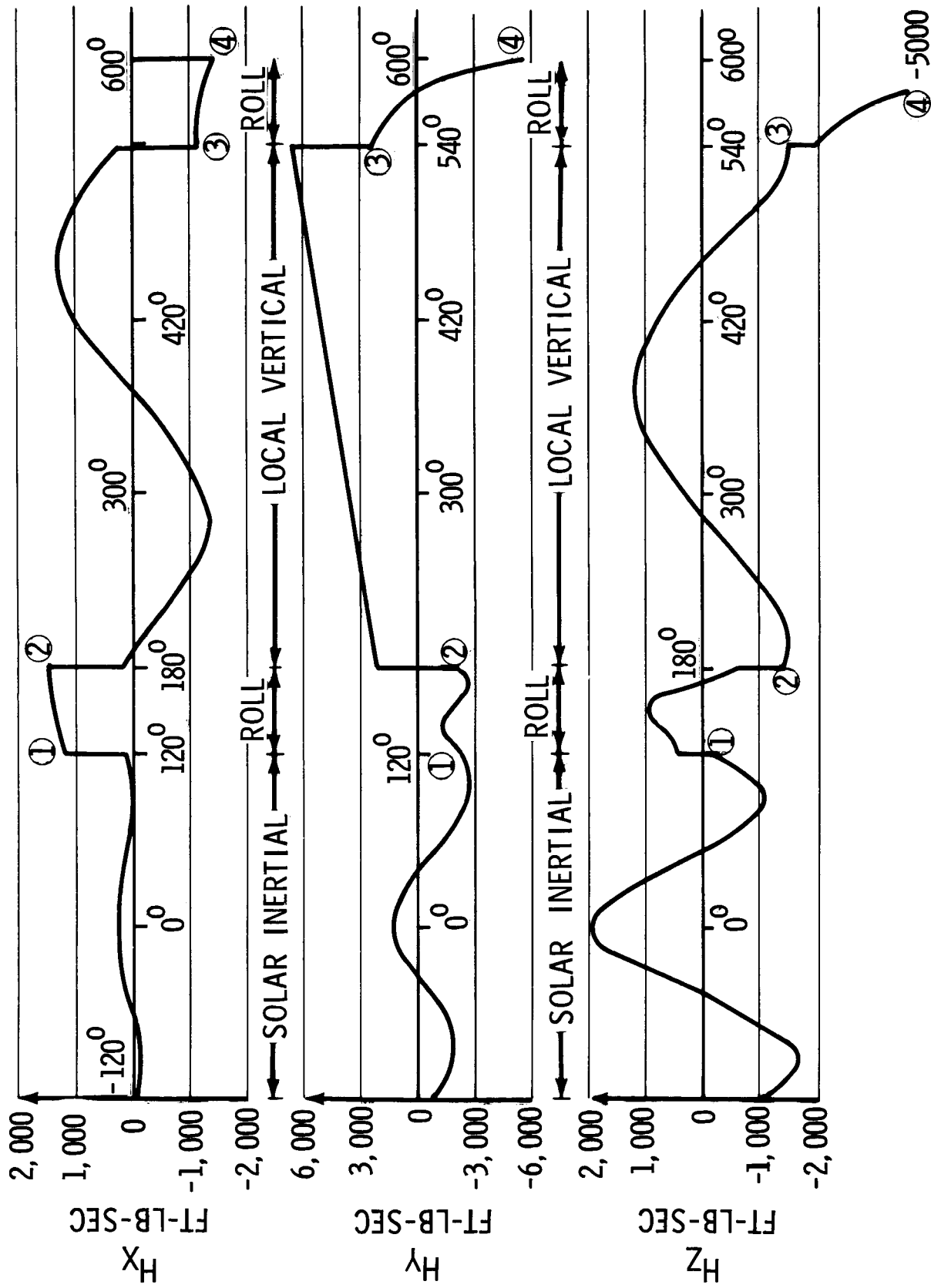


FIGURE 4 - ATTITUDE OPTION 2 - CONTROL OPTION 1
CMG MOMENTUM VARIATION VS. ORBIT ANGLE ($\beta = 45^\circ$)

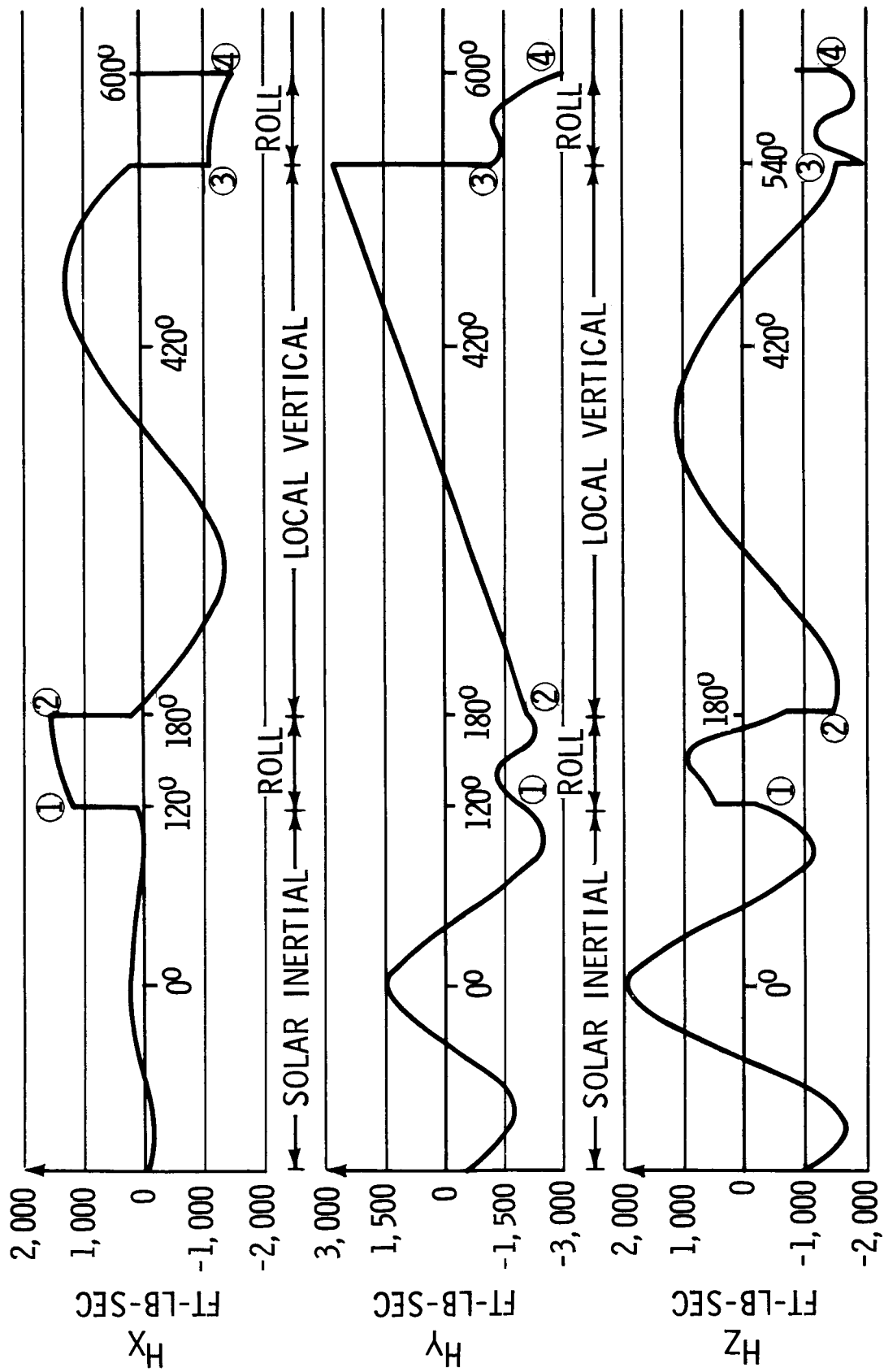
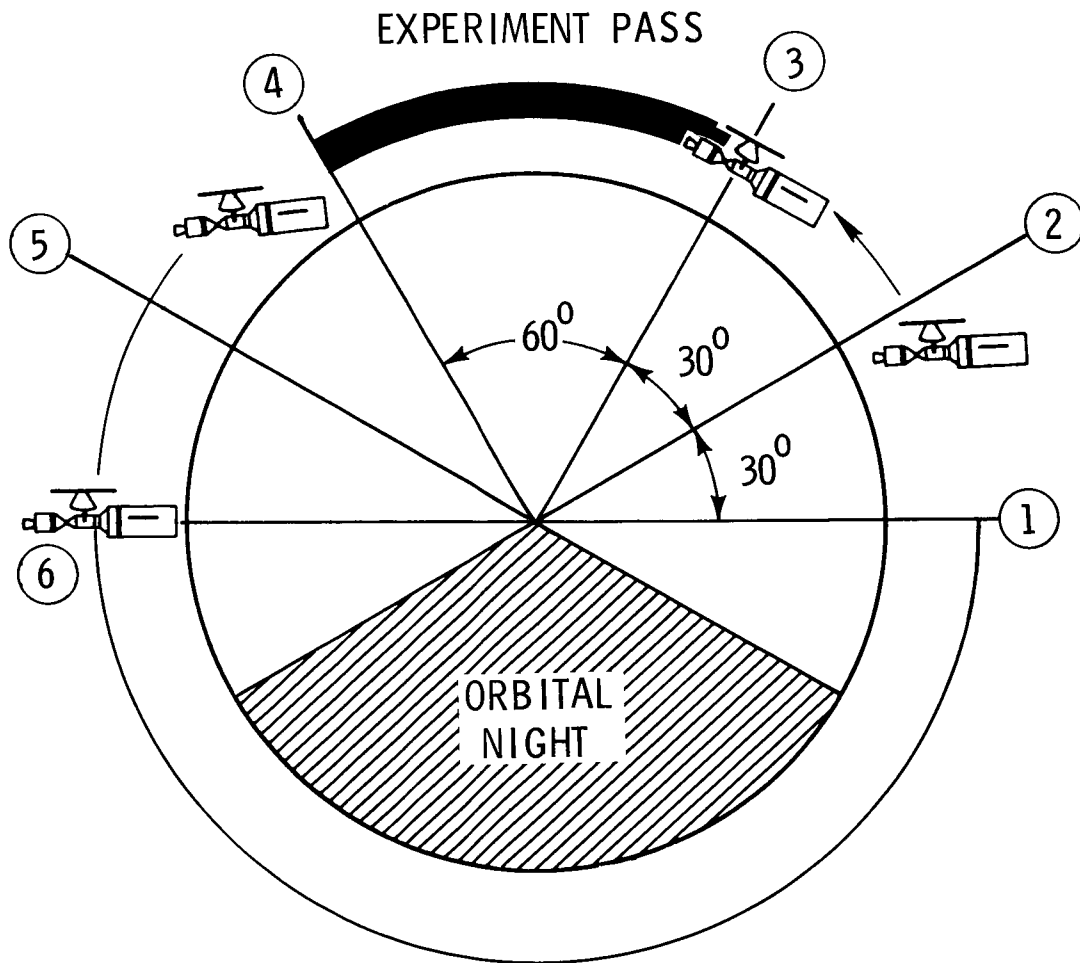


FIGURE 5 - ATTITUDE OPTION 2 - CONTROL OPTION 3
CMG MOMENTUM VARIATION VS. ORBIT ANGLE ($\beta = 45^\circ$)

ATTITUDE OPTION 3



- ① INITIATE ROLL MANEUVER TO REMOVE β .
- ② REMOVE ROLL RATE, INITIATE PITCH MANEUVER.
- ③ REMOVE PITCH MANEUVER RATE, INITIATE PITCH ORBITAL RATE.
- ④ REMOVE PITCH ORBITAL RATE, INITIATE RETURN PITCH MANEUVER RATE.
- ⑤ REMOVE PITCH RATE, INITIATE ROLL RATE.
- ⑥ REMOVE ROLL RATE.

FIGURE 6

APPENDIX A

A GRAVITY-GRADIENT DUMP SCHEME

If the local vertical mode is acquired at noon or if successive orbits can be tolerated by the thermal and power systems of the spacecraft, then the dark side of the orbit has no scheduled maneuvers. Further, equation (8) suggests that a Y-axis maneuver might be scheduled such that the momentum which accumulates about this axis can be dumped by the Earth's gravitational field. This is verified by the following example.

Consider the dark side maneuver illustrated in Figure 2. A constant rate is imparted about the spacecraft Y axis at the sunset terminator ② causing the spacecraft axes to move away from the orbit referenced system (ORS). In order that the body axes be realigned with the ORS at the sunrise terminator, the rate is reversed at orbital midnight ③. Then, at the sunrise terminator ④, the return maneuver rate is removed and the spacecraft geometric axes (GS) are realigned with the ORS.

From equation (8), the Y-axis component of the gravity-gradient torque on the spacecraft as it rotates about the Y-axis through an angle θ away from the ORS is given by

$$(A-1) \quad N_{ggy} = 1.5\omega_o^2 [(I_{zz} - I_{xx}) \sin 2\theta + 2I_{xz} \cos 2\theta]$$

If the sunrise terminator is defined at $t = 2\pi/3\omega_o$ sec and if at this instant the Y axis velocity is changed from ω_o to $\omega_o(1-\epsilon)$, then θ is given by

$$(A-2) \quad \theta = -\epsilon\omega_o \left(t - \frac{2\pi}{3\omega_o}\right).$$

Now, since the accumulation of bias momentum about this axis is 4645 ft-lb-sec per orbit, there will be approximately 3100 ft-lb-sec accumulated between the terminators. This must be dumped on the dark side and, since the maneuver is symmetrical,

half of this amount or 1550 ft-lb-sec must be dumped between the sunset terminator and midnight. From equation (7) the change in Y-axis momentum is equal to the integral of the external torque over time. This leads to the following expression for the required dumping maneuver

$$(A-3) \quad -1550 = 1.5\omega_o^2 \int_0^{\pi/3\omega_o} [2I_{xz} \cos(2\epsilon\omega_o\tau) - (I_{zz} - I_{xx}) \sin(2\epsilon\omega_o\tau)] d\tau,$$

where the substitution $\tau = (t - 2\pi/3\omega_o)$ has been made. The solution of (A-3) can be expressed in the form

$$(A-4) \quad 1535\omega_o = 0.75\omega_o A [\cos\delta - \cos(2\pi\epsilon/3 - \delta)]$$

where: $A = [4I_{xz}^2 + (I_{zz} - I_{xx})^2]^{1/2}$, and

$$\delta = \tan^{-1} \left(\frac{2I_{xz}}{I_{zz} - I_{xx}} \right).$$

This is a transcendental equation and must be solved approximately. Using the mass properties of the SVWS leads to the solution (obtained graphically) $\epsilon = 0.45$. This implies a maximum angular variation from the ORS of -27 degrees at orbital midnight. That is,

$$(A-5) \quad \theta(\pi/\omega_o) = -27 \text{ degrees.}$$

COVER SHEET FOR TECHNICAL MEMORANDUM

TITLE- Effects of Target Lighting and β
Constraints on Skylab Ground Site
Photography

TM-70-1022-8

DATE- March 30, 1970

FILING CASE NO(S)- 620

AUTHOR(S)- B. D. Elrod

FILING SUBJECT(S)- Space Photography
(ASSIGNED BY AUTHOR(S)- Earth-Looking Experiments
Target Lighting Constraint

ABSTRACT

Lighting for ground site photography is considered adequate, when the angle between the solar vector and the target local vertical does not exceed some value, Λ (target lighting constraint). Evaluation of lighting conditions given orbital parameters and time is generally a deterministic problem. Since launch time for future missions and subsequent times of re-visit to orbiting spacecraft are not known precisely, the question of adequate lighting over an arbitrary target at any time is addressed here on a probabilistic basis. Target lighting probabilities calculated on the basis of uniformly distributed launch times, represent the average chance for adequate lighting given a target sighting at any arbitrary time.

In the Skylab mission with a 50° orbit inclination, northern hemisphere targets at latitudes up to 50° are available. The probability of adequate lighting at these latitudes for $\Lambda=60^\circ$ is relatively constant (~ 0.33) for random target sightings during the spring/summer period, but drops steadily with increasing latitude for the fall/winter period (0.04 at 50°N). These characteristics reverse for southern hemisphere targets.

Due to electrical power and thermal control limitations, ground site photography with the Skylab in the XIOP-ZLV mode may be limited to periods when $|\beta| \leq \beta_c$ (β constraint). If $\beta_c=30^\circ$, the lighting probability is reduced by 30% for equatorial targets and by 41% for targets at a 50° latitude. With a β constraint of $\beta_c=45^\circ$ the reduction is 10-13% and for $\beta_c \geq 60^\circ$, there is no effect at all.

DISTRIBUTIONCOMPLETE MEMORANDUM TO

CORRESPONDENCE FILES:

OFFICIAL FILE COPY
plus one white copy for each
additional case referenced

TECHNICAL LIBRARY (4)

NASA Headquarters

H. Cohen/MLR
J. H. Disher/MLD
W. B. Evans/MLO
L. K. Fero/MLV
J. P. Field, Jr./MLP
W. H. Hamby/MLO
T. E. Hanes/MLA
T. A. Keegan/MA-2
M. Savage/MLT
W. C. Schneider/ML

Goddard Space Flight Center

J. T. Skladany/713

Langley Research Center

P. R. Kurzahls/AMPD

MSC

R. G. Brown/ES-16
C. N. Crews/KS
W. R. Cunningham/CB
R. E. Durkee/ES-5
R. L. Frost/KS
O. K. Garriott/CB
F. C. Littleton/KM
R. M. Machell/KF
P. S. Miglicco/KS
O. G. Smith/KF
H. E. Whitacre/KM

MSFC

R. M. Aden/S&E-ASTR-E
W. B. Chubb/S&E-ASTR-SGD
J. C. Cody/S&E-ASTR-MA
C. B. Graff/S&E-ASTR-EP

COMPLETE MEMORANDUM TOMSFC (continued)

G. B. Hardy/PM-AA-EI
G. D. Hopson/S&E-ASTN-PL
E. H. Hyde/S&E-ASTN-PF
H. F. Kennel/S&E-ASTR-A
G. F. McDonough/S&E-CSE-A
E. F. Noel/S&E-ASTR-SI
W. C. Patterson/S&E-ASTN-PLA
J. W. Sims/S&E-ASTN-PTA
J. D. Stroud/S&E-ASTR-SE
J. W. Thomas/PM-AA
H. F. Trucks/S&E-ASTN-PTA
J. L. Vaniman/S&E-ASTN-PT
R. D. Wegrich/S&E-CSE-AA
A. P. Woosley/S&E-ASTR-SEC
H. E. Worley/S&E-AERO-DOI

Martin-Marietta

H. S. Nassen/Denver
E. F. Bjoro/Washington
M. S. Imamura/Denver
R. W. Wilson/Denver

McDonnell-Douglas

G. Weber/Eastern Division

Bellcomm

A. P. Boysen
D. R. Hagner
W. G. Heffron
B. T. Howard
J. Z. Menard
J. M. Nervik
I. M. Ross
P. F. Sennewald
J. W. Timko
R. L. Wagner
M. P. Wilson
Departments 2031, 2034 Supervision
Department 1024 File
Division 102
Central Files

SUBJECT: Effects of Target Lighting and β
Constraints on Skylab Ground Site
Photography - Case 620

DATE: March 30, 1970

FROM: B. D. Elrod

TM-70-1022-8

TECHNICAL MEMORANDUM

1.0 INTRODUCTION

As part of an earth resources program ground site photography is currently planned with the S190, Multi-Spectral Photographic Facility during the first Skylab mission. As presently baselined the Saturn V Workshop (SVWS) will be oriented in the XIOP-ZLV mode* with cameras pointed along the nadir.** Photographic opportunities will occur when:

- a) the target falls within the camera field-of-view (target sighting) and
- b) the angle between the target local vertical and the solar vector is within $\Lambda=60^\circ$ (target lighting constraint).

The target sighting problem has recently been studied⁽¹⁾ for general circular orbits and results given in terms of the maximum interval between successive sightings of a specific target. Another study⁽²⁾ has examined the impact of both sighting frequency and the lighting constraint on photographic opportunities for specific targets from the 50° , 235×235 NM Skylab orbit. Sighting opportunities are important when photography of specific targets is planned. For arbitrary targets*** along a particular parallel of latitude, only the lighting constraint is relevant.

If orbital parameters and time are specified, evaluation of target lighting is a deterministic problem. Because launch time for future missions and subsequent times of revisit

*XIOP - x geometric axis in the orbital plane; ZLV - z geometric axis (ATM axis) along upward local vertical.

**A more detailed description of the experiment is given in Reference 2.

***"Arbitrary" is used in the sense, "selected at random".

to an orbiting spacecraft are uncertain, the chances of adequate lighting over arbitrary targets at any time is of interest. In this memorandum target lighting for nadir photography is addressed on a probabilistic basis. With this view the question considered is:

Given a target sighting at a particular latitude at some arbitrary time, what is the probability that the target lighting constraint (Λ) is satisfied?

Because of electrical power and thermal control limitations, opportunities for operating in the XIOP-ZLV mode with the SVWS may be limited to occasions when $|\beta| \leq 30^\circ$.* The β constraint affects target lighting probabilities, since it has the effect of excluding occasions when the lighting constraint would otherwise be satisfied. Thus, a second question considered is:

Given a target sighting at a particular latitude at some arbitrary time, what is the probability that both target lighting and β constraints are satisfied?

2.0 TARGET LIGHTING PROBABILITY - GENERAL

The geometry associated with an arbitrary target sighting (T) for a particular orbit is shown in Fig. 1a in which the earth is represented as a unit sphere. Since

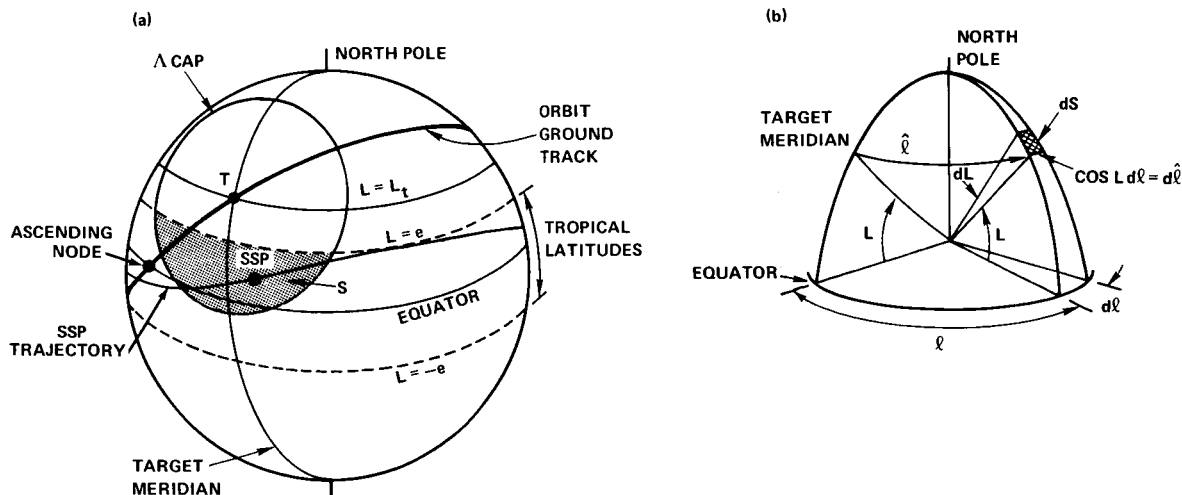


FIGURE 1. TARGET LIGHTING GEOMETRY

* $|\beta|$ is the minimum angle between the sunline and the orbital plane.

sightings of specific targets at a given latitude on the earth's surface are not involved here, the earth can be regarded as fixed relative to the orbit. The spherical cap centered at T is defined by the intersection with the earth's surface of a cone with vertex at the geocenter, half angle Λ and axis parallel to the target local vertical at latitude L_t . The lighting constraint is satisfied at T, if the solar vector (earth-sun line) pierces that region (S) of the spherical cap lying within the tropical latitudes, $|L| \leq e = 23.45^\circ$.

The solar vector orientation relative to an earth orbit varies slowly due to the earth's motion about the sun and the nodal motion caused by earth oblateness.⁽³⁾ A typical trajectory of the subsolar-point (SSP) relative to the orbit ground track is shown in Fig. 1a. For any particular orbit adequate lighting at T prevails over several days (while the SSP moves through S) and recurs at intervals.

For any particular orbit the probability (P_o) that the SSP lies in S at any arbitrary time within a mission depends on mission duration (T_M) and the initial location of the SSP relative to the orbit ground track (launch conditions). For short missions P_o may range between 0 and 1. However, it is intuitively clear that as T_M increases indefinitely, P_o tends to a constant (P_s), since orbits* corresponding to different launch times, all eventually experience the same solar vector variation. Furthermore, the ensemble average (at any arbitrary time) of P_o over all possible launch times must be P_s . Consequently, P_s is defined as the target lighting probability and can be evaluated as the ensemble average of P_o over all possible launch times. Hence P_s represents the average chance for adequate lighting given a target sighting at any arbitrary time.

*The exception is a sun-synchronous orbit⁽³⁾ where the orbit ascending node rotates in the equatorial plane in the same direction and at the same average rate as the solar vector in the ecliptic plane.

2.1 Evaluation of P_s

Consider an element of area $dS = \cos L \, d\ell \, dL = d\hat{\ell} \, dL$ on the unit sphere at latitude L and longitude ℓ relative to the target meridian as shown in Fig. 1b. The probability, $dP(\hat{\ell}, L)$, that the subsolar-point (SSP) lies within dS is given by

$$dP(\hat{\ell}, L) = f_{\hat{\ell}}(\hat{\ell}|L) f_L(L) d\hat{\ell} dL = f_{\hat{\ell}}(\hat{\ell}|L) f_L(L) \cos L \, d\ell \, dL \quad (1)$$

where

$$f_{\hat{\ell}}(\hat{\ell}|L) d\hat{\ell} = \begin{array}{l} \text{probability that SSP lies within} \\ \text{an increment of longitude,} \\ d\hat{\ell} = \cos L \, d\ell, \text{ given that SSP is at} \\ \text{latitude } L \text{ where } |L| \leq e, \end{array}$$

$$f_L(L) dL = \begin{array}{l} \text{probability that SSP lies within} \\ \text{the latitude band } (L, L + dL) \text{ at} \\ \text{some random instant} \end{array}$$

and $f_{\hat{\ell}}(\hat{\ell}|L)$, $f_L(L)$ are corresponding probability density functions. The target lighting probability is obtained by integrating $dP(\hat{\ell}, L)$ over S :

$$P_s = \int_S \int dP(\hat{\ell}, L) = \int_S \int f_{\hat{\ell}}(\hat{\ell}|L) f_L(L) \cos L \, d\ell \, dL \quad (2)$$

Expressions for $f_L(L)$ and $f_{\hat{\ell}}(\hat{\ell}|L)$ are derived in Appendix A based on treating launch time (date or time-of-day) as a uniformly distributed random variable.

To evaluate P_s for random target sightings over an entire year the expressions for $f_L(L)$ and $f_{\hat{\ell}}(\hat{\ell}|L)$ from Eqs. (A-11) and (A-7) are

$$f_{\hat{\ell}}(\hat{\ell}|L) = \frac{1}{2\pi \cos L} \quad |\hat{\ell}| < \pi \cos L \quad (3)$$

$$f_L(L) = \frac{1}{\pi} \frac{\cos L}{\sqrt{\sin^2 e - \sin^2 L}} \quad |L| < e \quad (4)$$

Substitution into Eq.(2) and integration over L yields

$$\begin{aligned} P_s &= \frac{1}{2\pi^2} \int_{\ell} \int_{L_1(\ell)}^{L_2(\ell)} \frac{\cos L}{\sqrt{\sin^2 e - \sin^2 L}} dL d\ell \\ &= \frac{1}{2\pi^2} \int_{\ell} \left\{ \sin^{-1} \left[\frac{\sin L_2(\ell)}{\sin e} \right] - \sin^{-1} \left[\frac{\sin L_1(\ell)}{\sin e} \right] \right\} d\ell \end{aligned} \quad (5)$$

where $L_2(\ell)$ and $L_1(\ell)$ represent the upper and lower boundaries of S at a longitude ℓ relative to the target meridian. Equations for evaluating the boundary of S formed by the spherical cap (Λ cap) in Fig.1 are given in Appendix B. Depending on L_t and Λ the region S may assume one of six forms as shown in Mercator projection in Fig.(B-3). Evaluation of P_s in Eq.(5) is normally a numerical process, since the integrand is usually intractable unless $L_1(\ell)$ and $L_2(\ell)$ are constant.

A comparison of target lighting probabilities for spring/summer and fall/winter periods can also be evaluated with only slight modification of these results. This arises for

random target sightings over six-month intervals centered at the summer and winter solstices. For the spring/summer period the lighting probability (P_{s1}) concerns only that portion of the spherical cap (around T in Fig.1) lying within the northern tropical zone ($0 < L \leq e$). For the fall/winter period only the region lying within the southern tropical zone ($-e \leq L \leq 0$) is involved in evaluating the lighting probability (P_{s2}). Corresponding expressions for $f_{\hat{\ell}}(\hat{\ell}|L)$ and $f_L(L)$ are given in Appendix A.

2.2 Effect of β Constraint on Lighting Probabilities

Opportunities for orbiting in a local vertical mode for ground site photography may be limited to periods when $|\beta| \leq \beta_c$ (β constraint).^{*} Hence, for a photographic opportunity at a random target sighting the subsolar-point is further restricted to that region in S between two spherical caps (β^+, β^-) shown in Fig.2. The caps are defined by the intersection with the earth's surface of two oppositely directed cones, each with vertex at the geocenter, half angle, $90^\circ - \beta_c$, and cone axis normal to the orbital plane.

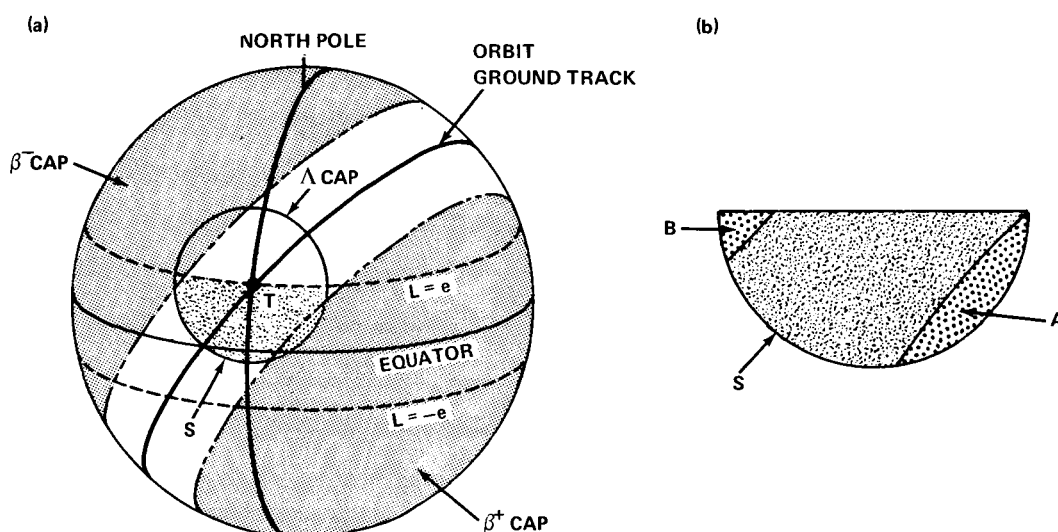


FIGURE 2. EFFECT OF β CONSTRAINT ON TARGET LIGHTING GEOMETRY

^{*}In the remainder of this work the β constraint is parameterized in terms of β_c .

The region excluded from S by the β constraint is the overlapping portion of the (β^+, β^-) caps on the Λ cap within S.* This is represented in Fig. 2b by the regions A and B. The corresponding probabilities for the subsolar-point in A and B are calculated analogous to Eq. (2) for S, that is

$$P_a = \int \int_A dP(\hat{\ell}, L) = \int \int_A f_{\hat{\ell}}(\hat{\ell}|L) f_L(L) \cos L \, d\ell \, dL \quad (6)$$

and

$$P_b = \int \int_B dP(\hat{\ell}, L) = \int \int_B f_{\hat{\ell}}(\hat{\ell}|L) f_L(L) \cos L \, d\ell \, dL \quad (7)$$

Thus, with the β constraint the target lighting probability (P_β) is

$$P_\beta = P_s - (P_a + P_b) \quad (8)$$

The reduction in the lighting probability due to the β constraint can be assessed from the ratio

$$\rho = \frac{P_s - P_\beta}{P_s} = \frac{P_a + P_b}{P_s} \quad (9)$$

which expresses the reduction as a fraction of P_s .

As there are six different forms for region S, there are also many possible forms for regions A and B. Typical cases are illustrated in Fig. (B-3). Equations for the boundaries of the β^+ and β^- caps necessary for evaluating P_a and P_b are also given in Appendix B.

3.0 TARGET LIGHTING PROBABILITIES FOR SKYLAB MISSION

The lighting probability, P_s , is a function of two parameters: L_t and Λ . With the β constraint, the lighting probability, P_β , is a function of four parameters: L_t, Λ, β_c

*Intersection of the β^+ and β^- caps with the Λ cap occurs if $\beta_c \leq \Lambda$.

and orbit inclination, i .* For the Skylab mission: $\Lambda=60^\circ$ and $i=50^\circ$ so that target latitudes in the range $-50^\circ \leq L_t \leq 50^\circ$ are available.

In Fig.3 lighting probabilities are plotted vs L_t for random target sightings:

- (a) over an entire year (P_s),
- (b) over a six-month interval centered at summer solstice (P_{s1}) and
- (c) over a six-month interval centered at winter solstice (P_{s2}).

The curve for P_s is symmetrical about $L_t=0^\circ$ with P_s a maximum for equatorial latitudes and a minimum at the northernmost latitudes. The curves for P_{s1} and P_{s2} are complimentary with $P_{s1} > P_{s2}$ for $L_t > 0^\circ$ and $P_{s1} < P_{s2}$ for $L_t < 0^\circ$. As L_t increases, the ratio P_{s1}/P_{s2} increases markedly with $P_{s1}/P_{s2}=8.2$ at $L_t=50^\circ$. For short duration missions, such as the 56-day Skylab mission, these results

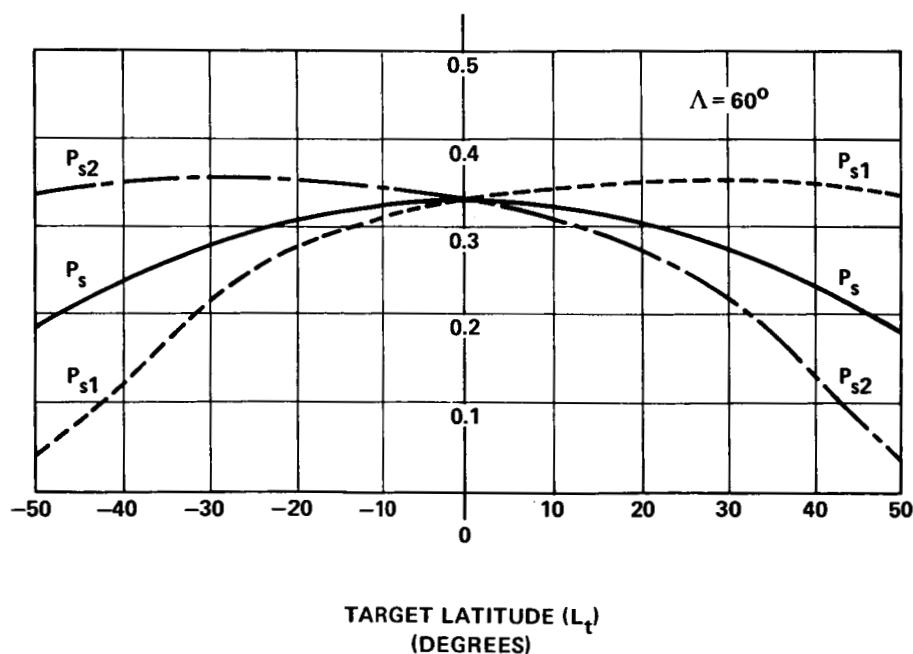


FIGURE 3. TARGET LIGHTING PROBABILITIES VS TARGET LATITUDE (L_t)

*Since i is the maximum latitude which the ground track reaches, only $|L_t| \leq i$ is of interest for nadir photography.

clearly illustrate the impact of spring/summer vs fall/winter launches on lighting probabilities for northern hemisphere targets.

In Fig.4 the effect of the β constraint on target lighting probabilities is shown for various values of β_c . If $\beta_c = 30^\circ$ is imposed on the Skylab mission, a 30-41% reduction in the lighting probability results with the higher value applicable to target latitudes near 50° , which are of particular interest.* For $\beta_c \geq \Lambda = 60^\circ$, the β constraint has no effect.

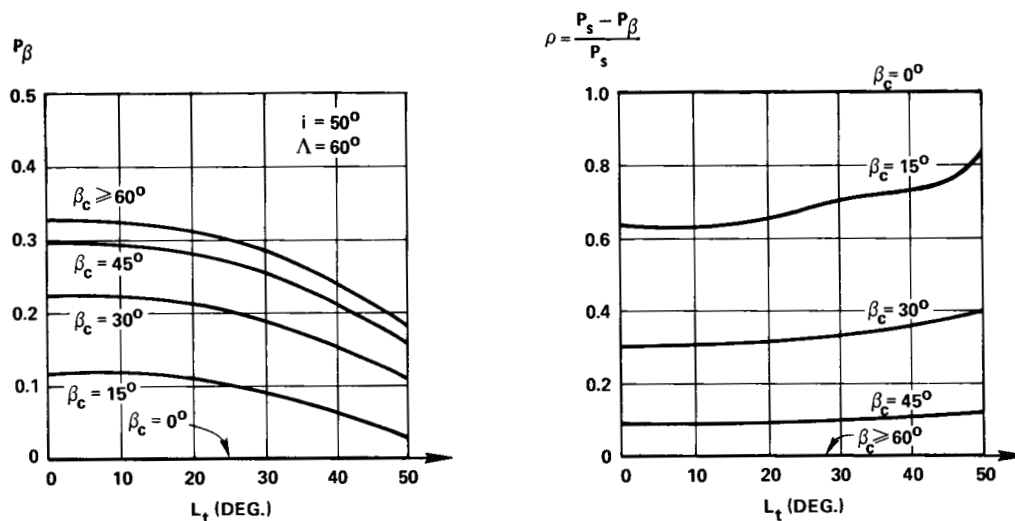


FIGURE 4. EFFECT OF β CONSTRAINT ON TARGET LIGHTING PROBABILITY

4.0 SUMMARY AND CONCLUSIONS

Adequate lighting for ground site photography is usually stated in terms of a target lighting constraint, which requires that the angle between the solar vector and the target local vertical not exceed some value, Λ . In this memorandum the question of adequate lighting at the time of passing over any arbitrary target is addressed on a probabilistic basis. Target lighting probabilities are evaluated for random target sightings over a year and over six-month intervals centered at the summer and winter solstices.

In the Skylab mission with a lighting constraint of $\Lambda = 60^\circ$, northern hemisphere targets at latitudes up to 50° are of

*A view of the region satisfying both target lighting and β constraints ($\Lambda = 60^\circ$, $\beta_c = 30^\circ$) for a western hemisphere target at $L_t = 50^\circ$ is shown in Fig. (B-4).

interest. The probability of adequate target lighting for random target sightings in the spring/summer period is relatively constant for northern latitudes with the average about 0.33. For random sightings in the fall/winter period the probability drops steadily as latitude increases, and reaches 0.04 at a 50° latitude. These characteristics reverse for southern hemisphere targets.

Because of electrical power and thermal control limitations, opportunities for ground site photography with the Saturn V Workshop in the XIOP-ZLV mode may be limited to periods when $|\beta| \leq \beta_c = 30^\circ$. This affects the lighting probability, since occasions when the lighting constraint would be satisfied, are excluded. The effect of requiring $\beta_c = 30^\circ$ is to reduce the lighting probabilities by 30-41% as shown in Fig. 4b. For a β constraint of 45° however, the reduction is only 10-13% and for $\beta_c \geq 60^\circ$, there is no effect at all.

ACKNOWLEDGEMENT

The author gratefully acknowledges the computer programming support of Mrs. P.R. Dowling.



B. D. Elrod

1022-BDE-cds

REFERENCES

1. S. Shapiro, "Low Altitude Orbits for Earth-Looking Experiments," Bellcomm Technical Memorandum, TM-69-1011-6, September 23, 1969.
2. D. A. DeGraaf and E. W. Radany, "Photography of Ground Sites from AAP Orbit," Bellcomm Memorandum for File, B70 02023, February 12, 1970.
3. B. D. Elrod, "Solar Pointing Variations in Earth Orbit and the Impact on Mission Design," Bellcomm Technical Report, TR-70-620-1, February 11, 1970.
4. A. Papoulis, "Probability, Random Variables and Stochastic Processes," McGraw-Hill Book Co., New York, N. Y., 1965, pp. 126-127.

APPENDIX APROBABILITY DENSITY FUNCTIONS FOR SUBSOLAR-POINT (SSP)
LATITUDE AND LONGITUDE

The purpose of this appendix is to derive probability density functions for a) SSP latitude (L) and b) SSP longitude ($\hat{\ell}$) relative to a ground site meridian given that the SSP is at a particular latitude. The analyses are based on treating time as completely arbitrary, i.e., a uniformly distributed random variable over some time interval.

A.1 SSP Latitude (L)

SSP latitude can be expressed in terms of an angle γ , which defines the earth-sun line location in the ecliptic plane.* The relationship between L and γ is **

$$L = \sin^{-1}(\sin \gamma \cdot \sin e) \quad (\text{A-1})$$

where $e=23.45^\circ$ is the angle between the equatorial and ecliptic planes. Three time intervals are of interest here: an entire year ($-\pi \leq \gamma \leq \pi$), a six-month interval centered at summer solstice ($0 \leq \gamma \leq \pi$) and a six-month interval centered at winter solstice ($-\pi \leq \gamma \leq 0$). The probability density function, $f_\gamma(\gamma)$, for γ in each case is***

$$\begin{aligned} \text{a) } & \underline{\text{Entire Year}} \\ f_\gamma(\gamma) = & \begin{cases} 1/2\pi & |\gamma| < \pi \\ 0 & \text{otherwise} \end{cases} \end{aligned} \quad (\text{A-2})$$

*Here γ is measured relative to the earth-sun line location at vernal equinox ($\gamma = 0$).

**At summer solstice, $\gamma = \pi/2$ so that $L = e$.

***The solar vector is assumed to rotate at a constant rate in the ecliptic plane, since the effect of earth's orbital eccentricity is small and unimportant for this analysis. Thus, γ is a uniformly distributed random variable in the stated interval.

$$\text{b) } \underline{\text{Spring/Summer}} \quad f_{\gamma}(\gamma) = \begin{cases} 1/\pi & 0 \leq \gamma \leq \pi \\ 0 & \text{otherwise} \end{cases} \quad (\text{A-3})$$

$$\text{c) } \underline{\text{Fall/Winter}} \quad f_{\gamma}(\gamma) = \begin{cases} 1/\pi & -\pi \leq \gamma \leq 0 \\ 0 & \text{otherwise} \end{cases} \quad (\text{A-4})$$

Corresponding probability density functions, $f_L(L)$, are to be determined with the procedure in Reference 4. A function $y=g(x)$ with x described by $f_x(x)$, has a probability density function $f_y(y)$ given by

$$f_y(y) = \sum_n \frac{f_x(x_n)}{|g'(x_n)|} \quad (\text{A-5})$$

where x_n are solutions of $y=g(x)$ for x in terms of y and $g'(x)=dg/dx$. Wherever $y=g(x)$ has no solutions, $f_y(y)=0$.

From Eq.(A-1) it follows that

$$\frac{dL}{d\gamma} = g'(\gamma) = \frac{\cos \gamma \cdot \sin e}{\sqrt{1 - \sin^2 \gamma \cdot \sin^2 e}} = \pm \frac{\sqrt{\sin^2 e - \sin^2 L}}{\cos L} \quad (\text{A-6})$$

Although $L=g(\gamma)$ has infinitely many solutions, $f_{\gamma}(\gamma_n)=0$ except in the intervals stated in Eqs.(A-2)-(A-4). In fact, for any L there are only two solutions for γ . Thus,

$$\text{a) } \underline{\text{Entire Year}} \quad f_L(L) = \sum_{n=1}^2 \frac{f_{\gamma}(\gamma_n)}{|g'(\gamma_n)|} = \begin{cases} \frac{\cos L}{\sqrt{\sin^2 e - \sin^2 L}} \left(\frac{2}{2\pi} \right) & |L| \leq e \\ 0 & \text{otherwise} \end{cases} \quad (\text{A-7})$$

b) Spring/Summer

$$f_L(L) = \sum_{n=1}^2 \frac{f_Y(\gamma_n)}{|g'(\gamma_n)|} = \begin{cases} \frac{\cos L}{\sqrt{\sin^2 e - \sin^2 L}} \left(\frac{2}{\pi}\right) & 0 \leq L \leq e \\ 0 & \text{otherwise} \end{cases} \quad (\text{A-8})$$

c) Fall/Winter

$$f_L(L) = \sum_{n=1}^2 \frac{f_Y(\gamma_n)}{|g'(\gamma_n)|} = \begin{cases} \frac{\cos L}{\sqrt{\sin^2 e - \sin^2 L}} \left(\frac{2}{\pi}\right) & -e \leq L \leq 0 \\ 0 & \text{otherwise} \end{cases} \quad (\text{A-9})$$

A.2 SSP Longitude ($\hat{\ell}$)

Since the axial rotation of the earth is fast relative to the annual motion of the earth about the sun, the SSP appears at essentially the same latitude over any given day. Assuming launch time-of-day as completely arbitrary implies that the SSP longitude relative to a ground site meridian is a uniformly distributed random variable. Hence, the probability, $dP(\hat{\ell}|L)$, that the SSP lies within an arc $d\hat{\ell} = \cos L d\ell^*$ given that the SSP is at latitude L , is simply the ratio of $d\hat{\ell}$ to the circumference of the parallel of latitude, $2\pi \cos L$. Expressed functionally this is

$$dP(\hat{\ell}|L) = \frac{d\hat{\ell}}{2\pi \cos L} = f_{\hat{\ell}}(\hat{\ell}|L) d\hat{\ell} \quad (\text{A-10})$$

so that

$$f_{\hat{\ell}}(\hat{\ell}|L) = \frac{1}{2\pi \cos L} \quad |\hat{\ell}| \leq \pi \cos L^{**} \quad (\text{A-11})$$

*See Fig. 1b. Note that $\hat{\ell} = \ell \cos L$.

**This is equivalent to $|\ell| \leq \pi$.

APPENDIX B

GEOMETRICAL RELATIONSHIPS FOR EVALUATING TARGET LIGHTING PROBABILITIES

Evaluation of lighting probabilities involves integration over sections of spherical caps lying within tropical latitudes and defined by constraints on target lighting (Λ) and the beta angle ($|\beta| \leq \beta_c$).^{*} In this appendix expressions for boundaries and intersections of the various caps ($\Lambda, \beta^+, \beta^-$) are given in terms of latitude L and longitude ℓ (relative to the target meridian).

B.1 Cap Boundary Equations

In Fig. (B-1a) a spherical cap with center Q at latitude L_q is shown. The cap boundary is defined by the

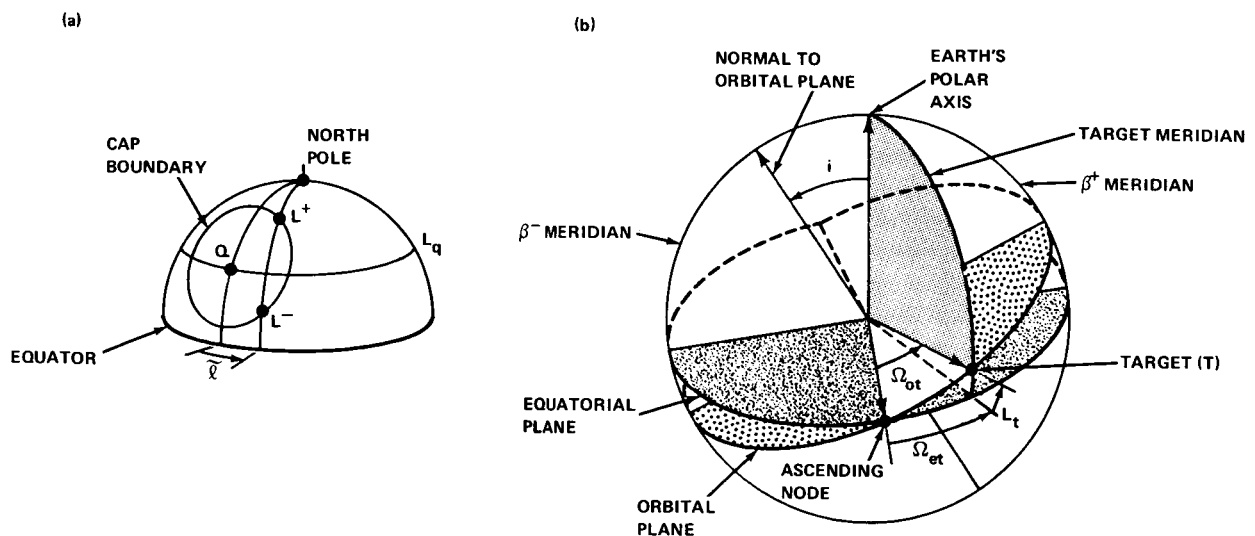


FIGURE (B-1) SPHERICAL CAP GEOMETRY AND RELATIONSHIP OF TARGET MERIDIAN TO ORBITAL PLANE

*See Figs.1 and 2.

intersection with the sphere's surface of a cone with vertex at the geocenter, half angle λ and axis parallel to the local vertical at Q. The cap boundary equations in terms of latitude L , longitude, $\tilde{\ell}$ (relative to the local meridian through Q), and cap parameters (λ, L_q) can be expressed as*

$$c\tilde{\ell} = \frac{c\lambda - sL_q sL}{cL_q cL} \quad (B-1)$$

or as

$$sL = \frac{c\lambda sL_q \pm cL_q c\tilde{\ell} \sqrt{s^2\lambda - s^2\tilde{\ell} c^2L_q}}{1 - s^2\tilde{\ell} c^2L_q} \quad (B-2)$$

where $|\tilde{\ell}| \leq \pi$ and $|L| \leq \pi/2$. The two solutions for L in Eq.(B-2) apply, if the cap does not include the north or south pole, i.e., $|L_q| < \pi/2 - \lambda$. When a cap includes a pole, only one solution for L applies.**

Specific boundary equations for a particular cap can be obtained from Eqs.(B-1) and (B-2) by specifying the cone half angle (λ) and the latitude L_q corresponding to the cap center. These are listed in Table B-1 for the Λ, β^+ and β^- caps. Since Eqs.(B-1) and (B-2) express longitude ($\tilde{\ell}$) relative to the meridian through the cap center, a common reference is adopted, specifically, longitude (ℓ) relative to the target meridian (Λ cap). The corresponding modification of $\tilde{\ell}$ for the β^+ and β^- cap boundary equations is also listed in Table B-1. This can be seen from Fig.(B-1b), which shows the relationship between the target meridian and the orbital plane for a particular orbit inclination (i). The angle Ω_{et} is given by

$$\Omega_{et} = \sin^{-1}(\tan L_t / \tan i) \quad |L_t| \leq i \quad (B-3)$$

*For brevity the trigonometric operations $\sin()$ and $\cos()$ are written as $s()$ and $c()$.

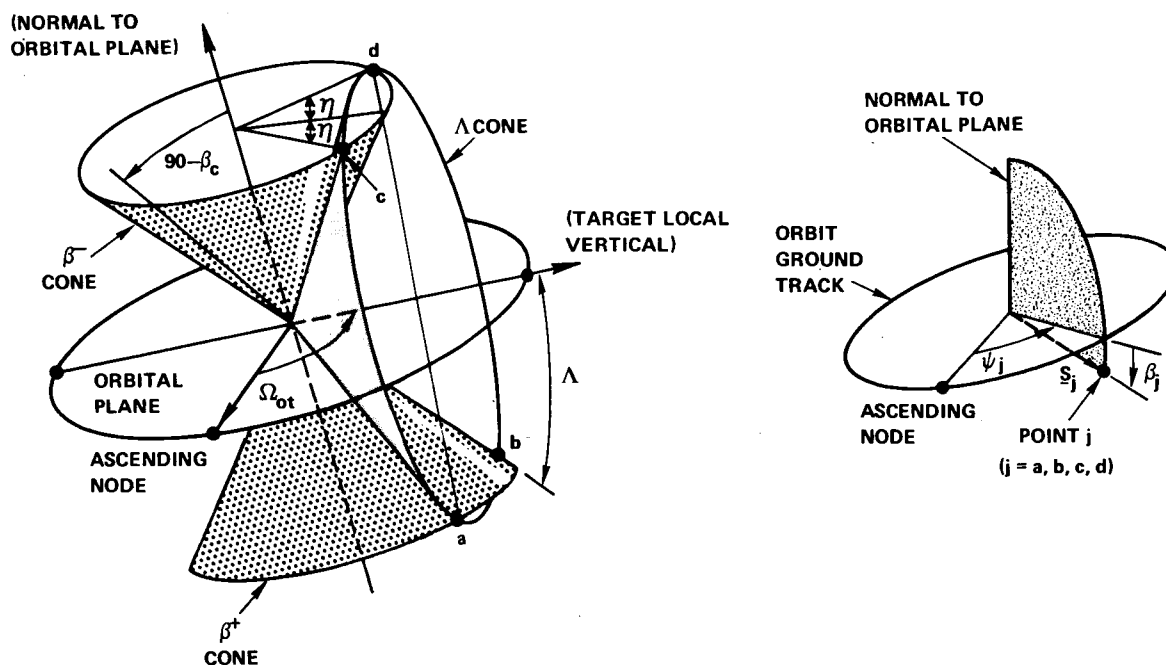
**If $L_q > \pi/2 - \lambda$, the solution for L in Eq.(B-2) with the negative radical applies, but if $L_q < -(\pi/2 - \lambda)$ then the positive radical applies.

TABLE B-1 PARAMETERS FOR $(\Lambda, \beta^+, \beta^-)$ CAP BOUNDARY EQUATIONS

CAP PARAMETER	Λ CAP	β^+ CAP	β^- CAP
L_q	L_t	$-(\pi/2-i)$	$(\pi/2-i)$
λ	Λ	$\pi/2 - \beta_c$	$\pi/2 - \beta_c$
$\bar{\ell}$	ℓ	$\ell - \pi/2 + \Omega_{et}$	$\ell + \pi/2 + \Omega_{et}$

B.2 Cap Intersections

Intersections of the β^+ and β^- caps with the Λ cap occur if $\beta_c \leq \Lambda$. This is illustrated in Fig. (B-2) which shows the terminal points (a,b,c,d) of the intersections on bases of the cones which define the boundaries of the $(\Lambda, \beta^+, \beta^-)$ caps. Location of the points (a,b,c,d) in terms of latitude L and longitude ℓ (relative to the target meridian) can be found by

FIGURE (B-2) GEOMETRY FOR EVALUATING $(\Lambda, \beta^+, \beta^-)$ CAP INTERSECTIONS

determining with appropriate coordinate transformations, the orientation (L_j, ℓ_j) of a unit vector \underline{S}_j ($j = a, b, c, d$) along the local vertical to each point. Based on the geometry in Figs. (B-2) and (B-1b) it can be shown that

$$sL_j = s\psi_j c\beta_j si - s\beta_j ci \quad (B-4)$$

$$\tan \ell_j = \frac{s\psi_j c\beta_j c\Omega_{et} ci + s\beta_j c\Omega_{et} si - c\psi_j c\beta_j s\Omega_{et}}{s\psi_j c\beta_j s\Omega_{et} ci + s\beta_j s\Omega_{et} si + c\psi_j c\beta_j c\Omega_{et}} \quad (B-5)$$

$$j = a, b, c, d$$

where β_j, ψ_j are given in Table B-2,

$$s\Omega_{ot} = sL_t/si \quad |L_t| \leq i \quad (B-6)$$

$$c\eta = c\Lambda/c\beta_c \quad |\beta_c| \leq \Lambda \quad (B-7)$$

$$\psi^+ = \Omega_{ot} + \eta \quad (B-8)$$

$$\psi^- = \Omega_{ot} - \eta \quad (B-9)$$

and Ω_{et} is given by Eq. (B-3).

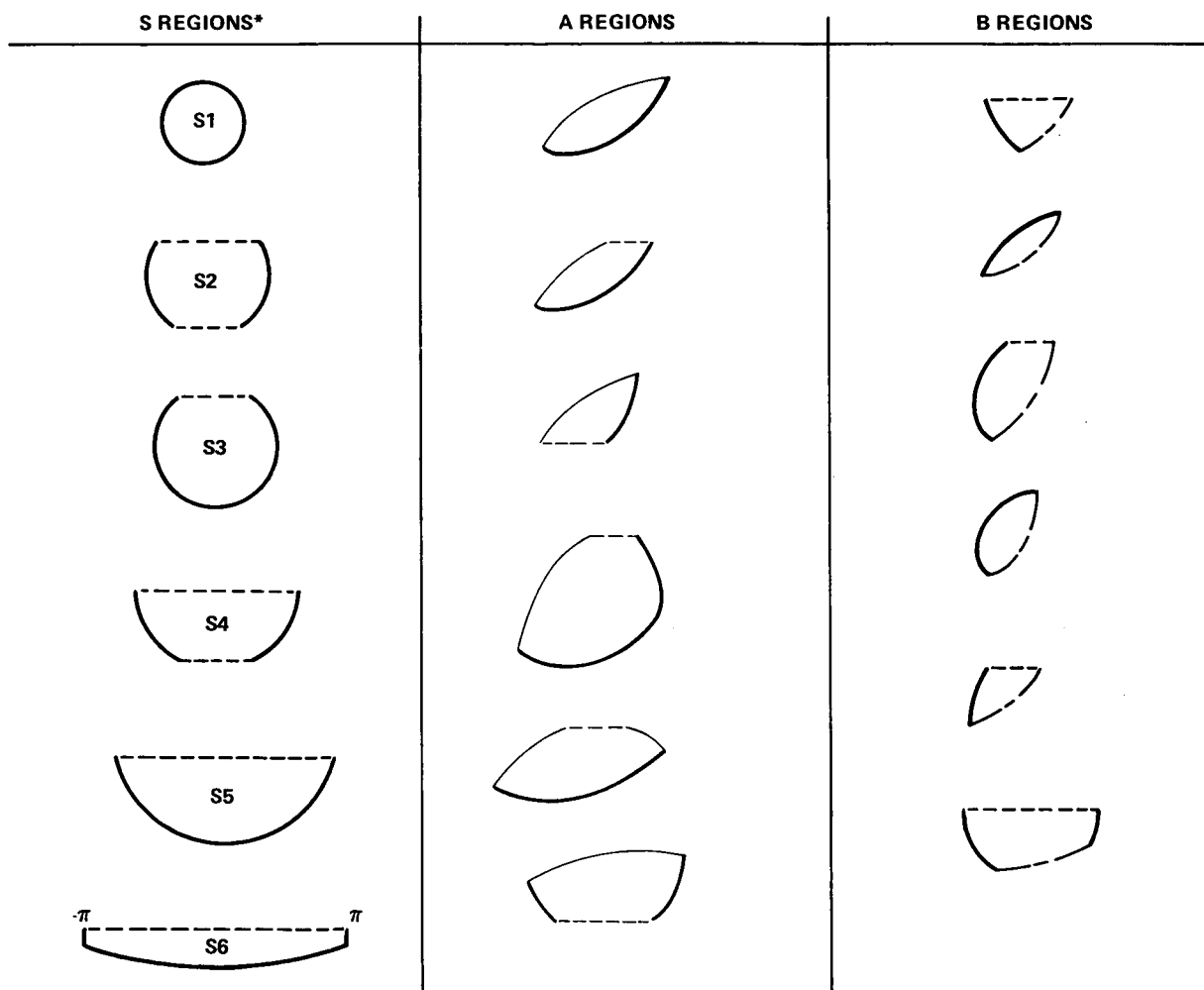
TABLE B-2 (β_j, ψ_j) PARAMETERS FOR $(\Lambda, \beta^+, \beta^-)$ CONE INTERSECTIONS

j	a	b	c	d
β_j	β_c	β_c	$-\beta_c$	$-\beta_c$
ψ_j	ψ^-	ψ^+	ψ^-	ψ^+

B.3 S, A and B Regions

The portion of the Λ cap lying within the tropics represents the region S where the target lighting constraint is satisfied. The form of S may take any of six forms depending on L_t and Λ , as shown in Fig.(B-3). Portions of S excluded by the β constraint represent regions $(A,B)^*$ where the lighting constraint is satisfied, but the β constraint is not. The A and B regions may take many forms, some of which are shown in Fig.(B-3). These correspond to cases when the target sighting occurs at an ascending intersection with latitude L_t . However, the situation is symmetrical for the descending intersection. A special case corresponding to $\beta_c=30^\circ$, $i=50^\circ$ and $\Lambda=60^\circ$ for a target at latitude $L_t=50^\circ$ in the western hemisphere is shown in Fig.(B-4).

*See Fig.2.



*REGIONS S2-S6 CORRESPOND TO NORTHERN
HEMISPHERE TARGETS ($L_t \geq 0$). FOR $L_t < 0$,
S2-S6 ARE INVERTED.

LEGEND:





 Λ CAP BOUNDARY
 β^+ CAP BOUNDARY
 β^- CAP BOUNDARY
 TROPICAL BOUNDARY

FIGURE (B-3) - S REGIONS AND TYPICAL (A,B) REGIONS

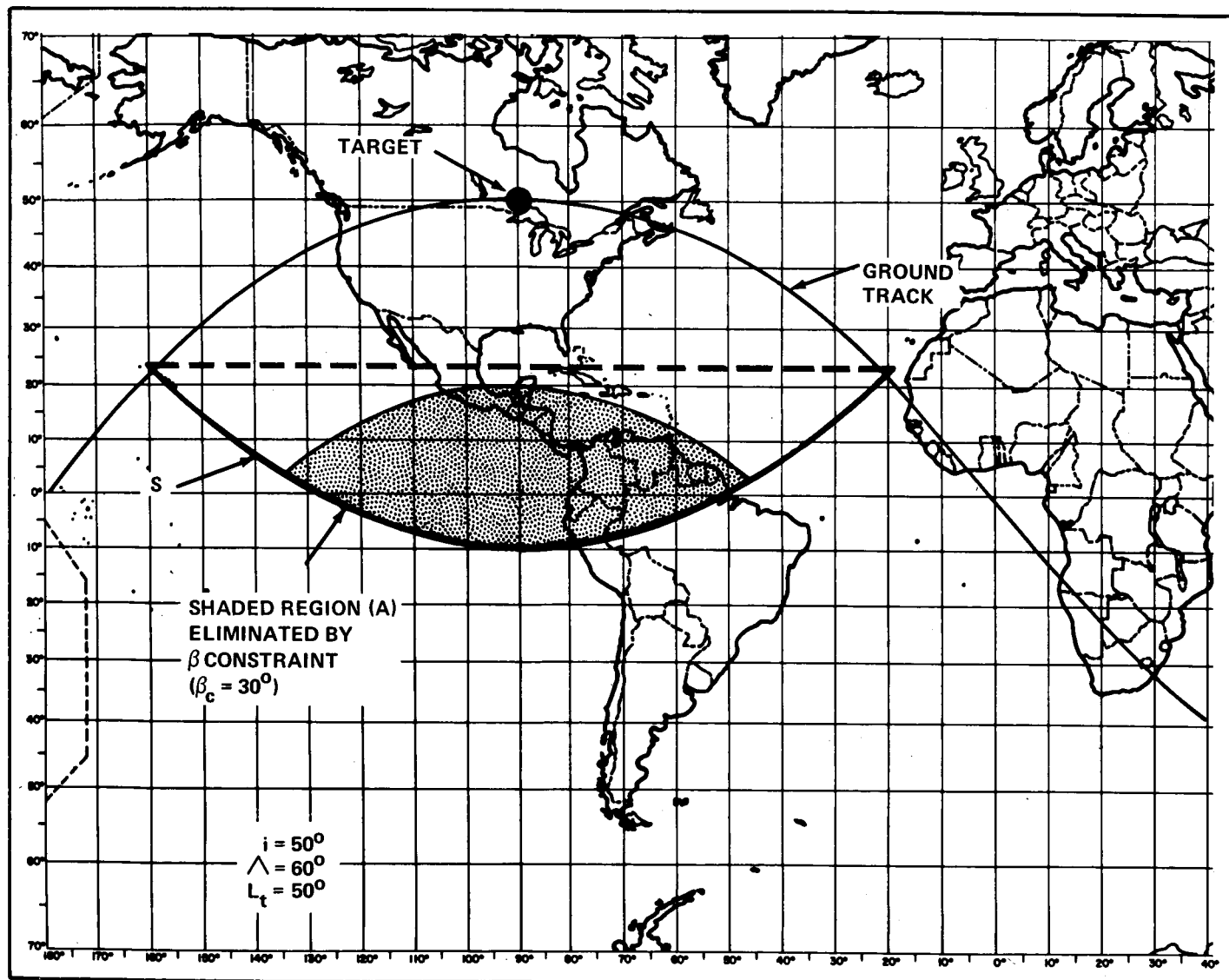


FIGURE (B-4) - TROPICAL REGION SATISFYING TARGET LIGHTING AND β CONSTRAINTS FOR A WESTERN HEMISPHERE TARGET AT 50° N LATITUDE.

BELLCOMM, INC.

955 L'ENFANT PLAZA NORTH, S.W., WASHINGTON, D.C. 20024

COVER SHEET FOR TECHNICAL MEMORANDUM

TITLE-AAP Electrical Power System Capabilities TM- 70-1022-6
in the Earth Resources Mission Mode

DATE- March 23, 1970

FILING CASE NO(S)- 620

AUTHOR(S)- W. W. Hough
B. W. Moss
J. J. Sakolosky

FILING SUBJECT(S) Apollo Applications Program
(ASSIGNED BY AUTHOR(S))- Electrical Power Systems
Earth Resources Experiments

ABSTRACT

During periods of earth resources experimentation, the AAP Cluster attitude will be controlled such that the fixed experiment axis is continuously aligned with the local vertical. In this attitude mode, solar array power output is substantially less than power generated in the usual solar inertial attitude when the arrays are continuously pointed at the sun. The fact that the angle of incidence of the sun's rays is other than zero causes a cosine loss in incident energy plus an increase in the energy reflected from the solar cell coverslides. The attitude is such that a larger average percentage of the arrays powering the Airlock system will be shadowed by the ATM arrays. On the positive side, the average temperature of the arrays will be lower than in the solar inertial mode, and therefore the electrical power output will be higher for a given incident solar flux.

The basic assumptions made for this analysis are that the experiment viewing axis is directly opposite the solar array outward normal, and that this axis is aligned with the local vertical at an orbital midnight and remains aligned until a subsequent midnight. In order to perform earth resources experimentation for one to several consecutive orbits, the system power requirements must be reduced, and/or an operational ground rule that the state-of-charge of each battery must return to 100% during the illuminated portion of each orbit must be set aside. It appears that an acceptable combination of decreased power requirements and permissible battery depth-of-discharge can be chosen such that two, and maybe three consecutive orbits are possible without imposing any severe restrictions on the sun-line/orbit-plane angle, β . Further, if the earth resources targets of interest are all north of 25° latitude (i.e. the U.S.A.), then the power capability can be substantially improved by locating the experiment axes 20-30 degrees away from their assumed location on the plus-Z Cluster axis toward the minus-Y axis.

DISTRIBUTIONCOMPLETE MEMORANDUM TO

CORRESPONDENCE FILES:

OFFICIAL FILE COPY
plus one white copy for each
additional case referenced

TECHNICAL LIBRARY (4)

NASA Headquarters

H. Cohen/MLR
J. H. Disher/MLD
W. B. Evans/MLO
L. K. Fero/MLV
J. P. Field, Jr./MLP
W. H. Hamby/MLO
T. E. Hanes/MLA
T. A. Keegan/MA-2
M. Savage/MLT
W. C. Schneider/ML

Goddard Space Flight Center

J. T. Skladany/713

Langley Research Center

P. R. Kurzhals/AMPD

MSC

R. G. Brown/ES-16
C. N. Crews/KS
W. R. Cunningham/CB
R. E. Durkee/ES-5
R. L. Frost/KS
O. K. Garriott/CB
F. C. Littleton/KM
R. M. Machell/KF
P. S. Miglicco/KS
O. G. Smith/KF
H. E. Whitacre/KM

MSFC

R. M. Aden/S&E-ASTR-E
W. B. Chubb/S&E-ASTR-SGD
J. C. Cody/S&E-ASTN-PLA

COMPLETE MEMORANDUM TOMSFC (continued)

D. N. Counter/S&E-ASTR-MA
C. B. Graff/S&E-ASTR-EP
G. B. Hardy/PM-AA-EI
G. D. Hopson/S&E-ASTN-PL
E. H. Hyde/S&E-ASTN-PF
H. F. Kennel/S&E-ASTR-A
G. F. McDonough/S&E-CSE-A
E. F. Noel/S&E-ASTR-SI
W. C. Patterson/S&E-ASTN-PLA
J. W. Sims/s&E-ASTN-PTA
J. D. Stroud/S&E-ASTR-SE
J. W. Thomas/PM-AA
H. F. Trucks/S&E-ASTN-PTA
J. L. Vaniman/S&E-ASTN-PT
R. D. Wegrich/S&E-CSE-AA
A. P. Woosley/S&E-ASTR-SEC
H. E. Worley/S&E-AERO-DOI

Martin-Marietta

H. S. Nassen/Denver
E. F. Bjoro/Washington
M. S. Imamura/Denver
R. W. Wilson/Denver

McDonnell-Douglas

G. Weber/Eastern Division

Bellcomm

A. P. Boysen
D. R. Hagner
W. G. Heffron
B. T. Howard
J. Z. Menard
J. M. Nervik
I. M. Ross
P. F. Sennewald
J. W. Timko
R. L. Wagner
M. P. Wilson
Departments 2031, 2034 Supervision
Department 1024 File
Division 102
Central Files

BELLCOMM, INC.

955 L'ENFANT PLAZA NORTH, S.W.

WASHINGTON, D. C. 20024

SUBJECT: AAP Electrical Power System
Capabilities in the Earth Resources
Mission Mode - Case 620

DATE: March 23, 1970

FROM: W. W. Hough
B. W. Moss
J. J. Sakolosky

TM-70-1022-6

TECHNICAL MEMORANDUM

I. INTRODUCTION

Electrical power for Apollo Applications Program spacecraft is generated by solar cell arrays. There are two solar array/battery systems; the AM system is mounted on the Workshop and Airlock Module and the ATM system is mounted on the Apollo Telescope Mount. When illuminated, the solar arrays convert incident solar energy into electrical energy. Some of this energy is used to power system loads and the rest is stored in batteries. Spacecraft power is supplied by these batteries when the array is not illuminated. Although they are the same in principal, the two systems are different in design and possess different operating characteristics. Although it is now planned to operate the systems in parallel for power sharing under nominal conditions, the systems have been treated separately in the past and that practice will be continued in this paper.

In the nominal AAP attitude mode, which is known as solar inertial, the vehicle is stabilized so that the arrays are pointed directly at the sun throughout the entire sunlit portion of the orbit, thus the per-orbit energy output of the arrays is maximized. Several earth-resources experiments have been proposed for AAP which, when operating, require a different attitude mode. In the earth-resources mission mode, the viewing axes of the spacecraft-fixed experiments must be continually aligned with the local vertical to within some small angular tolerance. These experiments will, in the main, perform observations of the sunlit earth and will therefore be fixed to the vehicle on the side opposite the active face of the arrays. The array energy output will therefore be reduced, but not eliminated.

The objective of the work reported in this paper has been to accurately determine the capabilities of the two AAP electrical power systems in the earth-resources mission mode.

Taking as a base the current AAP Cluster configuration as shown in Figure 1, system capabilities further depend on:

- a) the attitude profile,
 - b) the sun-line/orbit plane angle, β ,
 - c) the position of the experiment viewing axis relative to the solar arrays,
 - d) the time into the mission that the experiments are performed,
- and e) the maximum permissible depth of discharge of the batteries.

With all of the above specified, the number of consecutive experiment passes that are possible from the power standpoint can be determined if we also specify:

- f) the estimated average power requirements on both systems independent of the experiments
- and g) the power source for the experiments themselves (AM or ATM) and their power requirement.

II. ATTITUDE PROFILE

In Reference 1, three possible attitude profiles are discussed which meet the stated requirements of the earth resources experiments. They are alike in that all position the experiment viewing axes along the local vertical when the target (sub-spacecraft point) is properly illuminated by the sun, and in that the vehicle X-axis (roll axis) is kept in the orbital plane parallel to the velocity vector. They differ in how this attitude is acquired, starting from the solar inertial attitude..

It is shown in Reference 1 that to minimize the expense of attitude maneuvers while maximizing experiment opportunities in sunlight, an attitude profile known as midnight acquisition must be used. This profile begins with a vehicle roll maneuver between orbital sunset and orbital midnight to place the experiment viewing axis in the orbital plane such that the experiments will look directly down at midnight. At midnight, the orbital rate is induced about the normal to the orbital plane. The experiment axis then remains along the local vertical for some integral number of midnight-to-midnight orbits. After the last experimental pass, the opposite of the acquisition sequence is carried out; the orbital rate is removed at midnight and the vehicle is rolled back to solar inertial before orbital sunrise.

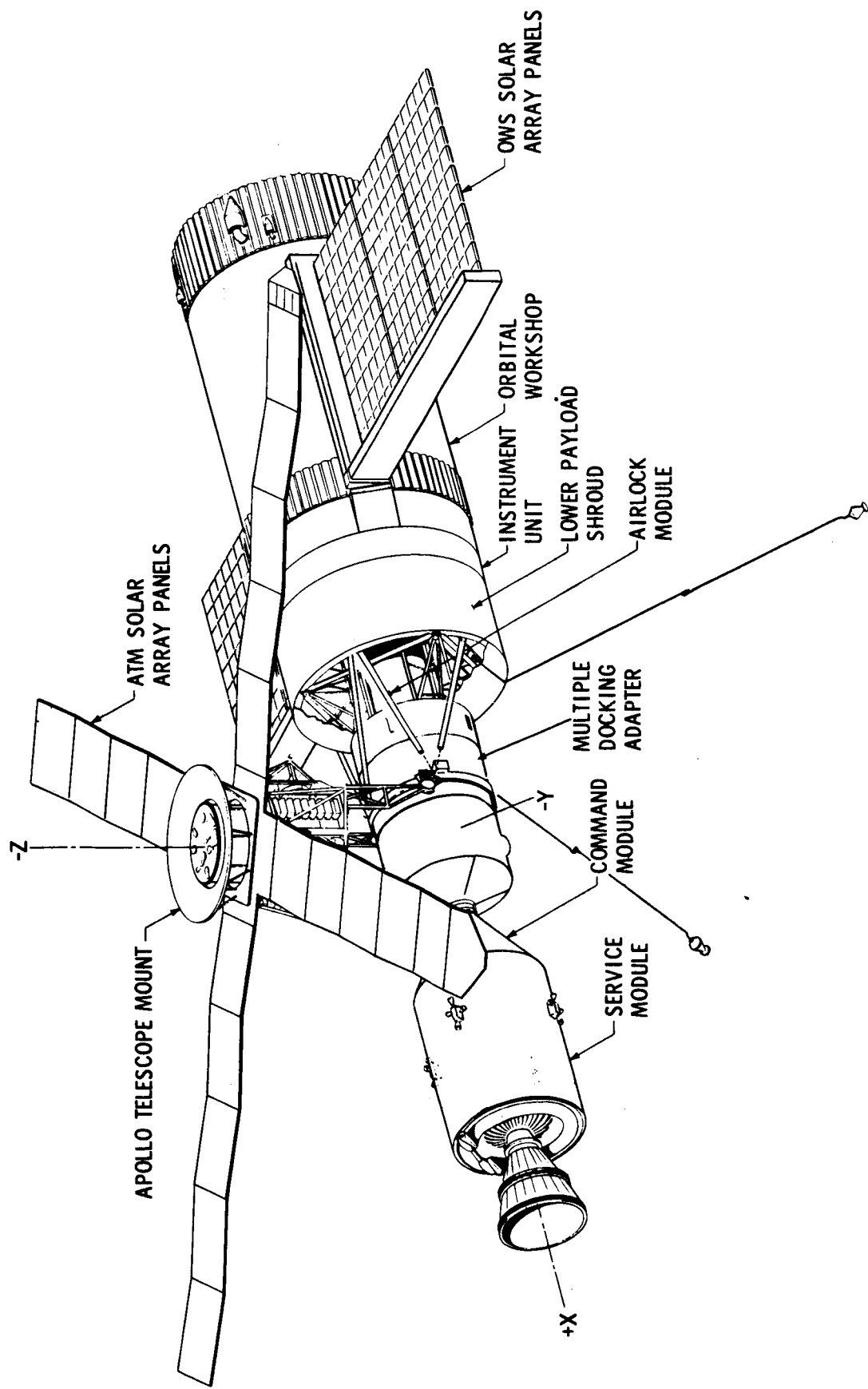


FIGURE 1 - AAP CLUSTER

The midnight acquisition profile has been adopted for this study. In the Baseline Reference Mission document (Ref. 2) the specification of the orientation of the Cluster in the solar inertial mode is such that the plus-X axis (CSM end) is in the direction of the velocity vector at orbital noon. The CSM will therefore lag at midnight, and the minus-X (OWS end) will be in the direction of the velocity vector throughout the earth resources mission mode. If either of the other two acquisition modes, noon acquisition or local target acquisition, discussed in Reference 1 are used, then the opposite is the case - the leading end in the earth resources mode will be the CSM end.

III. EXPERIMENT POSITION

The outward normals to the solar arrays of the AAP Cluster are all in the direction of the minus-Z Cluster axis. In the prior wet Workshop configuration, which was to use a different attitude profile and had movable solar arrays, the viewing axis of the multiband photography experiment was optimally located along the Cluster plus-Z axis. This experiment position has remained for all proposed earth resources experiments in the dry Workshop configuration. From electrical power and thermal control standpoints, the plus-Z experiment position is not necessarily the optimum in the attitude mode just described. The optimum depends on the range of target latitudes, the accessibility to these targets, and the direction of flight.

In this study, the plus-Z experiment position was adopted. In a later section optimal, or at least more favorable, positioning will be discussed.

IV. INSTANTANEOUS SOLAR ARRAY POWER OUTPUT

The instantaneous solar array power output in the earth resources mission mode, P_{SA} , can be evaluated by the following equation:

$$P_{SA} = \cos \lambda \cdot P_N(T) \cdot (1-L_R) \cdot (1-L_D) \cdot (1-L_S) \quad (1)$$

Each term of (1) is discussed in detail in the following paragraphs.

$\cos \lambda$:

λ is the angle of solar incidence; that is the angle between the vector to the sun and the outward normal to the solar array, which is the minus-Z Cluster axis. The incident solar power per unit area of the array is directly proportional to the cosine of λ . With the experiments along the plus-Z, the solar array normal will be coincident with the local vertical. In this attitude the cosine of λ is the product of the cosines of the minimum angle between the sun vector and the orbit plane, β , and the orbit position angle, η .

$$\cos \lambda = \cos \beta \cos \eta \quad (2)$$

These two angles are defined in Reference 3 and shown in Figure 2. β is positive if the sub-orbital-noon point is south of the sub-solar point.* (β as shown is negative.) η measures the angular position in the orbit of the spacecraft relative to orbital noon, and is positive (as shown) in the direction of the orbital velocity vector. Both β and η are time varying, and neither vary linearly. β varies due to the earth's rotation about the sun and orbital regression. Figure 3 is the time history of β for a mission launched at 3:00 p.m. EST on July 15 to a 235 NM, 50° inclination orbit. The limits on β are plus and minus the sum of the orbital inclination and the angle between the ecliptic and equatorial planes; for a 50° inclination, $-73^\circ 27' \leq \beta \leq +73^\circ 27'$. A pass of the satellite from one orbital noon to the next is equivalent to a 360° increase in η . The time rate of change of η is not constant, again because of orbital regression and the earth's rotation about the sun. In Appendix A, however, an expression for the average noon-to-noon satellite period, $T_{S \text{ AVG}}$, is derived, and that period has been used in this study in a linear approximation of the relation between η and time.

$$\dot{\eta} \approx 2\pi/T_{S \text{ AVG}} \quad \text{rad/hr} \quad (3)$$

With the assumed location of the experiment viewing axes along the Cluster plus-Z axis, the effect of β on power system capabilities is independent of the sign of β in the case of the ATM, and almost independent in the case of the AM. The slight dependency of the AM capabilities on the sign of β is due to nonsymmetric shadowing of the AM arrays, which is in turn

*This definition of positive β is consistent with the definition contained in the Baseline Reference Mission (Ref. 2), but opposite to the definition of Reference 3.

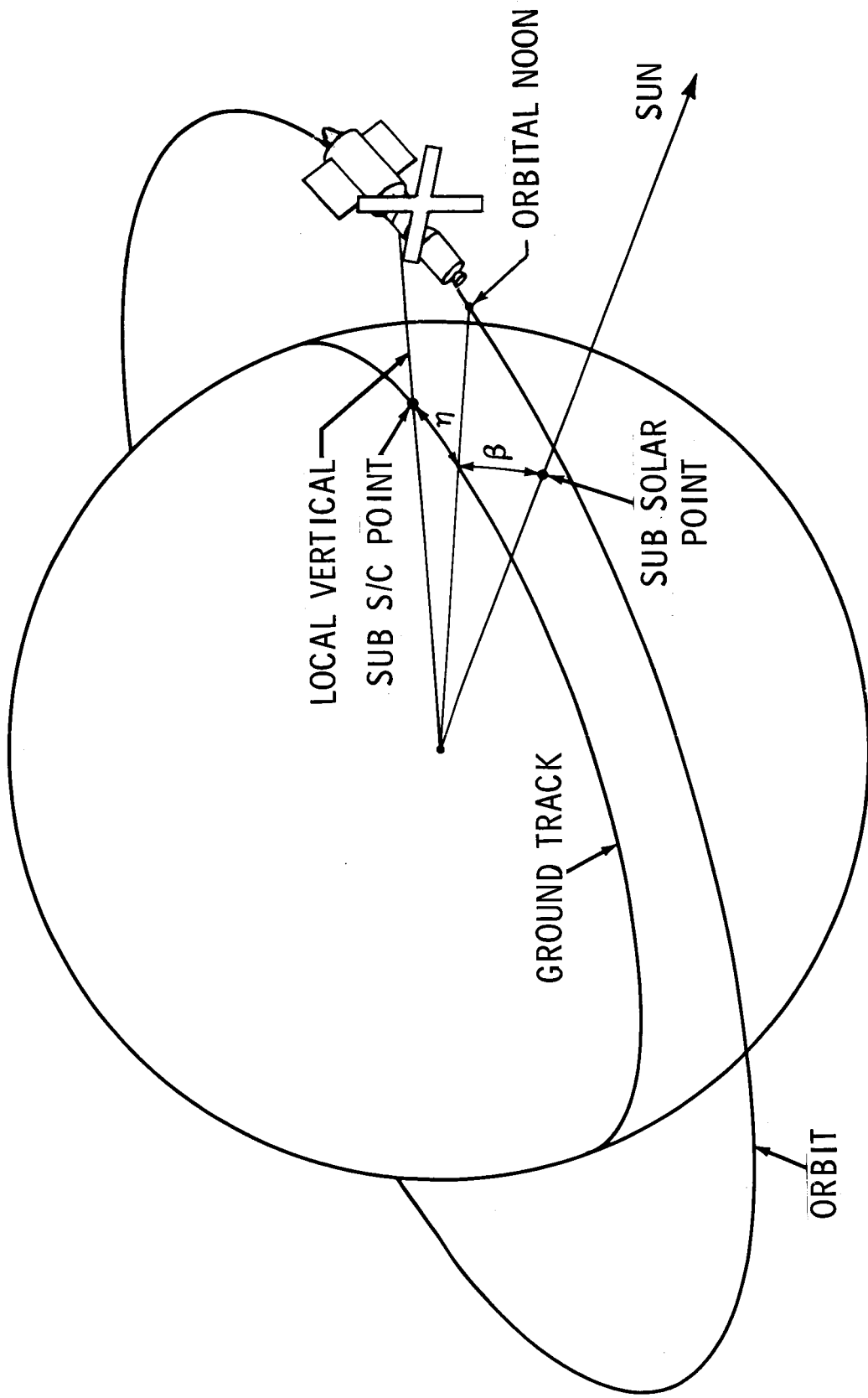


FIGURE 2 - ORBITAL GEOMETRY

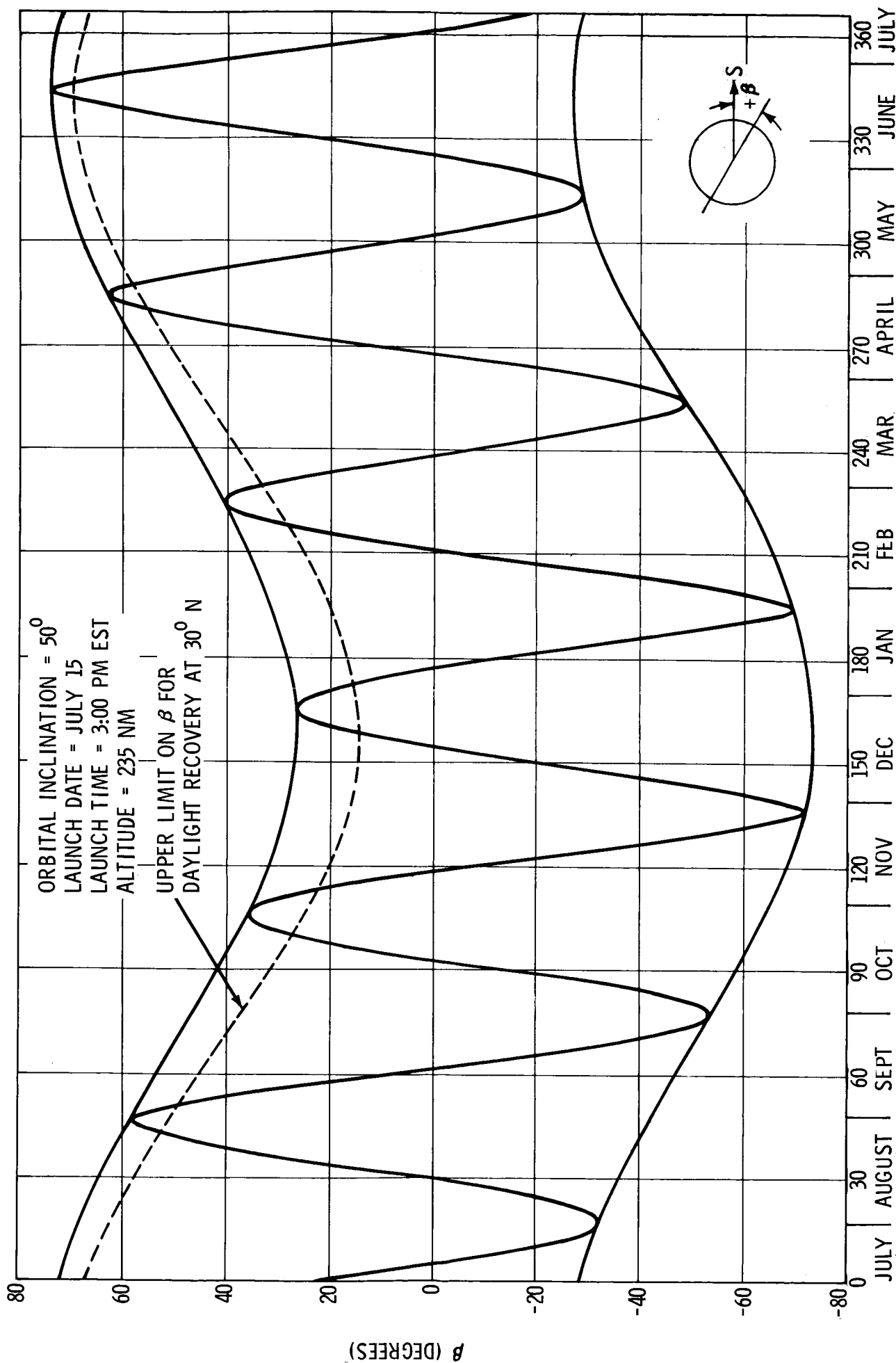


FIGURE 3 - BETA HISTORY

due to the offset of the arrays. However, the difference is undiscernable in plots of AM capabilities vs β . Therefore only positive values of β are used in plots of capabilities, with the understanding that the results apply equally well for negative β of the same absolute values.

It can be seen from equation (2) that $\cos \lambda$ will be negative whenever $\cos \eta$ is negative as $\cos \beta$ is always positive. However, P_{SA} in equation (1) can never be negative, but will be zero when $\cos \eta$ is zero or negative. In other words, the array will not see the sun and will not produce power when η is between 90° and 270° in the earth resources mission mode. Therefore, we need consider solar array output only when η is between -90° and $+90^\circ$.

$P_N(T)$:

$P_N(T)$ is the temperature dependent power output of the full array at normal solar incidence, air mass zero, and beginning of life. Solar arrays converting incident radiant energy into electrical energy are predictably affected by the temperature of the array which is itself affected by the incident radiant energy. It is well-known that the open-circuit voltage is an inverse function of temperature and is essentially unaffected by incident intensity while short-circuit current is a linear function of incident intensity and is essentially unaffected by temperature. The maximum power of an array at any given intensity, then, is an inverse function of temperature. Various sources give maximum power temperature coefficients ranging from -0.42% per $^\circ\text{C}$ to -0.485% per $^\circ\text{C}$. (-0.234% per $^\circ\text{F}$ to -0.27% per $^\circ\text{F}$.)

The two solar array systems in AAP both use identical solar cells arranged as modules to provide the desired power levels at the desired voltage levels. The cells are $2\text{ cm} \times 2\text{ cm}$ N on P silicon cells with a nominal base resistivity of 10 ohm-cm and an active area of 3.8 cm^2 . The conversion efficiency is taken as 10 per cent. From this, the nominal power output of each cell with incident normal solar power of 140 mw/cm^2 can be determined.

$$P_{\text{cell}} = 140 \times 3.8 \times 0.10 = 53.2\text{ mw/cell}$$

The AM array consists of 240 modules of 1136 cells each for a total of 272640 cells and the ATM array consists of 360 modules of 684 cells each for a total of 246240 cells. So,

$$P_{AM} = 53.2 \times 10^{-3} \times 272640 = 14504 \text{ w}$$

$$P_{ATM} = 53.2 \times 10^{-3} \times 246240 = 13100 \text{ w}$$

These nominal total array outputs are based on the cells being at a temperature of 30°C (86°F) and do not include losses for assembly into an array. The losses are summarized in the following table

	AM	ATM
Coverslides and adhesive	2.0%	2.0%
Cell mismatch	3.0	3.0
Diode loss (0.8v)	1.4	2.0
Line loss (1.0v)	1.75	2.5
	<hr/>	<hr/>
Total loss	8.15%	9.5%

The array power capabilities at 86°F are therefore

$$P_{AM} = 14504 (1-0.0815) = 13322 \text{ w}$$

$$P_{ATM} = 13100 (1-0.095) = 11855 \text{ w}$$

Taking the temperature coefficient as -0.465% per °C, or -.258% per °F, we can write the expressions for $P_N(T)$. For the AM system:

$$P_N(T) = 13322 (1-.00258 (T-86)) \quad (4-a)$$

BELLCOMM, INC.

and for the ATM system:

$$P_N(T) = 11855 (1 - .00258 (T - 86)) \quad (4-b)$$

where T is the temperature of the array in degrees F.

When these expressions are evaluated at the rated operating temperatures of the two systems, the results are in agreement with the MSFC published rated power capabilities to within 0.14%.

T:

To make use of the expressions for $P_N(T)$ just developed, an analysis of the array temperature profile is required. Several analyses of array temperature profiles for different attitude profiles have been performed by J. W. Powers, including the earth resources mission mode under consideration here. His work is reported in Reference 4. He modeled the array as a single two surface node with the appropriate absorptivity and emissivity on each face, and assumed these properties were identical for the two arrays. The array planar surfaces receive time varying direct solar, earth reflected solar, and earth emitted IR thermal fluxes as functions of altitude (taken as the baseline 235 NM circular orbit), attitude, and position angles relative to the sun, β and η . The incident flux profile together with the array physical properties were used to determine the array temperature profile. Power's results for the earth resources mission mode are shown in Figure 4 for the pertinent range of η and for four β angles.

The curves of Figure 4 can be duplicated to within a few percent with a fairly simple curve-fit equation, which was developed to ease computational effort within the computer program that predicts instantaneous solar array power output. Further, interpolation for different β angles is unnecessary. This expression is

$$T = A + B \sin \left(180^\circ \cdot \frac{\eta + 35 - C}{125 - C} \right) + D \quad (5)$$

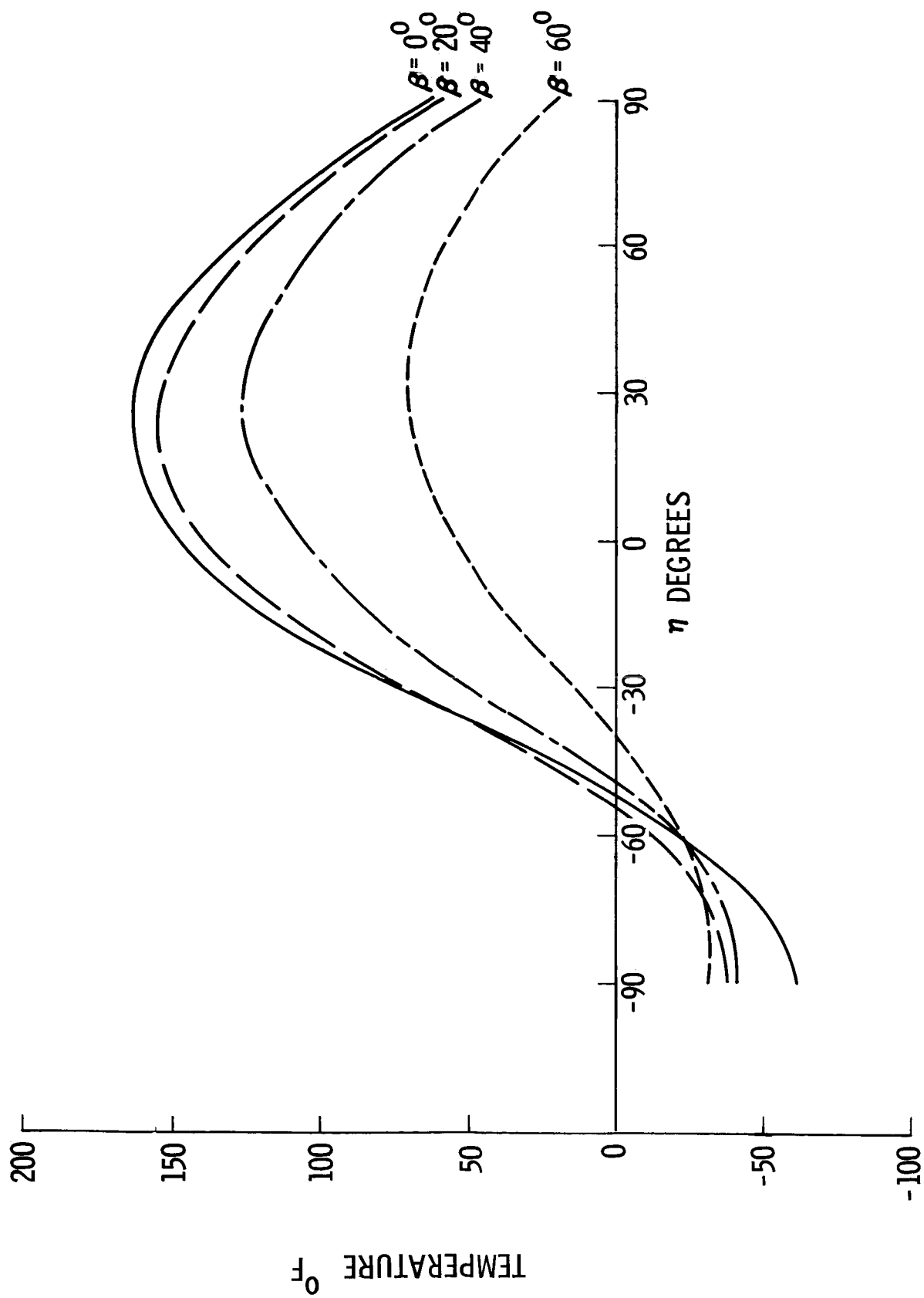


FIGURE 4 - SOLAR ARRAY TEMPERATURE VS. ORBITAL POSITION

where

$$A = 59 - .00088846 \beta^{2.617}$$

$$B = 104 - .02144 \beta^{1.907}$$

$$C = .00022212 \beta^{2.617}$$

$$D = \begin{cases} E + F, & \eta \leq +15^\circ \\ 0, & \eta > +15^\circ \end{cases}$$

where

$$E = -.09808 (60-\beta)^{1.081}$$

$$F = 0.14517 (60-\beta)^{1.107} \sin \left(180^\circ \cdot \frac{\eta+40}{70} \right)$$

When using these equations, η must be maintained in the range of $-90^\circ \leq \eta \leq +90^\circ$ (use of 280° rather than -80° will give an erroneous result), and β must be positive. Both must be input in degrees. The temperature, T , will be in degrees F.

$1-L_R$:

Because of reflection of incident light off the solar cell coverslide and because of transmission loss within the coverslide, the intensity of light reaching the surface of the cell is decreased from that reaching the coverslide. The transmission loss is assumed to be a constant 2%. The reflective loss is a function of the angle of incidence and the index of refraction of the coverslide material. In Reference 5, the following expression was developed for determination of the magnitude of the reflective loss:

$$\text{Percent loss} = 100\% \cdot \frac{\sin^2(\lambda-\chi)}{\sin^2(\lambda+\chi)} \left[1 + \frac{\cos^2(\lambda+\chi)}{\cos^2(\lambda-\chi)} \right] \quad (6)$$

where λ is the angle of incidence and χ is the angle of refraction. λ and χ are related to the index of refraction of the coverslide material by Snell's law:

$$\frac{\sin \lambda}{\sin \chi} = \text{index of refraction}$$

For the fused silica coverslides used in AAP, the index of refraction averages 1.47 over the wave lengths of interest.

At normal incidence, equation (6) reduces through small angle approximations to

$$\text{Percent loss at normal incidence} = 100\% \cdot \frac{(\text{index of refraction} - 1)^2}{(\text{index of refraction} + 1)^2} \quad (7)$$

which, when evaluated, gives a 3.63% loss. Applying this loss to (4a) and (4b) gives rated solar array power outputs at normal incidence that would be lower than the MSFC published capabilities by approximately the amount of the loss. Presumably, therefore, the loss due to reflection at normal incidence is already included in (4a) and (4b) through the assumed conversion efficiency of 10%. This presumption is supported by the fact that 10 ohm-cm N on P silicon cells characteristically have a conversion efficiency of approximately 10.5%. In this study, therefore, the degraded transmittance of the coverslide due to reflection at the cover-slide-space interface has been normalized to 100% at normal incidence. The normalized transmittance, 1-reflective loss ($1-L_R$), in percent is

$$100\% (1-L_R) = \frac{100\% - \text{percent loss by (6)}}{100\% - \text{percent loss at normal incidence by (7)}} \quad (8)$$

The normalized transmittance is plotted in Figure 5 vs the angle of incidence.

$1-L_D$:

The solar-to-electrical power conversion efficiency of solar cells degrades due to environmental radiation. The purpose of the coverslides is to minimize this degradation, but they do not eliminate it. The time dependent degradation used in AAP has been legislated at 1/2% per month. The term L_D in equation

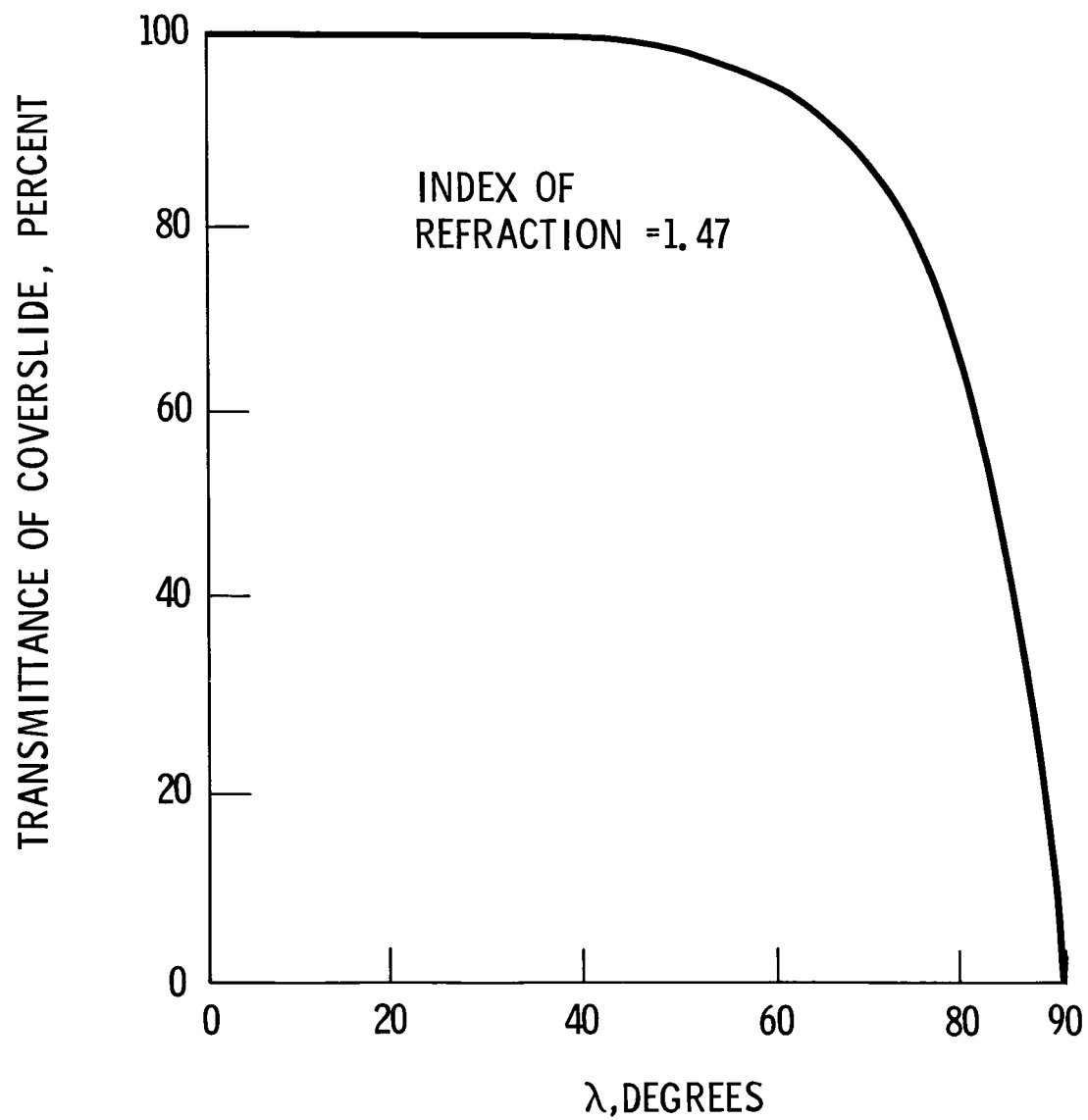


FIGURE 5 - PERCENT INCIDENT LIGHT TRANSMITTED THROUGH COVERSLIDE (NORMALIZED TO 100% AT NORMAL INCIDENCE)

(1) is therefore simply $0.005 d$ where d is the time into the mission in months.

$$1-L_D = 1 - 0.005 d \quad (9)$$

$1-L_S$:

This term accounts for the degradation in power output of the AM solar arrays due to shading by the ATM array.

$$L_S = \frac{\text{Shaded Area of Solar Array}}{\text{Total Area of Solar Array}} \quad (10)$$

L_S is equal to zero when calculating power at the ATM array since this array is never shaded during the portion of the orbit where $\cos \lambda$ is positive.

Shading of the AM arrays by the ATM array is a function of the sun angle, β , and the orbital position angle, η . A computer program (documented in Reference 6) which calculates shading of the AM arrays has been used to obtain the data required for this study. This program is used as a subroutine in the more general computer program used to calculate instantaneous power produced by the solar arrays.

Figure 6A illustrates the ratio of unshaded area to the total area (i.e., $1-L_S$) of the AM solar arrays as a function of η for β angles of 0° , 20° , 40° , and 60° . Figure 6B shows the same ratio for β angles of 0° , -20° , -40° , and -60° . The sign of β makes a difference because of the difference in the Z location of the two AM panels (see Figure 1). These data apply for the midnight acquisition attitude profile where the CSM is the lagging vehicle and shading occurs in the later part of the sunlit portion of the orbit, roughly between η angles of -5° and $+80^\circ$ for medium and small sun angles. For large β angles ($\beta > 50^\circ$), the portion of the orbit during which shading occurs is considerably less.

If an attitude profile is used that results in the opposite vehicle orientation, that is with the CSM the leading vehicle, the array shadowing will occur in the opposite half of the orbit. Shadowing data for this case can be taken directly from Figures 6 by reversing the signs on the η scale and the β angle.

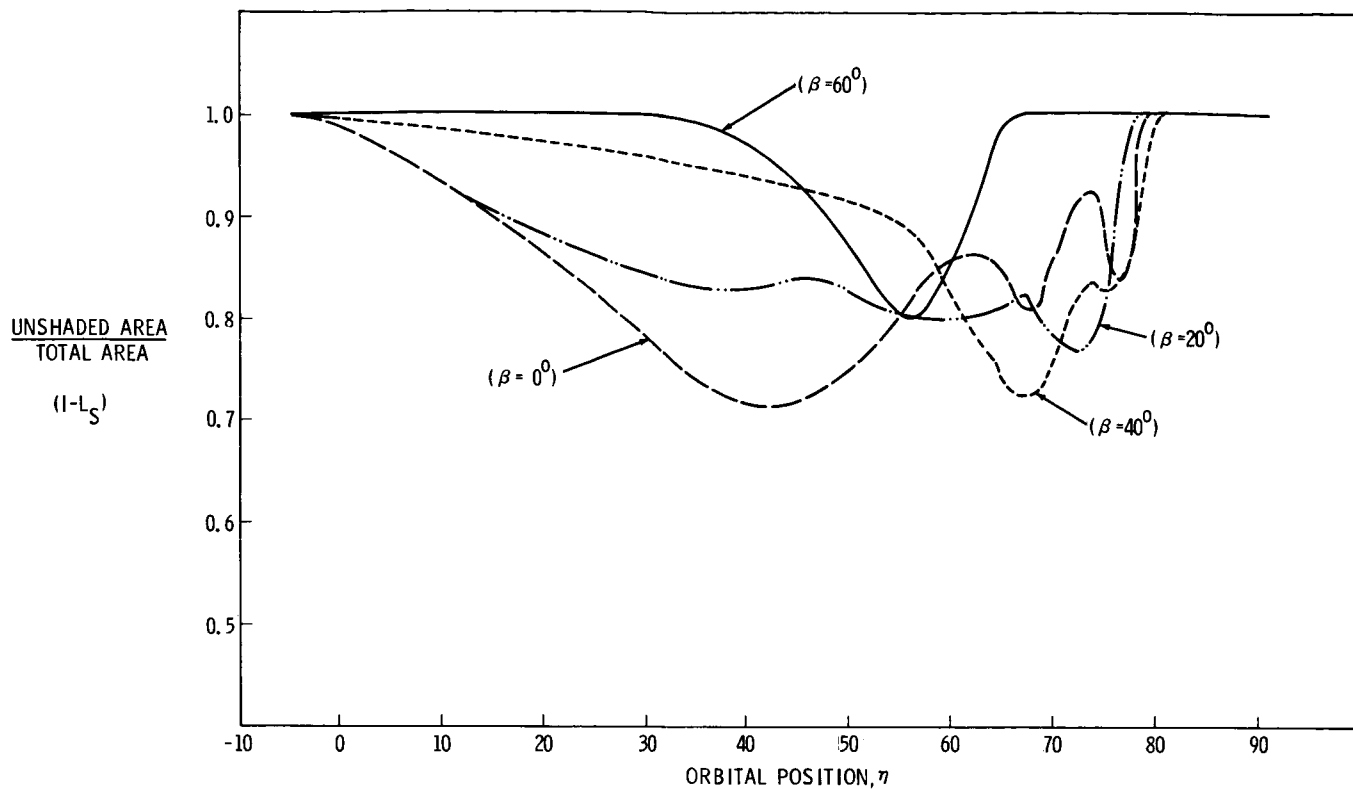


FIGURE 6A - SUN ANGLES GREATER THAN OR EQUAL TO ZERO

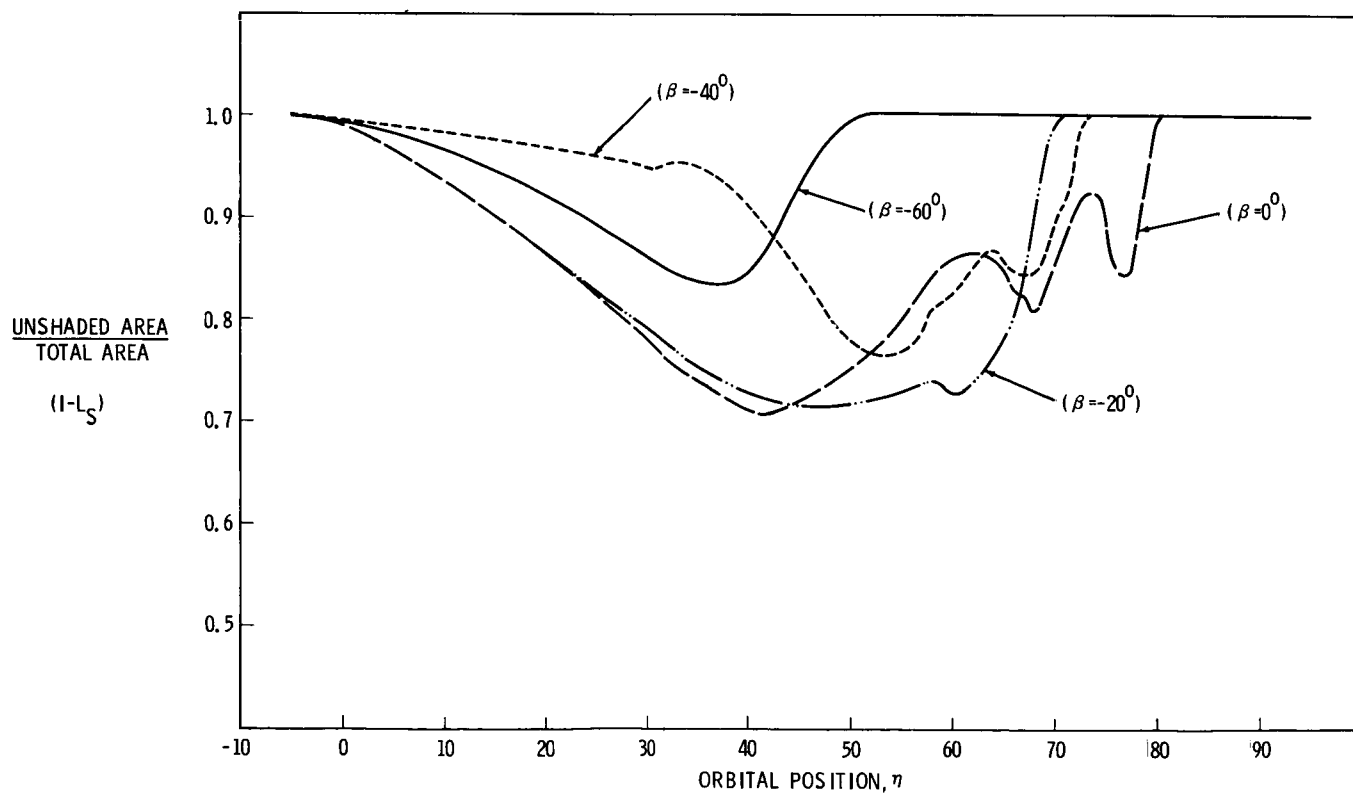


FIGURE 6B - SUN ANGLES LESS THAN OR EQUAL TO ZERO

FIGURE 6 - RATIO OF UNSHADED AREA TO TOTAL AREA OF AM SOLAR ARRAYS AS A FUNCTION OF SUN ANGLE AND ORBITAL POSITION.

Notice from Figure 6 that there is no readily predictable or consistent pattern that the shaded area follows as a function of β angle. This results from the geometry of the situation. The cruciform pattern of the ATM solar array causes a sequential shading of the AM panels as the Cluster changes its orbital position. The unequal displacements of the two AM panels from the plane of the ATM array also add to the effect of non-symmetric shading patterns. As can be seen from Figure 6, worst case shading occurs for small β angles. The maximum shading of the AM arrays occurs for orbital position angles between 40° and 50° . At this point in the orbit, approximately 30% of the total area of the AM arrays is shaded.

V. SOLAR ARRAY ENERGY OUTPUT

The energy output of the solar array between the time t_1 and the time t_2 is simply the integral of (1) over the time increment

$$W_{SA} = \int_{t_1}^{t_2} P_{SA} dt \quad (11)$$

Since time and orbit position angle, η , are related approximately by a constant given by (3),

$$\eta = \int \dot{\eta} dt \approx \frac{2\pi}{T_{S_{AVG}}} t \quad (12)$$

we can express the energy output of the array as:

$$W_{SA} = \frac{T_{S_{AVG}}}{2\pi} \int_{\eta_1}^{\eta_2} P_{SA} d\eta \quad (13)$$

In the earth resources mission mode, the array sees the sun only between orbital 6 a.m. and orbital 6 p.m. The energy output in a single orbit is

$$W_{SA0} = \frac{T_{S_{AVG}}}{2\pi} \int_{-\pi/2}^{\pi/2} P_{SA} d\eta \quad (14)$$

Because of the complexities introduced into P_{SA} by the temperature, time into the mission, coverslide reflection, and array shadowing, (14) must be integrated numerically. A rough approximation for the per-orbit energy output, which is useful in determining trends for different β 's or different attitude profiles, can be made by neglecting all terms of (1) except $P_N(T) \cos \lambda$ and treating T as a constant. Then

$$W_{SA0} \approx \frac{T_{S_{AVG}}}{\pi} P_N(T) \cos \beta \quad (15)$$

The accuracy of the result by (15) depends strongly on the assumed constant temperature, T . With T at 100°F and $\beta=0$, (15) gives a result 4.8% higher than the more accurate ATM energy output predicted by (14).

VI. POWER SYSTEM ENERGY PROFILE

The total electrical energy used (and lost through inefficiencies) during the mission cannot be greater than the total energy output of the solar arrays plus the initial stored energy in the batteries. Further, to insure continuous capability to supply loads, the stored energy must at no time reach zero. The SWS will be launched with all batteries fully charged. Once the solar inertial attitude is acquired, normal operating conditions will permit full recharge of all batteries during the sunlit portion of the orbit, and depth of discharge (DOD) of the batteries during the dark portion of the orbit will not normally be beyond 30%. Higher loads or lower solar array output are occasionally acceptable as long as the stored energy does not vanish. Subsequent to the occurrence of such conditions, the batteries must be allowed to recover so the long-term energy balance requirement will be met.

The earth resources mission mode is an example of a condition where the solar array output is substantially below the output in the solar inertial mode. In this attitude, it is unlikely that energy can be balanced on an orbit-to-orbit basis. That is, it is likely that the batteries will not return to 100% state of charge each orbit. In this section, the method for determination of the battery state of charge after some number of orbits in the earth resources mode is given. From this, we can state the capabilities of the power systems during earth resources experimentation.

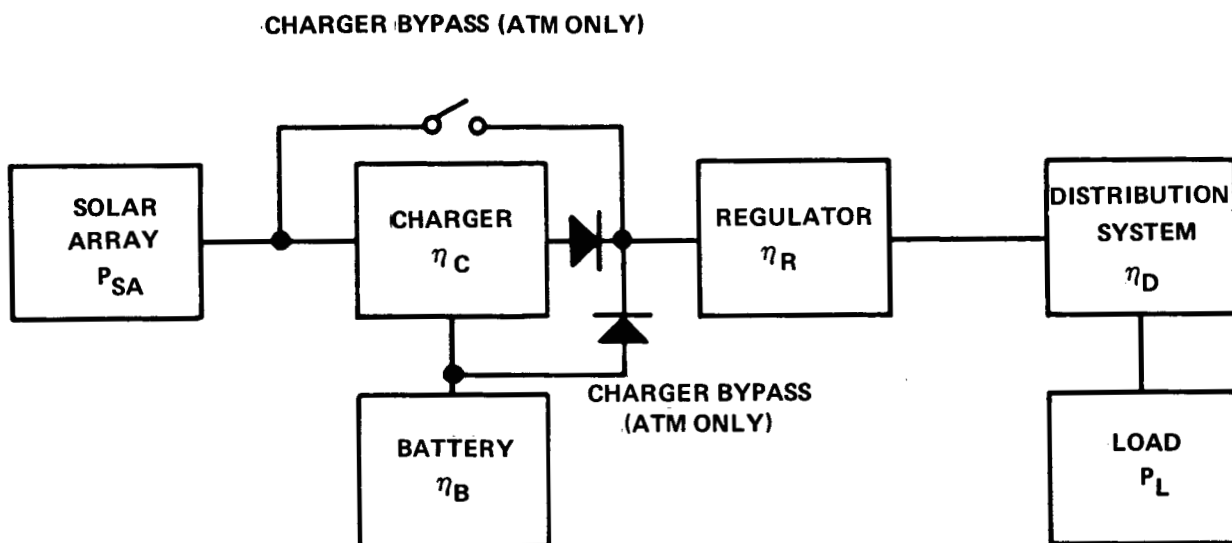


FIGURE 7 - SOLAR ARRAY/BATTERY ELECTRICAL POWER SYSTEM

Figure 7 is a simplified schematic of a solar array/battery power system. P_{SA} is the instantaneous solar array output, and P_L is the instantaneous load on the system. When the load, increased by the power lost in the distribution system and the regulator, is greater than the array output, there is over a time Δt a net loss of energy from the battery.

$$W_{LOSS} = \left(\frac{P_L}{\eta_R \eta_D} - P_{SA} \right) \Delta t \quad (16)$$

If the array output exceeds the demand, there is a gain in energy in the battery,

$$W_{GAIN} = \eta_C \eta_B \left(P_{SA} - \frac{P_L}{\eta_R \eta_D} \right) \Delta t \quad (17)$$

where η_C and η_B account for the power lost in the charger and battery. The definitions and values of the efficiencies for the two systems are given in the following table.

	AM	ATM
η_C = charger efficiency	.95	.96
η_B = battery charge utilization or watt hour efficiency	.677	.70
η_D = distribution efficiency	.826	.877
η_R = regulator efficiency	.95	.875

The value of the distribution efficiency for the AM accounts for the fact that power is supplied to the load from either source through the charger. This is not the case in the ATM.

The change in battery state of charge over the time Δt is obtained by dividing the change in energy, given by (16) and (17), by the total energy capacity of the battery system, W_{CAP} . The total capacity of the eight AM batteries is taken as 9108 watt-hours and the eighteen ATM batteries have a total capacity of 9936 watt-hours.

To track the battery state of charge, it is first necessary to determine whether energy is being gained or lost, but this simply entails picking the positive result of (16) or (17). That result is then divided by the capacity and appropriately added to or subtracted from the state-of-charge at the beginning of the period Δt . Continuing this process over time will give a time profile of the battery state of charge. The only restriction is that the state of charge must be within the limits $0 \leq SOC \leq 1$ (i.e.: $0 \leq SOC \leq 100\%$).

In the earth resources mode, the entire state-of-charge profile is not of as much interest as the minimum state of charge that occurs. Specification of a minimum allowable SOC is needed before the capability of the system to support the experiment mode can be stated.

If the system load is constant, or at least repetitive from orbit to orbit, the minimum SOC can be calculated without calculating the entire SOC profile. This can be best explained with the help of Figure 8, which is illustrative of a two-orbit earth resources sequence. On Figure 8, four points are numbered. Point 1 is the point in the orbit where the spacecraft, which is in the solar inertial mode, enters earth shadow.

The value of η at point 1, called η_{es} (for earth shadow) in Reference 3, is dependent on β and the altitude of the orbit. It is given by:

$$\eta_{es} = \cos^{-1} \left(-\sqrt{1 - \left(\frac{R}{R+H} \right)^2} / \cos \beta \right) \quad (18)$$

where R is the radius of the earth and H is the altitude of the orbit. η_{es} is limited to $90^\circ < \eta_{es} \leq 180^\circ$; if the numerator of the argument of the arc-cosine of (18) is greater than the denominator, η_{es} is to be taken as 180° , for in this case, the vehicle is constantly in sunlight. For the range of β studied here and the nominal AAP altitude of 235 NM, there will always be earth shadow.

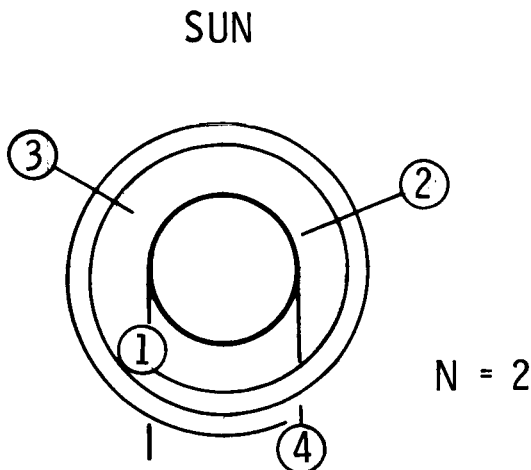


FIGURE 8

Points 2 and 3 are the points where the load, P_L , is exactly equal to the array output times the regulator and distribution efficiencies, $P_{SA} \eta_R \eta_D$.

At point 2, the batteries cease to discharge and begin to charge; at point 3, the opposite occurs. Even with a constant load, points 2 and 3 are not symmetric about $\eta=0$ (noon) because of the non-symmetry in the array temperature profile and, in the case of the AM array, the non-symmetry in shadowing.

Point 4 is the point where the vehicle leaves earth shadow having reacquired the solar inertial attitude, and the arrays abruptly begin delivering more power than the load requires. Neglecting the small change in β over the period in the earth resources mission mode, point 4 and point 1 are symmetric about $\eta=0$.

The segments of the orbit determined by the points just defined are periods when energy is either lost or gained by the batteries. Between points 1 and 2, the energy lost is

$$W_{\text{LOSS } 1-2} = \int_1^2 \left(\frac{P_L}{\eta_R \eta_D} - P_{SA} \right) dt$$

and the percent decrease in state of charge is

$$\Delta C_{1-2} = 100 \times \frac{W_{\text{LOSS } 1-2}}{W_{\text{CAP}}}$$

The energy gained between 2 and 3 is

$$W_{\text{GAIN } 2-3} = \int_2^3 \eta_C \eta_B \left(P_{SA} - \frac{P_L}{\eta_R \eta_D} \right) dt$$

and the percent increase in state of charge is

$$\Delta C_{2-3} = 100 \times \frac{W_{\text{GAIN } 2-3}}{W_{\text{CAP}}}$$

We can similarly define ΔC_{3-2} and ΔC_{3-4} as the percent decreases in state of charge between points 3 and 2, and 3 and 4, respectively.

It is assumed that at point 1, the initial state of charge is 100% since the vehicle has just completed a full sunlit pass in the solar inertial attitude. With this initial condition, values for the four ΔC 's defined above, and a specified number of orbits (N) in the earth resources mission mode, it is a simple matter to determine the minimum state of charge that the batteries reach. There are, however, several cases that must be examined:

a) If $\Delta C_{2-3} \geq \Delta C_{3-2}$, then the system is operating at or below its continuous power capability. Every orbit the batteries regain their full state of charge. The same minimum occurs every orbit but the first one and is

$$C_{\text{MIN}} = 100 - \Delta C_{3-2} \quad (19-a)$$

b) If $\Delta C_{1-2} \leq \Delta C_{2-3} < \Delta C_{3-2}$, then the batteries will return to 100% SOC at point 3 after the first experiment pass, but not thereafter. The minimum state of charge might occur at one of two places.

b-1) If $\Delta C_{2-3} > \Delta C_{3-4}$, then the minimum will occur at point 2 just before the last experiment pass and will be

$$C_{\text{MIN}} = 100 - (N-1) \Delta C_{3-2} + (N-2) \Delta C_{2-3} \quad (19b-1)$$

b-2) If $\Delta C_{2-3} \leq \Delta C_{3-4}$, the minimum will occur at point 4 and will be

$$C_{\text{MIN}} = 100 - (N-1) (\Delta C_{3-2} - \Delta C_{2-3}) - \Delta C_{3-4} \quad (19b-2)$$

c) If $\Delta C_{1-2} > \Delta C_{2-3}$, the batteries will not return to 100% SOC at point 3. As in b, we must treat two possible cases.

c-1) If $\Delta C_{2-3} > \Delta C_{3-4}$ the minimum occurs before the last experiment pass

$$C_{\text{MIN}} = 100 - \Delta C_{1-2} - (N-1) (\Delta C_{3-2} - \Delta C_{2-3}) \quad (19c-1)$$

c-2) If $\Delta C_{2-3} \leq \Delta C_{3-4}$, the minimum will occur just before the vehicle enters sunlight after the earth resource sequence.

$$C_{\text{MIN}} = 100 - \Delta C_{1-2} - (N-1) (\Delta C_{3-2}) + N(\Delta C_{2-3}) - \Delta C_{3-4} \quad (19c-2)$$

Cases b-2 and c-1 would not have to be included if ΔC_{1-2} and ΔC_{3-4} were exactly equal. The necessary conditions for applicability of these cases could not be satisfied. ΔC_{1-2} and ΔC_{3-4}

would be equal if temperature and shadowing profiles were symmetric about $\eta=0$. Given one set of temperature and shadowing profiles, we can say that it is possible for only one of these cases to occur. We can also say that the range of power requirement over which it will occur is small, because the values of ΔC_{1-2} and ΔC_{3-4} will be close.

VII. RESULTS

Presentation of power system capabilities for the earth resources mission mode is complicated by the large number of variables that enter the calculations. As the earth resources experiments will be operated only for a short time over the sun-lit earth, it is logical to specify P_L (required to evaluate (16) and (17)) as a profile that peaks when the experiments are on. In this analysis, we have taken the peak as 1070 watts for ten minutes centered about noon, which amounts to an orbital average requirement of 114 watts. In doing so, however, we are forced to specify which system, AM or ATM, is to power the experiments. Both cases have been analyzed. For each case, we are still faced with the problem of displaying the relationship between

- the minimum battery state-of-charge, C_{MIN} ,
 - the power requirement for everything else, P_L ,
 - the angle β ,
 - the number of experiment passes, N ,
- and
- the time into the mission, d .

The last variable listed, d , has the least effect on performance, and we will, for the time being, eliminate it by specifying that it is the beginning of the mission. We will also forget the very small difference in AM power output between cases where β is of the same magnitude but of different sign, which is due to the slightly different shadowing profile. To the accuracy with which the following curves can be plotted and read, the sign of β is immaterial. Then for a given system, a given β , and a choice as to which system powers the experiments, we can present a set of curves like those of Figure 9. These particular curves relate the minimum battery state-of-charge to the average power requirement in the AM system, which includes

the 114 watt average experiment requirement* for one through five and 10 consecutive experiment passes. For more than one consecutive pass, the curves all intersect at a power requirement of approximately 2.1 kw. This is the continuous power capability at $\beta=0$, beginning of life. Equation (19a) for C_{MIN} applies at lower power requirements, and (19b-1) applies to approximately the point where all curves bend downward. This bend occurs when ΔC_{1-2} , ΔC_{2-3} , and ΔC_{3-4} (see page 23) are all approximately equal. At higher power levels (19c-2) gives C_{MIN} .

Figures 10 and 11 for the AM are for identical conditions except for β , which is stated on the Figures. Note that for given minimum state-of-charge and number of passes, the power capability decreases with increasing β . This suggests another way to plot the data, namely that of Figure 12. This plot shows the average power capability vs β and N if the minimum state of charge is permitted to drop to 40%.

Figure 13 is like the former plots that show minimum state of charge vs the power requirement, but is for the ATM system at $\beta=30^\circ$. The power requirement, P_L , used to generate this data was constant over an orbit; that is, it included no increase around noon for experiment requirements. It therefore complements the earlier AM data, which did include the peaks.

The dashed lines on the curves just referenced, at an AM average power of 2454 watts and an ATM average power of 2022 watts, correspond to estimates of the minimum average power that might satisfy requirements during the earth resources mission mode. The AM requirement includes the 114 watt average requirement of the experiments. As there is presently much disagreement and/or uncertainty concerning AAP mission power requirements, these estimates should be considered as examples of how the charts can be used to state system capabilities. For instance, from either Figure 11 or Figure 12, we can state that the AM system is capable of two consecutive experiment passes at a 2454 watt average reduced requirement with β up to 60° if the maximum depth of discharge is permitted to reach 60%.

If the experiments are powered by the ATM rather than the AM, or if (as now planned) the systems are operated in parallel, we can state that three consecutive passes are feasible at the reduced estimated power levels. If the battery depth-of-discharge is limited to 50%, then β must be below 42° ; if 60%

* P_L for the AM for this case is the average power requirement less 114 watts except for the 10 minutes centered about noon, when it is the average plus 956 watts.

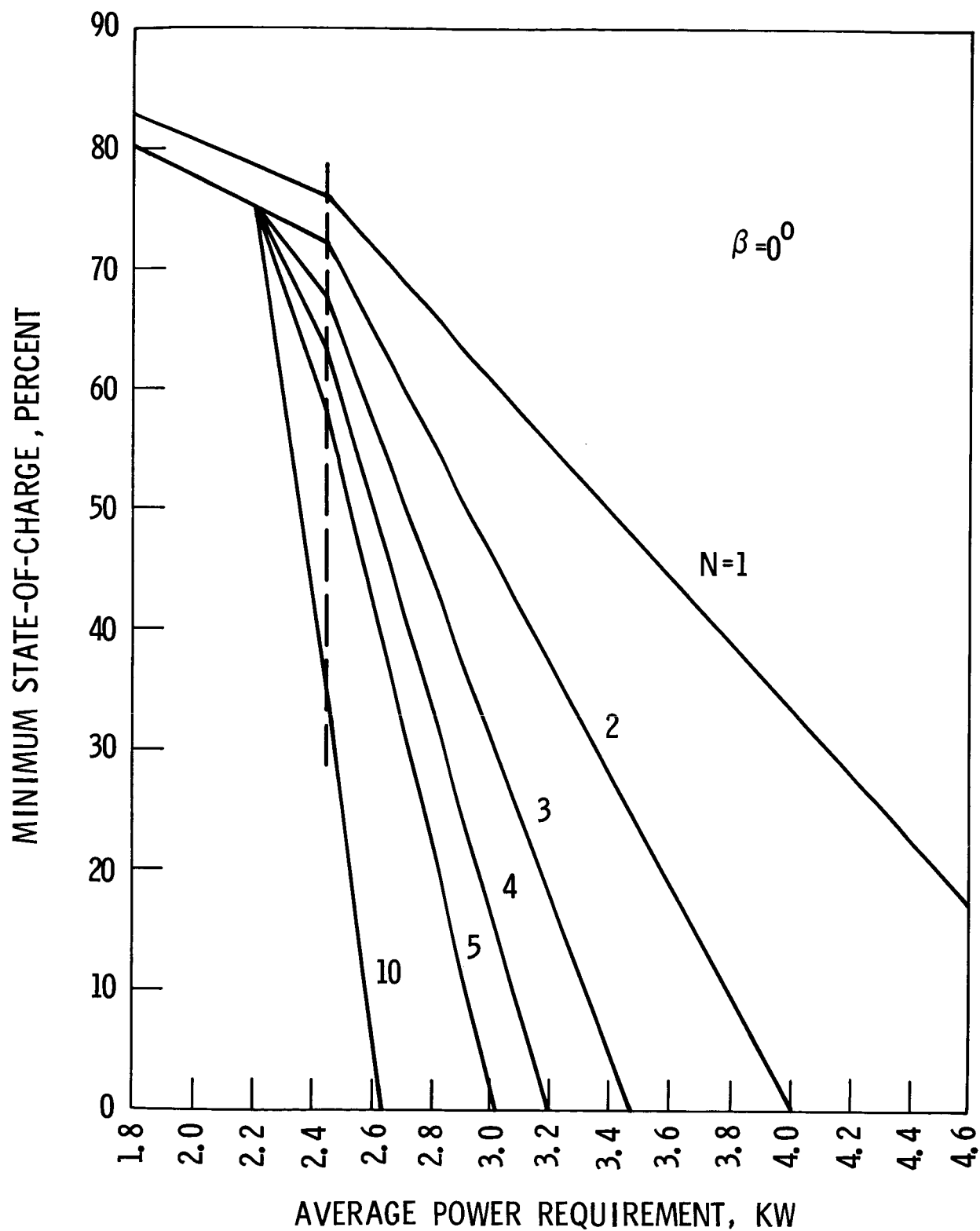


FIGURE 9 - AM BATTERIES — MINIMUM STATE-OF-CHARGE VS. POWER REQUIREMENT DURING N ORBITS IN EARTH POINTING MODE

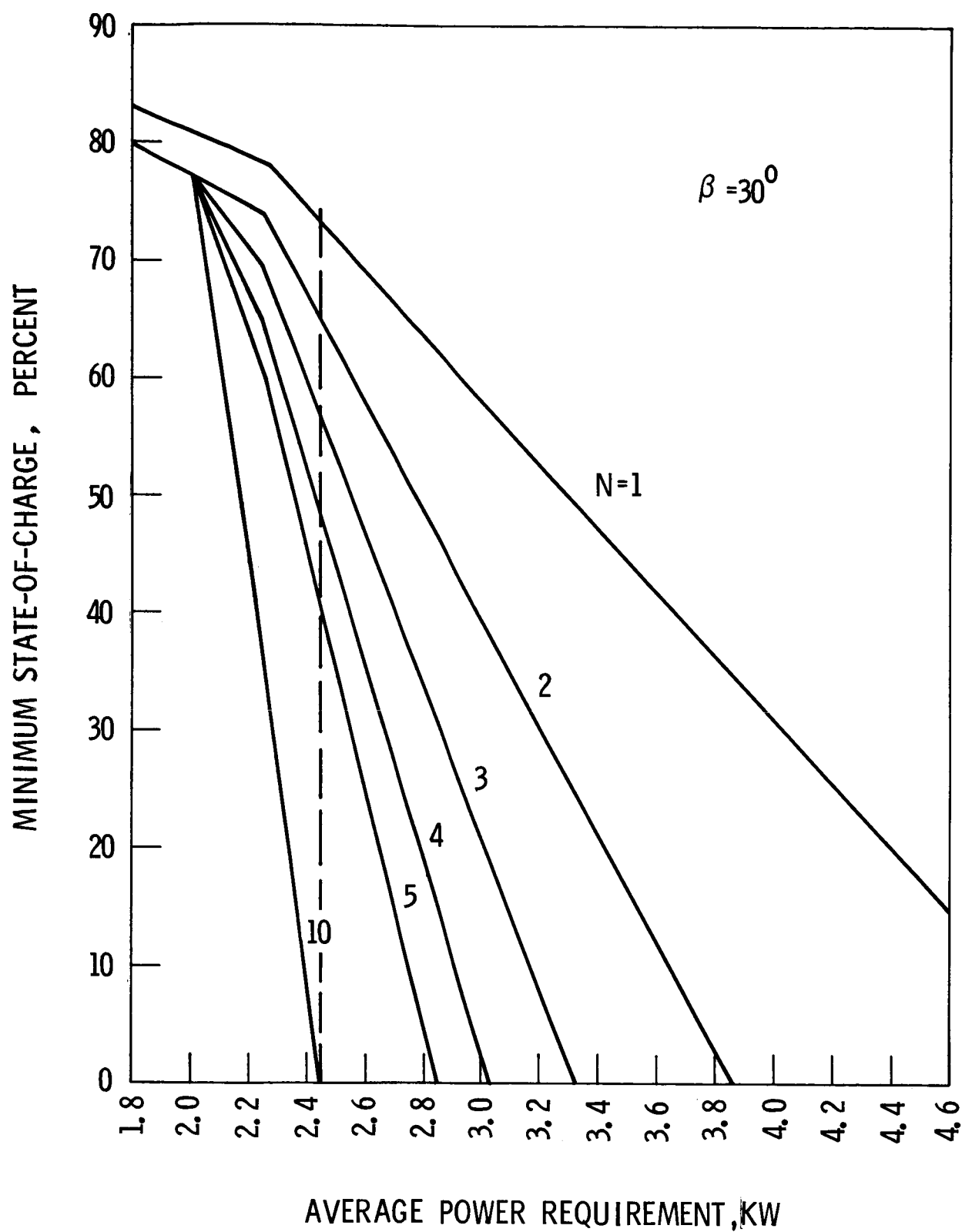


FIGURE 10 - AM BATTERIES — MINIMUM STATE-OF-CHARGE VS. POWER REQUIREMENT DURING N ORBITS IN EARTH POINTING MODE

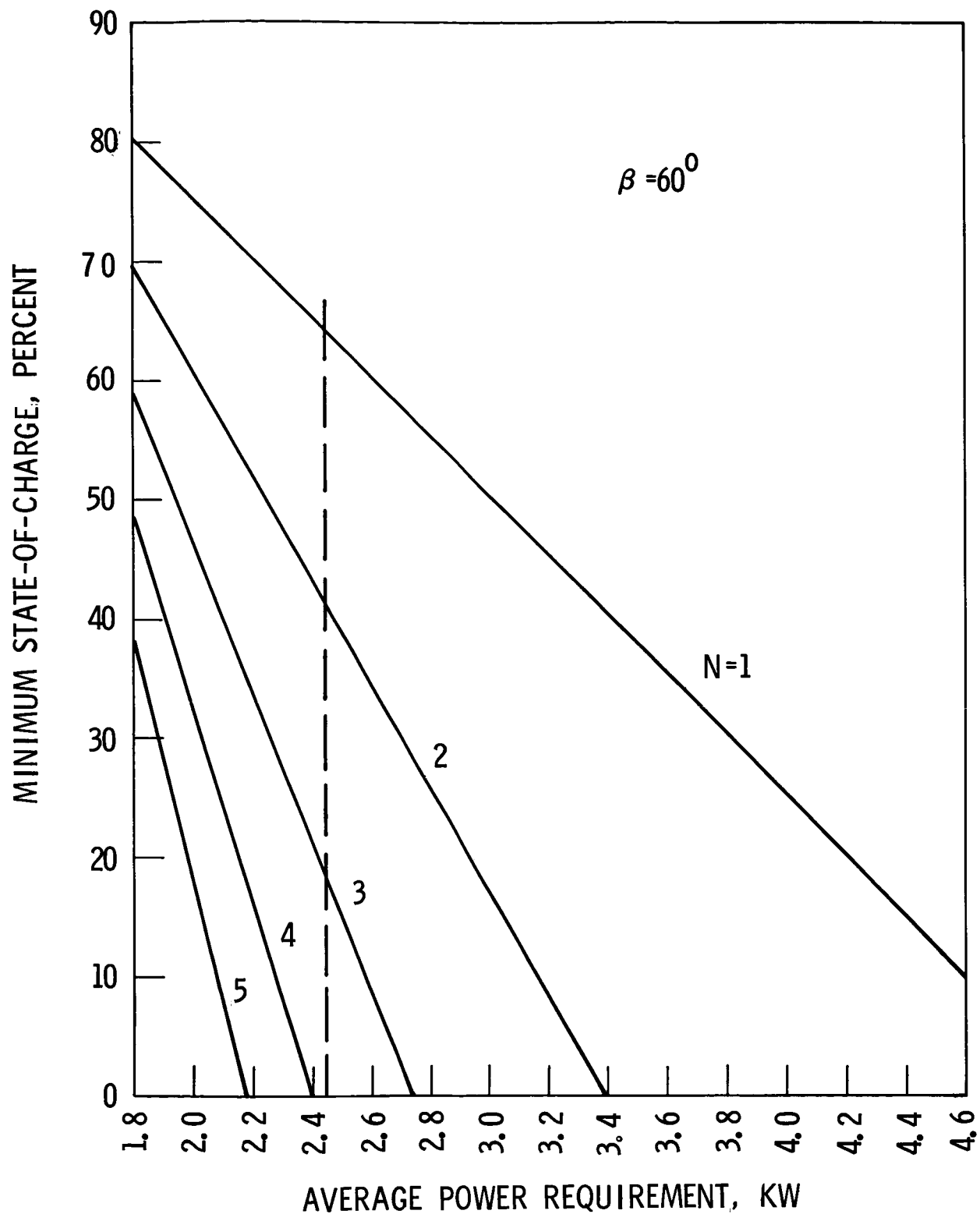


FIGURE 11 - AM BATTERIES — MINIMUM STATE-OF-CHARGE VS. POWER REQUIREMENT DURING N ORBITS IN EARTH POINTING MODE

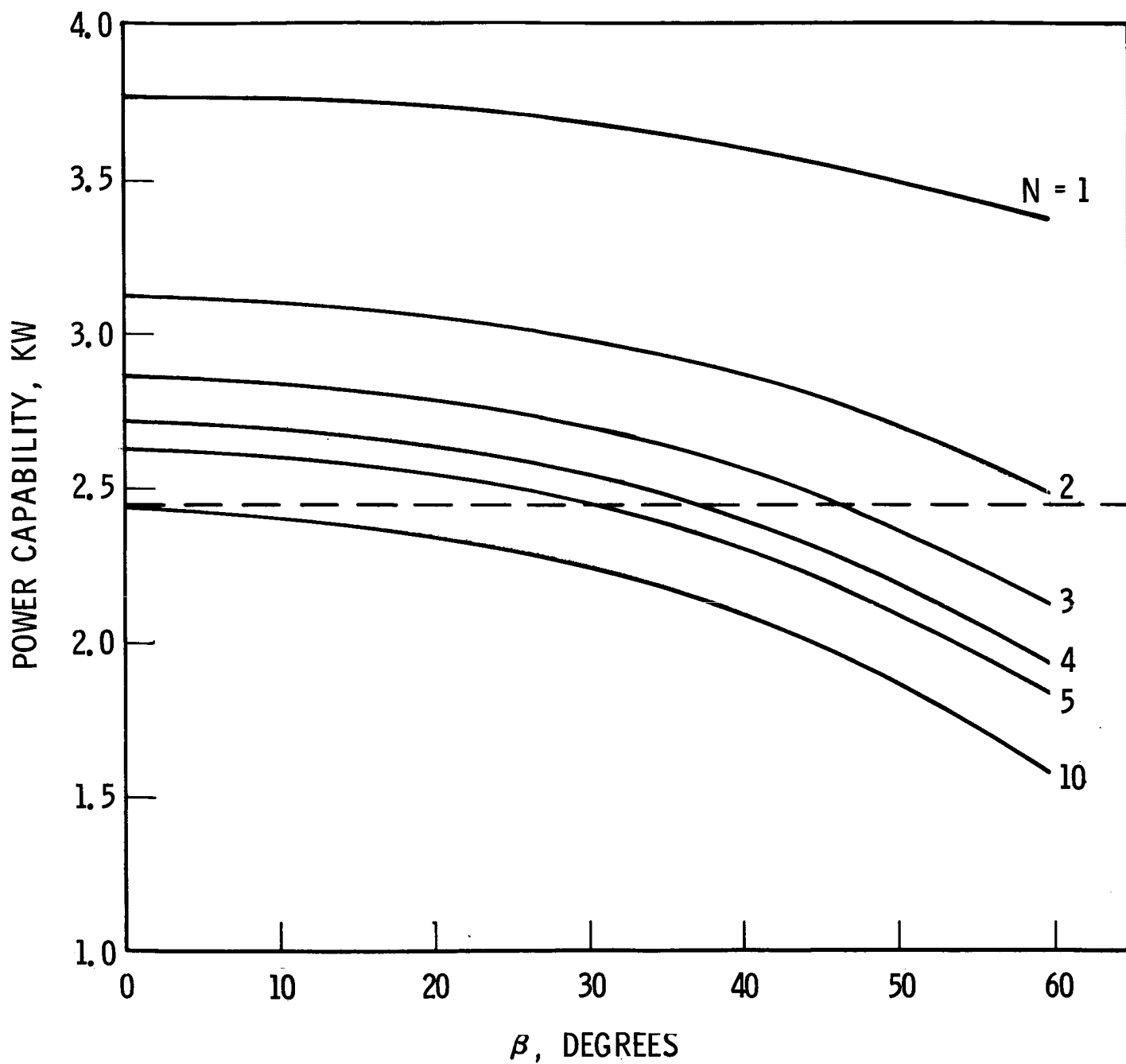


FIGURE 12 - AM POWER CAPABILITY WITHOUT EXCEEDING 60% DOD

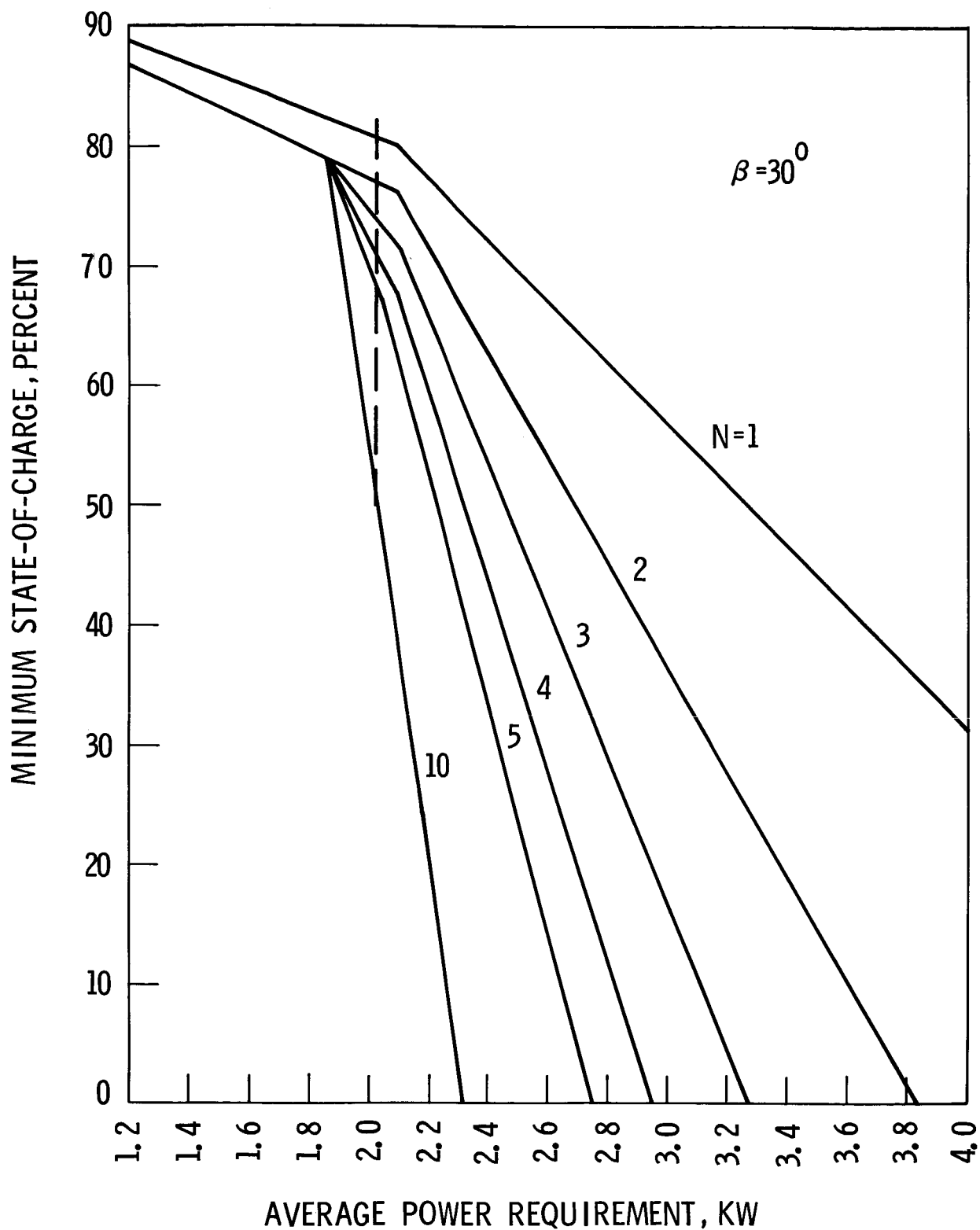


FIGURE 13 - ATM BATTERIES — MINIMUM STATE-OF-CHARGE VS. POWER REQUIREMENT DURING N ORBITS IN EARTH POINTING MODE

DOD is permitted, β can be up to 50° , and if three-pass capability over the full range of β (up to 60°) is desired, then the batteries must be permitted to discharge by 70% of their capacity. Such statements are clearly dependent on the assumed power requirement. For a higher power requirement, the capability in terms of number of consecutive orbits or range of β is less.

Let us now look at the effect of lifetime on the power capability. The total life of AAP Workshop I is to be eight months. Figure 14 shows the minimum state-of-charge after three experiment passes vs β at the beginning of life and at the end of life for a 2400 watt load on the AM. We observe that the decrease in the minimum state of charge due to solar cell degradation (difference between curves) is less as the minimum state of charge itself decreases (as β increases). This is logical; as β increases the batteries supply more and the solar arrays supply less of the same total energy, and only the arrays are affected by radiation damage.

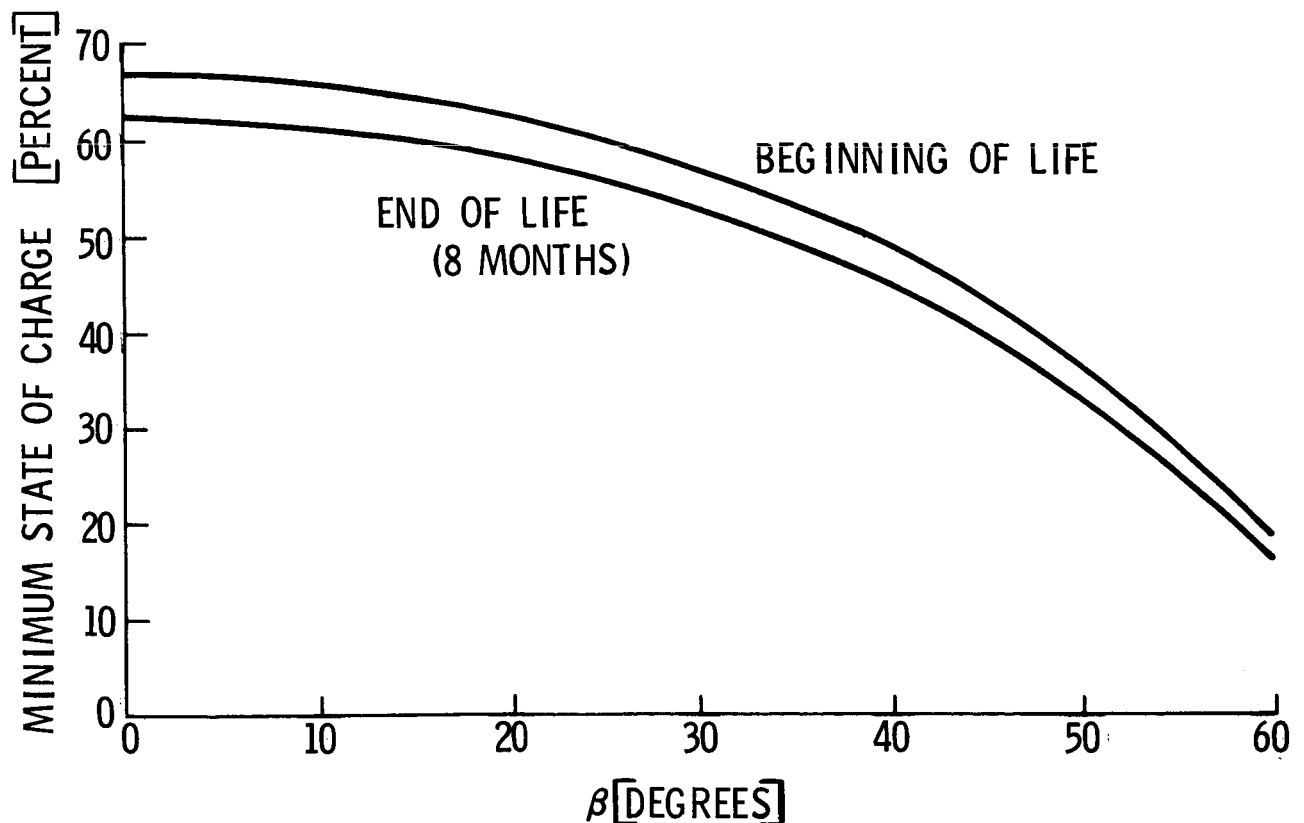


FIGURE 14 - EFFECT OF SOLAR CELL DEGRADATION

VIII. SUMMARY AND DISCUSSION

It is impossible to firmly state the capability of the AAP power systems to support the earth resources mission mode in terms of number of consecutive orbits and limits on β without knowing exactly both the minimum power requirement and the maximum permissible battery depth of discharge. When these numbers are known, however, one need only go to the curves generated in this study to accurately determine the capability. If the estimated minimum power requirements given in the last section are close, then it is fairly safe to say that two, and perhaps three consecutive earth resources passes are feasible without severe restrictions on β .

In determining the permissible battery depth of discharge, we must realize that the specified level will be reached infrequently, and possibly never. Assuming a constant power requirement in the earth resources mode, a specified limit on battery DOD will be reached only when $|\beta|$ is at an associated upper operational limit. For instance, 70% might be specified as an acceptable DOD when $|\beta| = 60^\circ$, which is the experimental limit due to ground lighting restrictions. However, we would not expect the batteries near 70% DOD very often simply because $|\beta|$ is seldom in the neighborhood of 60° . With the initial conditions used to generate Figure 3, $|\beta| = 60^\circ$ will occur only four times during the life (eight months) of the Workshop mission, and not at all during the first 4-1/2 months. In the first manned mission (28 days), $|\beta|$ will not get larger than about 32° .

Observation of Figures 10 and 11 shows that a power requirement that results in two-orbit minimum state of charge of 30% (70% DOD) at $\beta = 60^\circ$ does not require even a 50% discharge at $\beta = 30^\circ$. The same calculation for three orbits gives a discharge less than 35% at $\beta = 30^\circ$. From these considerations, plus the fact that even if it did occur a few times it would not be damaging, specification of a maximum permissible battery depth of discharge of 70% at $|\beta| = 60^\circ$ does not appear unreasonable.

If the targets for earth resources experimentation are all in the latitude range of 30°N to 50°N (i.e. the U.S.A.), then the plus-Z Cluster axis is not the optimum location for the experiments. When the limits on the subsolar point, determined by target lighting constraints and the tropics, are plotted relative to the ground track, it is found that β will be predominantly of one sign. The subsolar point will usually be south of the sunlit ground track, which is equivalent to a negative β . Figure 15 indicates why, under these circumstances, an experiment location away from the plus-Z toward the minus-Y

axis by 20° to 30° would be better. Not only will the average pointing angle, λ in Equation (1), be less, but the arrays will be sunlit for more than half the orbit, assuming the experiments are continually aimed along the local vertical.

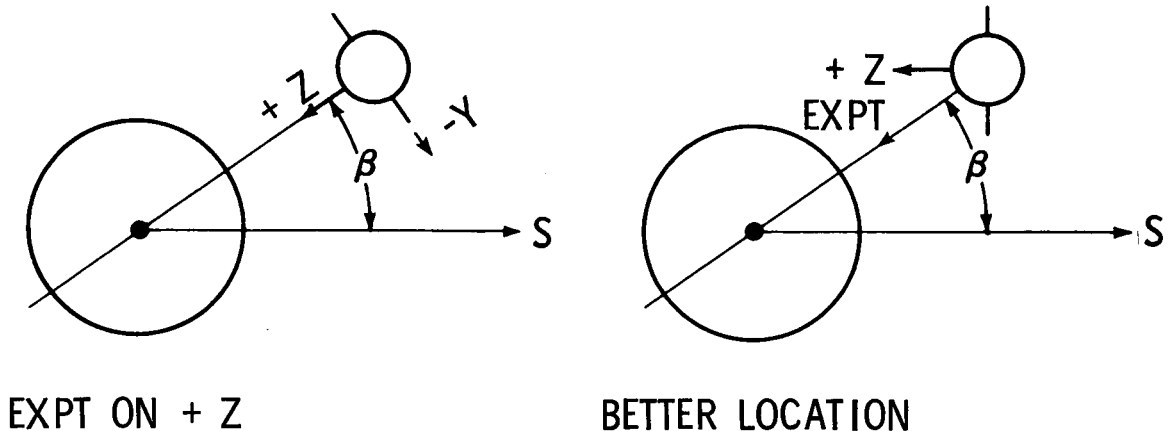


FIGURE 15 - ALTERNATE EXPERIMENT LOCATION FOR U.S.A. TARGETS

Derivation of the optimum angle for positioning the experiments vs β is the identical problem that is discussed as the Fixed Roll Case in Reference 3. One only need recognize that, in both problems, we have one spacecraft axis pointed directly down and are optimizing the position of the arrays relative to that axis with an angular degree of freedom about a line tangent to the orbit.

If targets for the earth resources experiments are equally distributed north and south of the equator, then the optimum experiment position is along the plus-Z axis.

IX. ACKNOWLEDGEMENT

The authors acknowledge the work of Mrs. Patricia Dowling which led to the numerical results presented.

W. W. Hough
W. W. Hough

B. W. Moss
B. W. Moss

J. J. Sakolosky
J. J. Sakolosky

WWH
1022-BWM-cf
JJS

BELLCOMM, INC.

REFERENCES

1. Fearnside, J. J., "A Study of Some Attitude and Control Options Compatible with the Performance of Earth-Pointing Experiments by the AAP Cluster," Technical Memorandum TM-70-1022-2, Bellcomm, Inc., February 3, 1970.
2. Apollo Applications Program - Baseline Reference Mission (Rev. A), MSC-KM-D-68-4A, NASA, Manned Spacecraft Center, Houston, Texas, October 27, 1969.
3. Hough, W. W. and Elrod, B. D., "Solar Array Performance as a Function of Orbital Parameters and Spacecraft Attitude," Journal of Engineering for Industry, Trans. ASME, Series B, Vol. 91, No. 1, February 1969, pp. 13-20.
4. Powers, J. W., "Solar Array Temperatures during the AAP-SWS Earth Pointing Experiments Mission Mode," Memorandum for File B70 01059, Bellcomm, Inc., January 28, 1970.
5. Moss, B. W., "The Effect of Quartz Coverslides on Radiant Energy Incident on Solar Cells," Memorandum for File B69 04094, Bellcomm, Inc., April 24, 1969.
6. Sakolosky, J. J., "Shading of the AAP Workshop Solar Arrays by the ATM Arrays," Technical Memorandum TM-70-1022-9, Bellcomm, Inc., March 31, 1970.

APPENDIX ANOON-TO-NOON SATELLITE PERIOD

The period of a satellite in a circular orbit about a spherical earth is given by:

$$T_0 = 2\pi \sqrt{\frac{(R+H)^3}{\mu}} \quad A-1$$

where: R is the radius of the earth = 3443.93 NM

H is the altitude of the orbit

μ is the earth's gravitational constant =

$$4.68427 \cdot 10^{14} \text{ NM}^3/\text{Day}^2$$

When the earth's oblateness is considered to the order of the dominant oblateness parameter, J, there is no longer a unique period for a satellite. [A-1, A-2] Commonly used periods are the anomalistic (perigee-to-perigee) and the nodical (node-to-node). There is a third period, which we'll call the noon-to-noon period, that gives the time required for the satellite to progress from one orbital noon to the next. This is the period in which the orbit position angle used in this report, η , changes by 360° .

In reference A-3, the angle ψ is used to describe the position of orbital noon ($\eta=0$) relative to the ascending node of the orbit. The angle ψ increases with time, but not linearly, and therefore $\dot{\psi}$ is not constant. However, the average value of $\dot{\psi}$ is shown to be the difference between the rate of the earth's rotation about the sun, $\dot{\gamma}$, and the orbital regression rate, $\dot{\Omega}$.

That is:

$$\dot{\psi}_{\text{AVG}} = \dot{\gamma} - \dot{\Omega} \quad A-2$$

where (for circular orbits)

$$\dot{\Omega} = - \frac{JR^2 \mu^{1/2} \cos i}{(R+H)^{7/2}} \quad A-3$$

and

$$\dot{\gamma} = 360^\circ/\text{solar year} = 0.01720279 \text{ rad/day}$$

with J being the first-order oblateness parameter $= 1.6234 \cdot 10^{-3}$, and i the orbital inclination.

In one noon-to-noon orbit, the angle ψ increases on the average by $\dot{\psi}_{\text{AVG}}$ times the noon-to-noon period. However, since $\dot{\psi}_{\text{AVG}}$ is already to the order J , it is sufficient to set

$$\Delta\psi_{\text{AVG}} = \dot{\psi}_{\text{AVG}} T_0 \quad \text{A-4}$$

The time needed for the satellite to traverse through $\Delta\psi_{\text{AVG}}$ is approximately

$$\Delta T_{\text{AVG}} = \Delta\psi_{\text{AVG}} / \omega_0 \quad \text{A-5}$$

where ω_0 is the orbital rate based on a spherical earth $= 2\pi/T_0$. Thus:

$$\Delta T_{\text{AVG}} = \dot{\psi}_{\text{AVG}} \frac{T_0^2}{\pi} \quad \text{A-6}$$

ΔT_{AVG} is a measure of the average additional time required to reach orbital noon after passing the ascending node over the time to traverse between the same two points on the preceeding orbit. To obtain the average noon-to-noon period, the nodical period must be added.

$$T_{\text{S}_{\text{AVG}}} = T_{\text{N}} + \Delta T_{\text{AVG}} \quad \text{A-7}$$

where $T_{\text{S}_{\text{AVG}}}$ is the average noon-to-noon period and T_{N} is the nodical period, which is given to the order J by: [A-2]

$$T_{\text{N}} = T_0 \left(1 - J \left(\frac{R}{R+H} \right)^2 \left(\frac{7 \cos^2 i - 1}{4} \right) \right) \quad \text{A-8}$$

Thus the average noon-to-noon period is, to the order J

$$T_{S_{AVG}} = T_0 \left(1 - J \left(\frac{R}{R+H} \right)^2 \left(\frac{7 \cos^2 i - 1}{4} \right) \right) + \frac{\dot{\psi}_{AVG}}{\omega_0} \quad A-9$$

The values of these parameters for a 235 NM altitude, 50° inclination orbit are:

$$T_0 = .06478004 \text{ days} = 1.5547209 \text{ hours}$$

$$T_N = .06473644 \text{ days} = 1.5536745 \text{ hours}$$

$$\Delta T_{AVG} = .00007073 \text{ days} = .0016975 \text{ hours}$$

$$T_{S_{AVG}} = .06480717 \text{ days} = 1.5553720 \text{ hours}$$

REFERENCES FOR APPENDIX A

- A-1 Space Technology Laboratories, Flight Performance Handbook for Orbital Operations, Raymond W. Wolverton, Editor, John Wiley and Sons, New York, 1963, pp. 2-228 through 2-230.
- A-2 NASA Sp 33 Part 1, Orbital Flight Handbook, NASA Office of Scientific and Technical Information, Washington, 1963, pp. IV-21 through IV-23.
- A-3 Elrod, B. D., Solar Pointing Variations in Earth Orbit and the Impact on Mission Design, Bellcomm TR-69-1022-1, February 11, 1970.

BELLCOMM, INC.

955 L'ENFANT PLAZA NORTH, S.W., WASHINGTON, D.C. 20024

COVER SHEET FOR TECHNICAL MEMORANDUM

TITLE- Shading of the AAP Workshop Solar
Array by the ATM Array

TM- 70-1022-9

FILING CASE NO(S)- 620

DATE- March 31, 1970

AUTHOR(S)- J. J. Sakolosky

FILING SUBJECT(S)
(ASSIGNED BY AUTHOR(S))- Electrical Power
Shadow

ABSTRACT

Shading of the SIVB solar array by the ATM array has been determined for any spacecraft attitude and position as the AAP Cluster traverses the sunlit portion of its orbit. The panels of the ATM array are divided into sample areas; the centerpoint of each sample area is then projected along the sun vector to the planes of the SIVB solar array wings. Projected points lying within the boundaries of each wing are summed and converted to a percentage of the total array area that is shaded.

In the earth resources mission mode, shading of the SIVB array follows no easily predictable pattern as a function of sun angle or orbital position. In general, shading becomes worse as the sun angle decreases. As much as 30% of SIVB solar array area is shaded for certain sun angles and positions in orbit during the earth resources mode.

DISTRIBUTIONCOMPLETE MEMORANDUM TO

CORRESPONDENCE FILES:

OFFICIAL FILE COPY
plus one white copy for each
additional case referenced

TECHNICAL LIBRARY (4)

NASA Headquarters

H. Cohen/MLR
J. H. Disher/MLD
W. B. Evans/MLO
L. K. Fero/MLV
J. P. Field, Jr./MLP
W. H. Hamby/MLO
T. E. Hanes/MLA
T. A. Keegan/MA-2
M. Savage/MLT
W. C. Schneider/ML

Goddard Space Flight Center

J. T. Skladany/713

Langley Research Center

P. R. Kurzhals/AMPD

MSC

R. G. Brown/ES-16
C. N. Crews/KS
W. R. Cunningham/CB
R. E. Durkee/ES-5
R. L. Frost/KS
O. K. Garriott/CB
F. C. Littleton/KM
R. M. Machell/KF
P. S. Miglicco/KS
O. G. Smith/KF
H. E. Whitacre/KM

MSFC

R. M. Aden/S&E-ASTR-E
W. B. Chubb/S&E-ASTR-SGD
J. C. Cody/S&E-ASTR-MA
C. B. Graff/S&E-ASTR-EP

COMPLETE MEMORANDUM TOMSFC (continued)

G. B. Hardy/PM-AA-EI
G. D. Hopson/S&E-ASTN-PL
E. H. Hyde/S&E-ASTN-PF
H. F. Kennel/S&E-ASTR-A
G. F. McDonough/S&E-CSE-A
E. F. Noel/S&E-ASTR-SI
W. C. Patterson/S&E-ASTN-PLA
J. W. Sims/S&E-ASTN-PTA
J. D. Stroud/S&E-ASTR-SE
J. W. Thomas/PM-AA
H. F. Trucks/S&E-ASTN-PTA
J. L. Vaniman/S&E-ASTN-PT
R. D. Wegrich/S&E-CSE-AA
A. P. Woosley/S&E-ASTR-SEC
H. E. Worley/S&E-AERO-DOI

Martin-Marietta

H. S. Nassen/Denver
E. F. Bjoro/Washington
M. S. Imamura/Denver
R. W. Wilson/Denver

McDonnell-Douglas

G. Weber/Eastern Division

Bellcomm

A. P. Boysen
D. R. Hagner
W. G. Heffron
B. T. Howard
J. Z. Menard
J. M. Nervik
I. M. Ross
P. F. Sennewald
J. W. Timko
R. L. Wagner
M. P. Wilson
Departments 2031, 2034 Supervision
Department 1024 File
Division 102
Central Files

SUBJECT: Shading of the AAP Workshop
Solar Array by the ATM Array

DATE: March 31, 1970

FROM: J. J. Sakolosky

TECHNICAL MEMORANDUM

1.0 INTRODUCTION

The configuration of the AAP Cluster results in shading of the SIVB solar panels by the ATM solar array during the sunlit portion of the orbit. The shaded portion of the Workshop panels is constant and relatively insignificant ($\sim 1.3\%$) when the Cluster is in a solar inertial attitude, and the solar arrays are pointing directly at the sun. However, when the Cluster is operating in the earth resources mode, variable shading does occur since the orientation of the solar arrays with respect to the sun is not constant. In this attitude, the vehicle roll axis is kept in the orbital plane parallel to the velocity vector, and the planes of the solar arrays are maintained perpendicular to the orbital plane. The percent of the SIVB array that is shaded varies with sun angle* and spacecraft position in orbit and can be as high as 30%. This memorandum discusses the shading problem and describes a computer program which has been written to determine SIVB array shading by the ATM array. Data are presented for the case when the AAP Cluster is in the earth resources attitude mode.

2.0 CLUSTER CONFIGURATION AND RELATED COORDINATE SYSTEMS

The AAP Cluster coordinate system (X_{sc} , Y_{sc} , Z_{sc}) is illustrated in Figure 1. The Z_{sc} axis is perpendicular to the planes of the ATM and SIVB solar arrays with $-Z_{sc}$ extending outward from the active side of the arrays. X_{sc} is the roll axis of the Cluster; the CSM is located on the positive X_{sc} axis. The Y_{sc} axis completes the right hand coordinate system.

The relationships between the spacecraft coordinate system and other coordinate systems referred to in this memorandum are illustrated in Figure 2. The orbit referenced coordinate system (X_o , Y_o , Z_o) is defined with Z_o perpendicular to the orbital plane, positive in the direction of the spacecraft

*The sun angle, designated β , is the minimum angle between the sun vector and the orbital plane. (See Figure 2.)

angular velocity vector (north). Y_O is formed by the intersection of the orbit noon meridian plane and the orbital plane, and X_O completes the right hand set. The local vertical coordinate system (X_{LV} , Y_{LV} , Z_{LV}) has Z_{LV} parallel to Z_O and Y_{LV} pointing from the nadir and located in the orbital plane at an angle η from the noon meridian plane. Completing the right hand system, the X_{LV} axis also lies in the orbital plane. The (X_{yaw} , Y_{yaw} , Z_{yaw}) coordinate system is defined to allow yaw attitude maneuvers of the spacecraft. The X_{yaw} axis and Y_{yaw} axis lie in the plane of X_{LV} - Y_{LV} and are displaced through a negative rotation θ (about Z_{LV}) from the respective X_{LV} and Y_{LV} axes. Note that X_{yaw} is coincident with the spacecraft X_{sc} axis. Z_{yaw} is parallel to Z_{LV} . In the sun-referenced system (X_s , Y_s , Z_s), Y_s is pointing at the sun and X_s is parallel to X_O . Z_s completes the right hand system.

The coordinate systems discussed above are related through the angles β , η , θ , and α . The sun angle, β , is the angle formed by the orbital system Y_O axis and the Y_s axis of the sun system. Note that in this memorandum β is positive when the sub-solar point is south of the sub-orbital noon point.* The position of the spacecraft in the orbit is specified by the angle η , which is measured from orbital noon and increases as the vehicle progresses in its orbit. The angle θ is the angle between the spacecraft roll axis and the orbit tangent (between X_{sc} and X_{LV}); it is equal to η when the spacecraft is in a solar inertial attitude.** The angle α is used to specify the roll attitude of the spacecraft. It is defined as the angle between the Z_{LV} axis and the Z_{sc} axis, measured positive for a positive rotation about X_{sc} . α is the angle between the planes of the spacecraft solar arrays and the orbital plane.

*There are two definitions of the polarity of the sun angle in use. The definition used here allows that a positive rotation of the Y_s and Z_s axes (about the X_s axis) through the angle β transforms from the sun referenced coordinates to the orbital coordinates.

**Note that the spacecraft X_{sc} axis is never allowed out of the orbital plane. This is because all the spacecraft attitudes with which we are concerned constrain the Cluster roll axis to be in the orbital plane.

The active area of the Cluster solar arrays has been modeled as shown in Figures 3 and 4. Figure 3 gives the vertices of each of the panels in spacecraft coordinates. The panels are labeled (e.g., ATM1, S-IVB2, etc.) for ease of future reference. It is obvious from Figure 3 that in a solar-inertial attitude mode ($-Z_{sc}$ pointing at the sun) a relatively small amount of shading of the SIVB panels takes place. Figure 4 views the Cluster from the $+X_{sc}$ axis (i.e., the CSM end).

The centerline of the fairing for each wing of the SIVB solar array is displaced equally from the $X_{sc}-Y_{sc}$ plane. This leads to an unequal displacement of the active surface of each solar array wing from the plane of the ATM array. The distance between each SIVB wing and the ATM array is indicated in Figure 4.

3.0 DETERMINATION OF SHADOW

Shading of the SIVB panels by a point on the ATM array can be determined for any attitude and position of the spacecraft in its orbit by projecting that point along the sun vector to the planes of the SIVB panels. If the projected point lies within the boundaries of either of the AM solar array wings, then the initiating point on the ATM array does cast a shadow for the particular values of β , η , θ , and α considered. The problem of determining SIVB solar array shadow, then, becomes primarily that of obtaining an expression for the sun vector in spacecraft coordinates for any spacecraft position and attitude in its orbit. This expression is obtained in the Appendix by successively transforming the sun vector from the sun-referenced system to the spacecraft system. The method used in projecting a point on the ATM array to the planes of the SIVB panels and determining its location relative to the panel boundaries is also outlined.

Each of the ATM panels is divided into sample areas twenty-one inches on a side, as indicated in Figure 3. This allows for a total of 275 sample areas in ATM panel 1; ATM panels 2 and 3 each contain 125 sample areas. Each sample area is less than 0.2% of the total active area of the SIVB array. The center point of each sample area is projected to the plane of each SIVB wing. If the projected point lies within the boundaries of the wing, then an area of the wing equal to the area of the ATM sample is assumed to be shaded. The total number of projected points within the boundaries of each wing are counted and converted into shaded area as a percentage of total array area.

4.0 DESCRIPTION OF COMPUTER PROGRAM

Input information required by the program consists of a variable called ICSM and the angles β , θ , and α . ICSM (i.e., ICSM = "FIRST," ICSM = "LAST") specifies whether the CSM is flying first or last as the Cluster traverses its orbit. This is important since in the earth resources mode, it determines the portion of the orbit during which shading occurs. The angles β , θ , and α are input as positive or negative degrees, not radians. The orbital position angle, η , is increased by a selected increment (e.g. one degree) within the program, and output information is printed at each increment of η . The percentage area of each SIVB wing shaded by each ATM panel, the total percent shaded area of each wing, and the average percent shaded area of both wings are provided as output.

5.0 DISCUSSION/RESULTS

Shadowing data have been obtained for various sun angles for the case when the planes of the SIVB and ATM solar arrays are perpendicular to the orbital plane ($\alpha=90^\circ$). The angle, θ , between the spacecraft roll axis and the orbital tangent was taken to equal zero for these calculations. This corresponds to the earth resources attitude mode of the AAP Cluster. The data plotted in Figures 5 and 6 display the ratio of unshaded area to total area of the SIVB solar array as a function of orbital position. Figures 5 and 6 both show data for the case when the CSM is flying last; Figure 5 is for positive β angles, and Figure 6 is for negative β angles. Data for the case when the CSM is flying first may also be obtained from Figures 5 and 6. In this case, sign inversions are required for η and β . Thus

$$S(\beta, \eta)_{\text{CSM last}} = S(-\beta, -\eta)_{\text{CSM first}}$$

where S is any shadowing function in Figures 5 or 6. For example, if the sign of η is reversed, the data of Figure 5 apply equally well to the case when the CSM is flying first and the sun angles are negative.

Notice that there is no readily predictable or consistent variation of shaded area as a function of sun angle. This results from the geometry of the situation. The cruciform pattern of the ATM array results in sequential shading of the SIVB array by the ATM panels as the spacecraft changes its position in orbit. The unequal displacements of the two SIVB wings from the plane of the ATM array also add to the effect of non-symmetrical shading patterns.

Comparing Figure 5 and Figure 6, notice that the primary effect of changing the sign of β is to vary the position in the orbit at which worst case shading occurs. This shift in η results from the unequal displacements of the SIVB solar array wings from the plane of the ATM array. If both SIVB wings were located in the same $X_{sc}-Y_{sc}$ plane, we would expect the data to be symmetrical with respect to β . In general, shading of the SIVB array gets worse as the sun angle gets smaller. Worst case shading occurs at an η between 40° and 50° when the sun angle is equal to zero. Approximately 30% of the total area of the SIVB array is shaded at these orbital positions.



J. J. Sakolosky

1022-JJS-cf

Attachment
Appendix

APPENDIX

The sun vector may be represented by the column vector $\{0, 1, 0\}$ in sun coordinates. (Refer to the sun oriented coordinate system in Figure 2.) We would like to express this vector in spacecraft coordinates for any position and attitude of the spacecraft in its orbit, i.e. for any β , η , θ , and α as shown in Figure 2. This may be accomplished by subjecting the sun vector to successive coordinate transformations through β (into the orbital coordinate system), η (into the local vertical coordinate system), θ (into the yaw coordinate system), and α (into the spacecraft coordinate system).

Transformation of the sun vector into the orbital coordinate system is accomplished by the transformation matrix, $T_{\beta}^{X_S}.$ *

$$\begin{bmatrix} X_O \\ Y_O \\ Z_O \end{bmatrix} = T_{\beta}^{X_S} \begin{bmatrix} X_S \\ Y_S \\ Z_S \end{bmatrix} = \begin{bmatrix} 1 & 0 & 0 \\ 0 & \cos\beta & \sin\beta \\ 0 & -\sin\beta & \cos\beta \end{bmatrix} \begin{bmatrix} X_S \\ Y_S \\ Z_S \end{bmatrix}$$

The resulting vector expressed in orbital coordinates may be expressed in local vertical coordinates through use of the $T_{\eta}^{Z_O}$ transformation matrix.

$$\begin{bmatrix} X_{LV} \\ Y_{LV} \\ Z_{LV} \end{bmatrix} = T_{\eta}^{Z_O} \begin{bmatrix} X_O \\ Y_O \\ Z_O \end{bmatrix} = \begin{bmatrix} \cos\eta & \sin\eta & 0 \\ -\sin\eta & \cos\eta & 0 \\ 0 & 0 & 1 \end{bmatrix} \begin{bmatrix} X_O \\ Y_O \\ Z_O \end{bmatrix}$$

*The superscript denotes the axis of rotation; the subscript denotes the angle of rotation.

We may then relate the local vertical coordinate system to the yaw coordinate system by a negative rotation through the angle θ and about the Z_{LV} axis.

$$\begin{bmatrix} x_{yaw} \\ y_{yaw} \\ z_{yaw} \end{bmatrix} = T_{-\theta}^{Z_{LV}} \begin{bmatrix} x_{LV} \\ y_{LV} \\ z_{LV} \end{bmatrix} = \begin{bmatrix} \cos\theta & -\sin\theta & 0 \\ \sin\theta & \cos\theta & 0 \\ 0 & 0 & 1 \end{bmatrix} \begin{bmatrix} x_{LV} \\ y_{LV} \\ z_{LV} \end{bmatrix}$$

Note that the two transformations, $T_{\eta}^{Z_O}$ and $T_{-\theta}^{Z_{LV}}$, from the orbital system to the yaw coordinate system have the net effect of a single rotation through the angle $(\eta-\theta)$ about Z_O .*

$$\begin{bmatrix} x_{yaw} \\ y_{yaw} \\ z_{yaw} \end{bmatrix} = T_{-\theta}^{Z_{LV}} T_{\eta}^{Z_O} \begin{bmatrix} x_O \\ y_O \\ z_O \end{bmatrix} = \begin{bmatrix} c\theta c\eta + s\theta s\eta & c\theta s\eta - s\theta c\eta & 0 \\ s\theta c\eta - c\theta s\eta & s\theta s\eta + c\theta c\eta & 0 \\ 0 & 0 & 1 \end{bmatrix} \begin{bmatrix} x_O \\ y_O \\ z_O \end{bmatrix}$$

$$\begin{bmatrix} x_{yaw} \\ y_{yaw} \\ z_{yaw} \end{bmatrix} = \begin{bmatrix} c(\eta-\theta) & s(\eta-\theta) & 0 \\ -s(\eta-\theta) & c(\eta-\theta) & 0 \\ 0 & 0 & 1 \end{bmatrix} \begin{bmatrix} x_O \\ y_O \\ z_O \end{bmatrix}$$

The yaw coordinate system can now be related to the spacecraft coordinate system by a rotation through the angle α about the x_{yaw} axis.

$$\begin{bmatrix} x_{sc} \\ y_{sc} \\ z_{sc} \end{bmatrix} = T_{\alpha}^{x_{yaw}} \begin{bmatrix} x_{yaw} \\ y_{yaw} \\ z_{yaw} \end{bmatrix} = \begin{bmatrix} 1 & 0 & 0 \\ 0 & \cos\alpha & \sin\alpha \\ 0 & -\sin\alpha & \cos\alpha \end{bmatrix} \begin{bmatrix} x_{yaw} \\ y_{yaw} \\ z_{yaw} \end{bmatrix}$$

*Note that c is shorthand notation for cos; s is shorthand notation for sin.

Thus the initial vector in sun coordinates may be expressed in spacecraft coordinates by the following series of transformations.

$$\begin{bmatrix} X_{sc} \\ Y_{sc} \\ Z_{sc} \end{bmatrix} = T_{\alpha}^{X_{yaw}} T_{-\theta}^{Z_{LV}} T_{\eta}^{Z_O} T_{\beta}^{X_s} \begin{bmatrix} X_s \\ Y_s \\ Z_s \end{bmatrix}$$

Performing the indicated matrix multiplication results in the following.

$$\begin{bmatrix} X_{sc} \\ Y_{sc} \\ Z_{sc} \end{bmatrix} = \begin{bmatrix} c(\eta-\theta) & s(\eta-\theta)c\beta & s(\eta-\theta)s\beta \\ -c\alpha s(\eta-\theta) & c\alpha c(\eta-\theta)c\beta - s\alpha s\beta & c\alpha c(\eta-\theta)s\beta + s\alpha c\beta \\ s\alpha s(\eta-\theta) & -s\alpha c(\eta-\theta)c\beta - c\alpha s\beta & -s\alpha c(\eta-\theta)s\beta + c\alpha c\beta \end{bmatrix} \begin{bmatrix} 0 \\ 1 \\ 0 \end{bmatrix}$$

Therefore, for any position and attitude of the spacecraft in its orbit the sun vector may be represented in spacecraft coordinates by the following vector.

$$\begin{bmatrix} X_{sc} \\ Y_{sc} \\ Z_{sc} \end{bmatrix} = \begin{bmatrix} s(\eta-\theta)c\beta \\ c\alpha c(\eta-\theta)c\beta - s\alpha s\beta \\ -s\alpha c(\eta-\theta)c\beta - c\alpha s\beta \end{bmatrix}$$

The negative of the above vector (call it \vec{S}) provides the line of sight from the sun through a point (X_{sc}, Y_{sc}, Z_{sc}) on the ATM array.

$$\vec{S} = -s(\eta-\theta)c\beta\vec{i} + [s\alpha s\beta - c\alpha c(\eta-\theta)c\beta]\vec{j} + [s\alpha c(\eta-\theta)c\beta + c\alpha s\beta]\vec{k}$$

Any point on the ATM array may be projected along this vector to the plane of the SIVB array by multiplying the vector by a number, N , such that

$$N[sac(\eta-\theta)c\beta + cas\beta] = H$$

where $sac(\eta-\theta)c\beta + cas\beta$ is the z direction cosine and H is the distance (parallel to the Z_{sc} axis) between the plane of the ATM array and the plane of the SIVB array. Then

$$N\vec{S} = - \frac{Hs(\eta-\theta)c\beta}{sac(\eta-\theta)c\beta + cas\beta} \vec{i} + \frac{H[sas\beta - cac(\eta-\theta)c\beta]}{sac(\eta-\theta)c\beta + cas\beta} \vec{j} + H\vec{k}$$

is a vector, parallel to the sun vector, originating at a point on the ATM solar array and terminating at a point in the plane of the SIVB solar array.

$$\Delta X_{sc} = - \frac{Hs(\eta-\theta)c\beta}{sac(\eta-\theta)c\beta + cas\beta}$$

$$\Delta Y_{sc} = \frac{H[sas\beta - cac(\eta-\theta)c\beta]}{sac(\eta-\theta)c\beta + cas\beta}$$

The termination point in the plane of the SIVB array has the following X-Y coordinates.

$$(X_{sc} + \Delta X_{sc}, Y_{sc} + \Delta Y_{sc})$$

This point may then be checked to determine if it lies within the boundaries of the SIVB array.

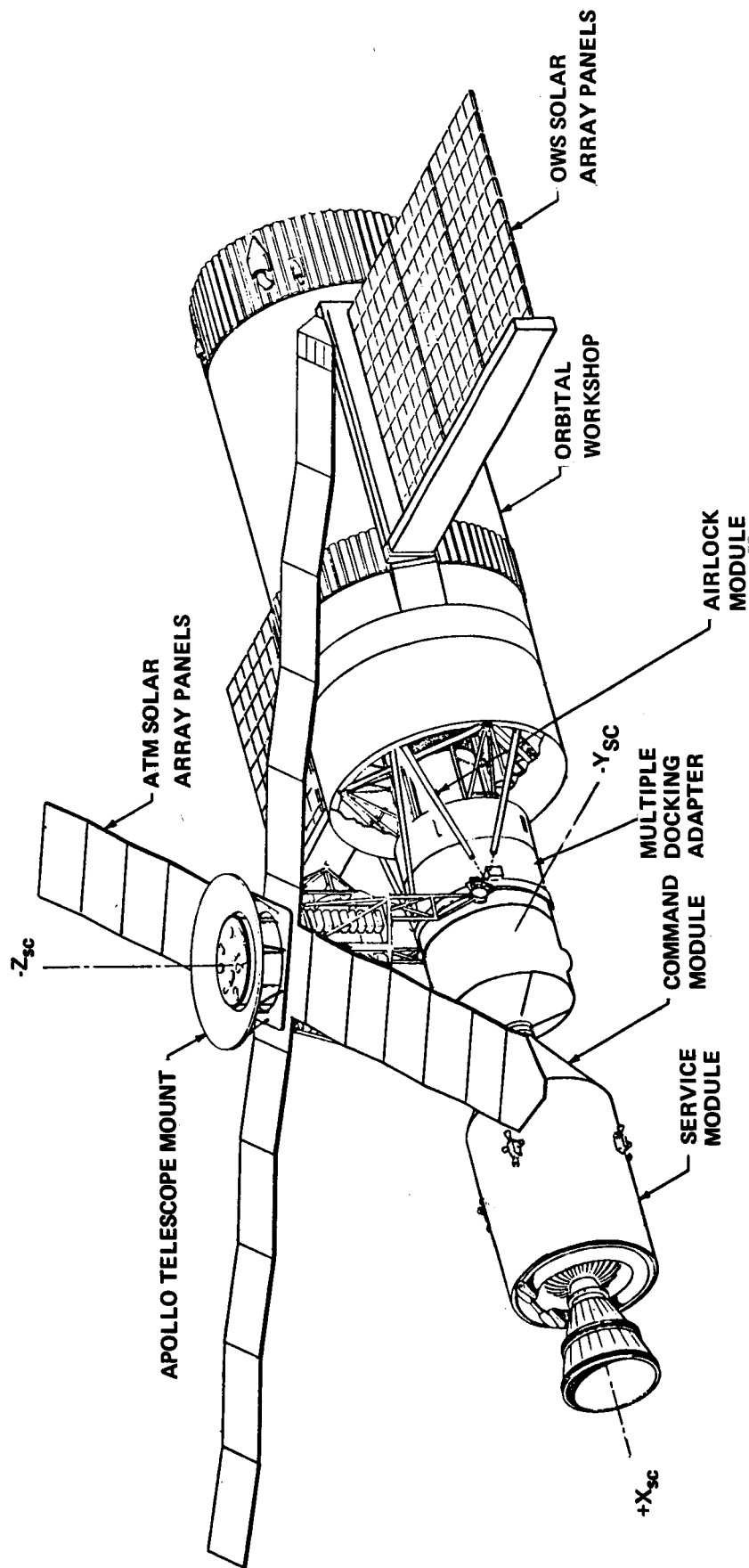


FIGURE 1 - DOCKED CONFIGURATION OF THE AAP CLUSTER

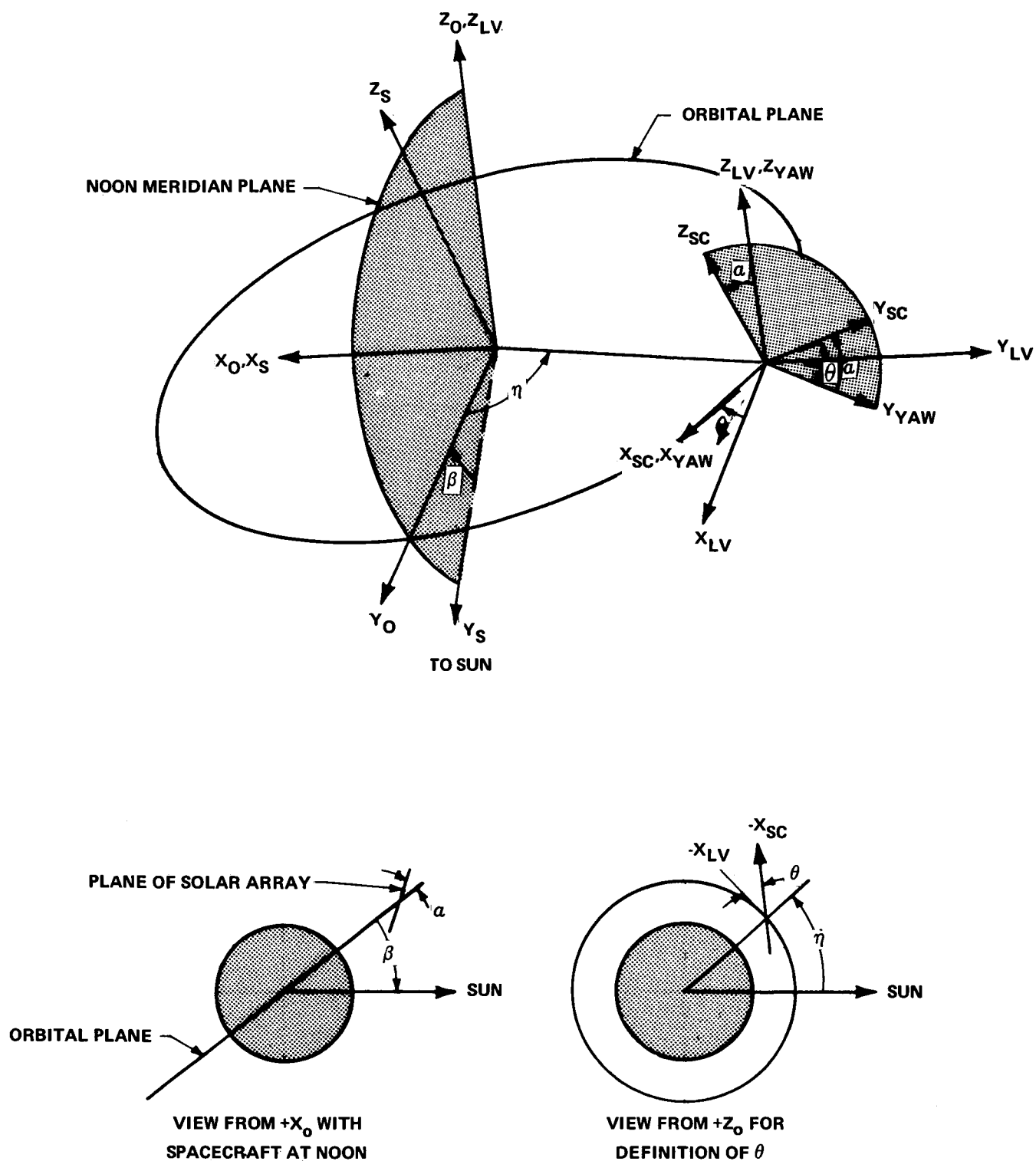


FIGURE 2 - DEFINITION OF SUN, ORBITAL, LOCAL VERTICAL, YAW, AND SPACECRAFT COORDINATE SYSTEMS

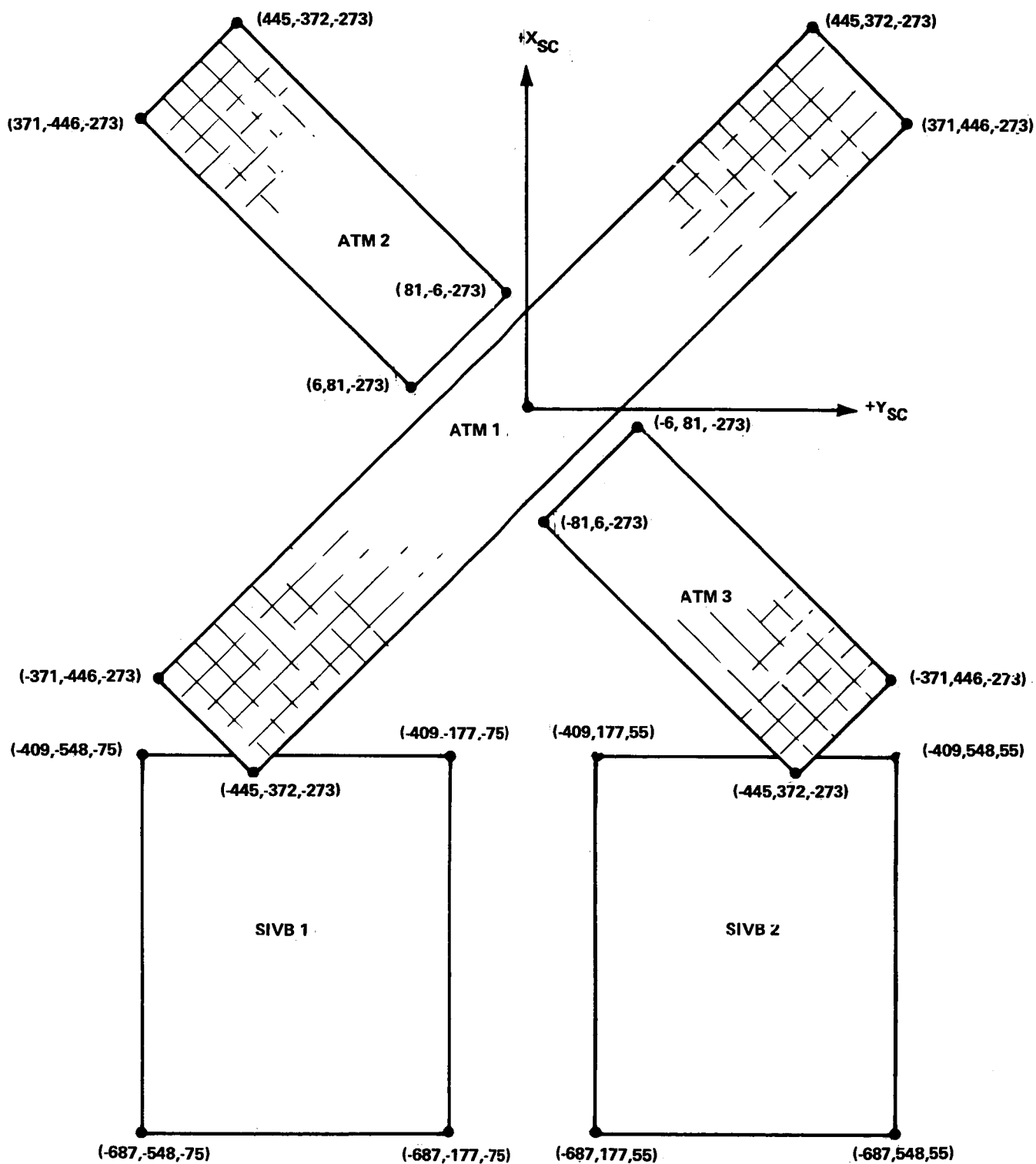


FIGURE 3 - ATM AND SWS SOLAR ARRAY CONFIGURATION AS VIEWED FROM $-Z_{SC}$ AXIS

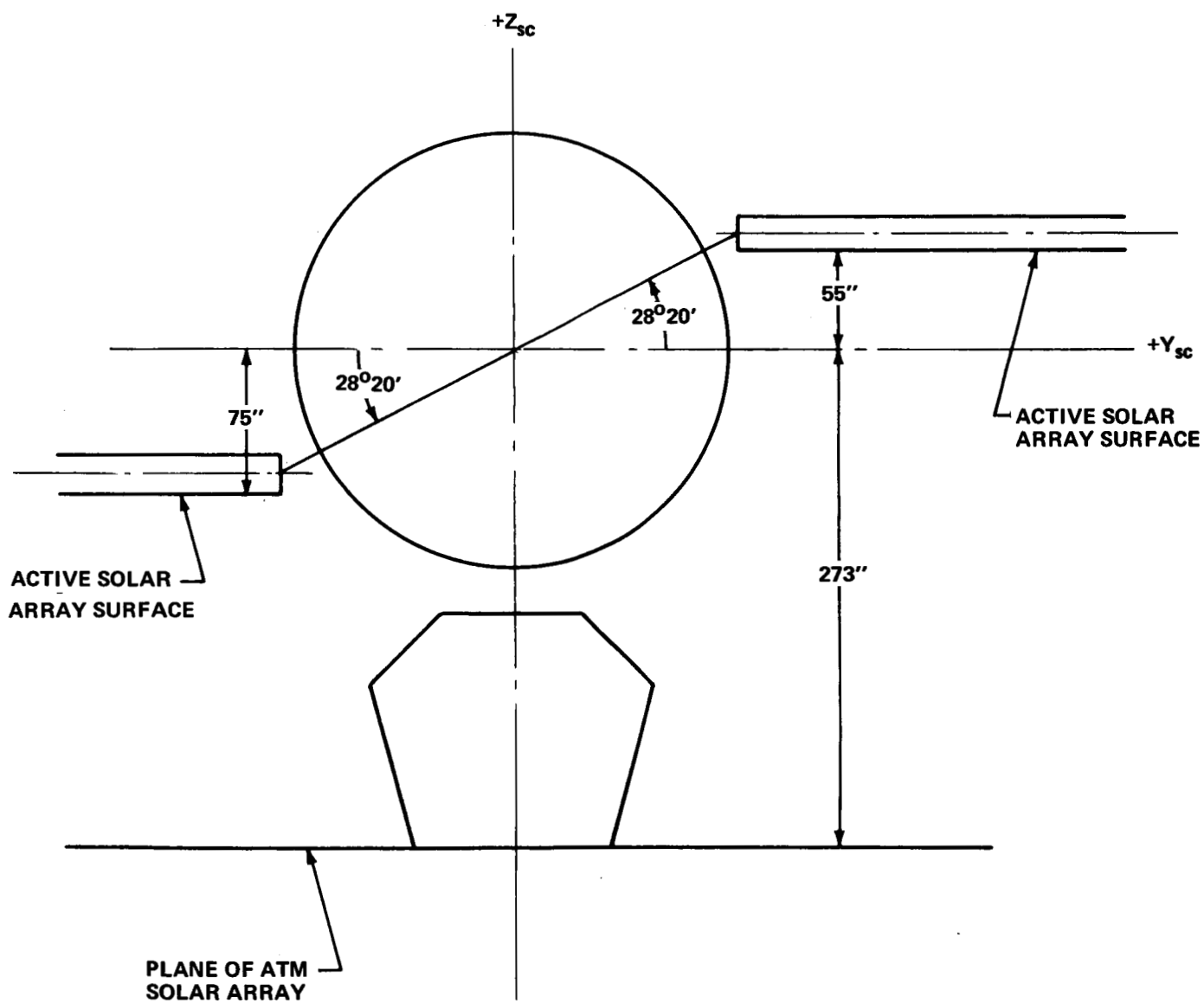
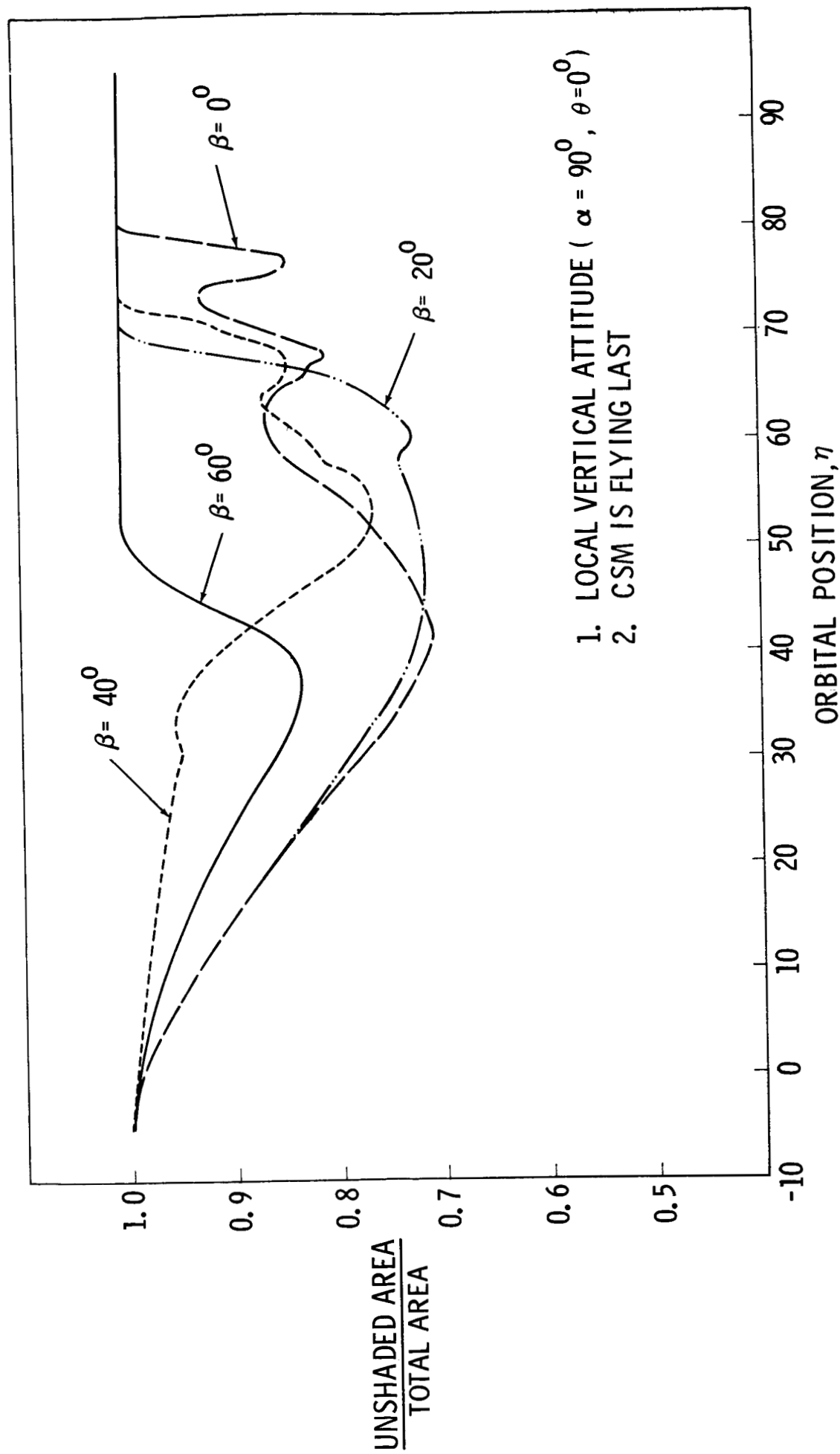


FIGURE 4 - CONFIGURATION OF THE ATM AND SIVB SOLAR ARRAYS



1. LOCAL VERTICAL ATTITUDE ($\alpha = 90^\circ, \theta = 0^\circ$)
2. CSM IS FLYING LAST

FIGURE 5 - RATIO OF UNSHADED AREA TO TOTAL AREA OF THE SIVB SOLAR ARRAY
FOR POSITIVE SUN ANGLES

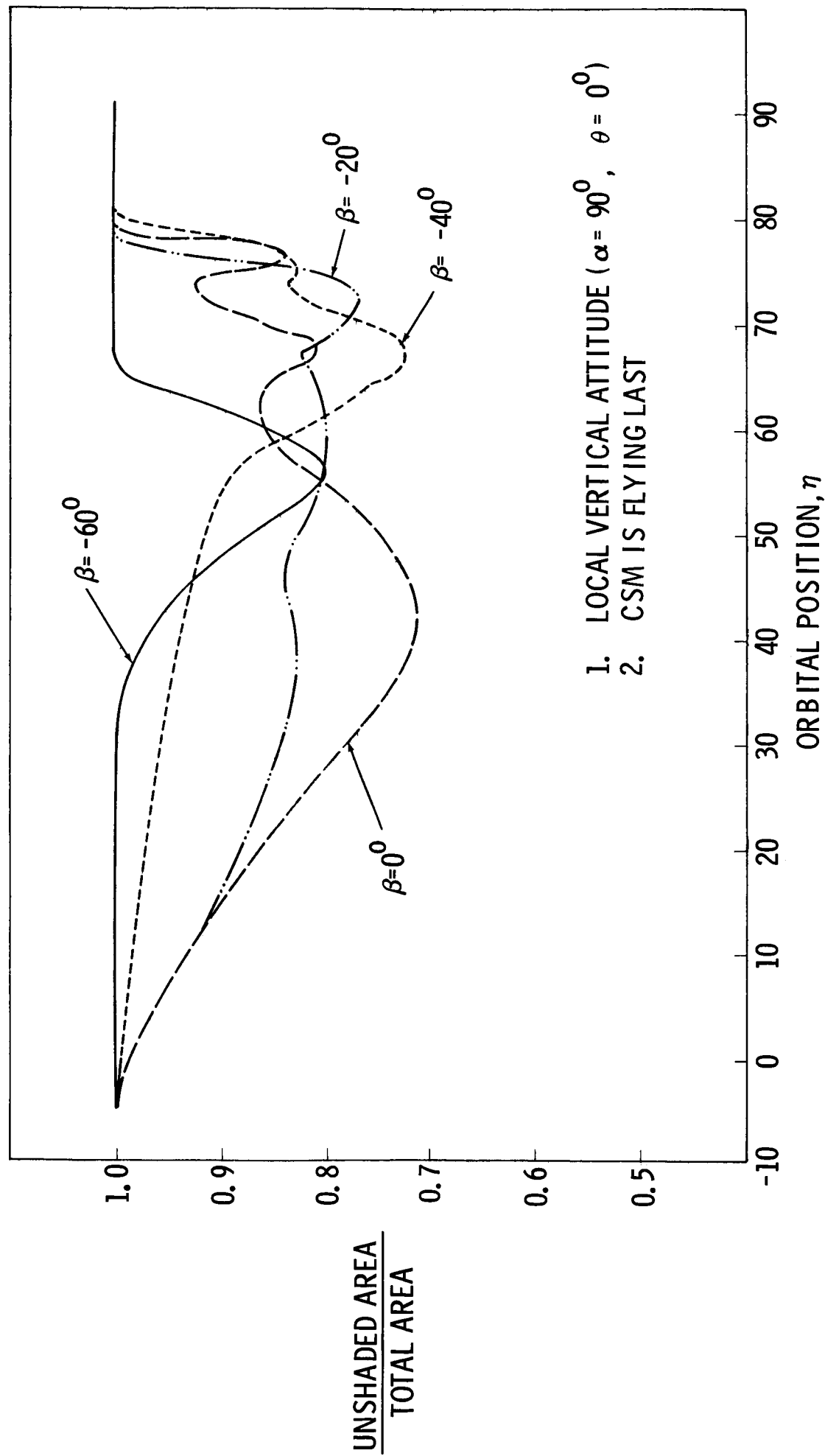


FIGURE 6 - RATIO OF UNSHADED AREA TO TOTAL AREA OF THE SIVB ARRAY FOR NEGATIVE SUN ANGLES

BELLCOMM. INC.

955 L'ENFANT PLAZA NORTH, S.W.

WASHINGTON, D. C. 20024

B70 03080

SUBJECT: Thermal Response of the ATM
Charger/Battery/Regulator
Modules During the Proposed
SL Earth Oriented Missions
Case 620

DATE: March 27, 1970
FROM: J. E. Waldo
D. P. Woodard
G. M. Yanizeski

ABSTRACT

The passively controlled ATM Charger/Battery/Regulator Modules (CBRM's) are shadowed in the solar inertial attitude. In the XIOP/ZLV attitude, needed for earth resources experiments, some CBRM's are exposed to direct solar heating, and the critical battery cells heat up. Five solar inertial to XIOP/ZLV missions were analyzed to determine transient cell temperatures. With a fully degraded thermal control coating, $\beta \leq 60^\circ$, and a 200 watt operating level, at least 1 sunlit pass can be completed. With a partially degraded coating or lower operating level, 2 or more consecutive passes can be completed.

SUBJECT: Thermal Response of the ATM
Charger/Battery/Regulator
Modules During the Proposed
SL Earth Oriented Missions
Case 620

DATE: March 27, 1970

FROM: J. E. Waldo
D. P. Woodard
G. M. Yanizeski

MEMORANDUM FOR FILE

I. INTRODUCTION

The Skylab Apollo Telescope Mount (ATM) is designed to operate in the thermal environment imposed by a solar inertial attitude. In the proposed XIOP/ZLV attitude for earth resources various passively controlled elements are exposed to space thermal environments that may be unsuited for their particular thermal characteristics. Of these elements, the ATM Charger/Battery/Regulator Modules (CBRM's) are critical.

The CBRM battery cells require relatively tight temperature control to insure adequate cell life. This is accomplished by the passive rejection of electrically generated waste heat. In the solar inertial attitude, the ATM shadow shield shades the CBRM's and acceptable cell temperatures are maintained. However, in the XIOP/ZLV attitude, direct solar heating may increase cell temperatures significantly.

The results and conclusions of this thermal study and other parallel studies conducted at the same time were presented to the Skylab Program Director and to the program offices at MSC and MSFC by D. R. Hagner/MLS.

II. BACKGROUND

The Charger/Battery/Regulator Modules accept electrical power from the ATM Solar arrays during the illuminated portion of the orbit and supply power to the ATM bus during the entire orbit. There is a total of 18 CBRM's, each consisting of 24 nickel cadmium battery cells, a series of 15 printed circuit boards, and various electronics mounted in a relatively heavy aluminum housing. Each CBRM weighs 110 lbs with the batteries (approximately 50 lbs) and the housing (approximately 25 lbs) comprising the majority of this total. Figure 1, illustrates the assembly of these

components for an earlier configuration. The current configuration is very similar except it is slightly larger (23.05" x 16.6" x 5.94"), and the connecting leads pass through the base instead of the sides.

A. Mounted Location

The CBRM's are mounted to the ATM rack shear panels in 3 arrays of 6 modules each. As indicated in Figure 2, the arrays are located adjacent to the 3 control moment gyros. The array in the -Y direction (Skylab coordinate) is radiantly illuminated by the CSM, which is axially docked to the MDA. All three arrays are radiantly illuminated by the ATM solar arrays and shadowed by the ATM solar shield while in the solar inertial attitude. However, in the XIOP/ZLV attitude, substantial direct solar heating can occur.

The details of the current array configurations are indicated in Figure 3. Although not shown, the CBRM's cover almost the entire shear panel except for a 3 inch strip exposed at the top and bottom. Each CBRM has six feet, which are bolted directly to the shear panel.

B. Thermal Characteristics

The electronics, the printed circuit boards, and the battery cells are mounted on the aluminum housing to remove by conduction the waste heat generated in these components. Part of the heat is radiated directly to space by the exposed surface of the CBRM housing, and the remainder is conducted to the shear panel and then rejected through a complex pattern of radiation and conduction through the ATM rack structure and the ATM cannister.

Ultimately, CBRM thermal control depends on the radiation of waste heat to space. Most of the ATM rack and its components are coated with S13-G thermal control paint which is well suited for rejecting heat in the solar inertial environment. This coating has a high stable emittance ($\epsilon=.9$) and a low initial solar absorptance ($\alpha=.2$). Although the absorptance is susceptible to ultraviolet degradation, this degradation is not an important factor in the solar inertial attitude because the ATM solar shield prevents direct solar heating. However, in the XIOP/ZLV attitude, substantial direct solar heating can occur and absorptance degradation is a consideration. Although ultraviolet degradation should be

insignificant based on earlier flight data³, MSFC is assuming a fully degraded coating ($\alpha=.5$) because of Skylab contamination effects.

C. CBRM Temperature Limits

Of the CBRM components, the battery cells are definitely the most sensitive to temperature. The specified temperature range is 32°F to 86°F, while a 41°F to 68°F is preferred. However, recent MSFC ASTR data indicate that cell temperatures up to 105°F can be tolerated for up to 2 hours a total of 15 times.

III. THE ANALYSIS

A. CBRM Configuration

The current CBRM configuration is used for this study and changes to the CBRM and ATM that might be beneficial to an XIOP/ZLV attitude are not considered. Therefore, this study analyzes the adequacy of the existing, unmodified system under various modeling assumptions described later in this section.

B. Sperry 430 Node Model of the CBRM

A 430 node CINDA* computer model¹ developed by the Sperry Rand Corporation for S&E-ASTR-MA is used in the analysis. This model was originally developed as a design tool to compute heat transfer and temperatures in the electronics and printed circuit boards. Consequently, the modeling detail generally expected in a 430 node model of this type is not reflected in and around the battery cells. However, the model is adequate in this study for battery cell thermal analysis in light of other uncertainties to be discussed.

C. Battery Heat Dissipation

Electrical waste heat profiles are important, but difficult to estimate. Battery waste heat dissipation is particularly difficult to determine, being an intricate, ill defined function of charge level, charge rate, and operating history. Calorimetry data² indicates that nickel cadmium battery cells generate most of their waste heat while discharging, which occurs primarily during the cool earth shadowed portion of the orbit in the solar inertial mission. However, overcharging at the end of the sunlit portion of the

*CINDA - "Chrysler Improved Numerical Difference Analyzer" is a general purpose thermal analyzer program that has been in general use by the Department 1022 Thermal Systems Group. It was developed at Chrysler for NASA.

orbit can cause a substantial peak in waste heat dissipation. Because of these uncertainties, the Sperry analysis simply uses a constant 20 watt heat dissipation rate for the 200 watt and 250 watt operating levels.

Recent tests indicate that present cell efficiency is better than expected; new, more efficient cells that guard against overcharge are likely to be flown. Therefore, 16 watt and 12 watt heat dissipation rates for the 200 watt and 150 watt operating levels were chosen as more reasonable in the Bellcomm analysis. Transient heat dissipation was not used because of the above uncertainties and because cell charge/discharge profiles had not been determined for the XIOP/ZLV missions at the time of the analysis.

D. Incident Thermal Radiation

The CBRM aluminum housing absorbs incident thermal radiation from the sun, the earth, and surrounding cluster surfaces. The calculation of these absorbed heats involved the combination of output from three complex computer programs:

1. "FLUX," developed at the Goddard Space Flight Center, is used to calculate incident solar, earth reflected solar, and earth-emitted thermal radiation.
2. "SHADE," also developed at the Goddard Space Flight Center, is used to calculate the solar shadowing of the housing front surface by other cluster elements.
3. "CONFAC," developed at North American Rockwell, is used to calculate geometric viewfactors from the ATM Solar Arrays and the CSM to the CBRM front surfaces.

The thermal inertia of the ATM solar arrays was introduced by using a simple one node model. The CSM shell was assumed to have zero thermal lag. CSM waste heat was ignored, and energy reflected from the CSM was assumed to be diffuse. The blockage of earth IR and albedo by cluster elements was ignored. In general, these simplifications and assumptions result in conservatively hot values. As a comparison, for the solar inertial attitude, $\beta=0^\circ$ * and $\alpha=.5$, ASTN calculated $52.7 \frac{\text{BTU}}{\text{HR FT}^2}$ orbit averaged absorbed energy on the

housing front while the Bellcomm value is $56.0 \frac{\text{BTU}}{\text{HR FT}^2}$. Table 1

* β as used here is positive, and the Y-axis CBRM's of interest are on the -Y side. There is a comparable case for negative β and the +Y side.

TABLE 1. ORBIT AVERAGED ABSORBED INCIDENT HEAT:

ATTITUDE	CBRM FACING AXIS	a	$Q_{AVG} \frac{BTU}{HR FT^2}$	ΔT_{CELL} FROM SI, $\beta = 0$
SOLAR INERTIAL $\beta = 0$	+X	.5	52.7 (ASTN)	—
			56.0	0°F
XIOP/ZLV $\beta = 0$	+X	.5	87.5	+11.7
XIOP/ZLV $\beta = 30$	-Y, +X	.5	76.6	+ 8.1
		.2	47.9	- 3.8
XIOP/ZLV $\beta = 60$	-Y	.5	172.3	+32.3
		.2	84.2	+10.5

lists the orbit averaged, incident heating values calculated at Bellcomm. Figure 4 illustrates three typical instantaneous orbital heating profiles.

E. Shear Panel Temperatures

Shear panel thermal behavior is linked intricately to the external space environment, the ATM rack structure, the rack-cannister enclosure, and the CBRM heat input. (The Sperry CBRM model includes shear panel temperature as an input constant which has been calculated by S&E-ASTN-PTE from a model which includes the above factors.)

Temperature differences between the $\beta = 0^\circ$, solar inertial case and the XIOP/ZLV cases have been estimated using an approximate model of the panel. The model includes the effects of the space environment, the ATM rack and interior, and the CBRM heat input as constants. The environmental loads were based on previously described orbital heat calculations; heat input from the CBRM's was obtained from the Sperry model; the cannister and ATM interior temperature was assumed to be 20°F as suggested by H. F. Trucks/S&E-ASTN-PTE. For the solar inertial environment, the model shows that a 37.2°F area-weighted-average panel temperature results when the panel edges are maintained at 35.6°F . For this case, only a small part (approximately 10%) of the total heat input to the panel leaves by conduction through the edges to the ATM rack structure; i.e., the panel edges appear to be isolated from the rack structure. This condition is assumed to apply for the XIOP/ZLV cases and is a conservative assumption provided the adjacent shear panels are not warmer than the hot CBRM housing.

Under these assumptions, the approximate analysis shows no significant change in steady state shear panel temperature from S/I, $\beta=0^\circ$, to XIOP/ZLV for $\beta=0^\circ$ and 30° . At $\beta=60^\circ$, XIOP/ZLV, the panel is approximately 19°F warmer. The resulting steady state cell temperature is increased approximately 10°F , but transient cell temperature in the first XIOP/ZLV orbit is not altered appreciably by changes in the shear panel. It is impractical to model the panel accurately for this study; consequently a panel temperature of 37.2°F , as used in the Sperry analysis for the hot, $\beta=0^\circ$, solar inertial case, has been used for all calculations.

F. Attitude Profile

Several attitude control schemes for acquiring the XIOP/ZLV attitude are possible; however, the effort required to thermally simulate all of them is not warranted in light of the relatively long CBRM thermal response time. Therefore, the following simplified attitude profile was devised: the solar inertial attitude is flown for four orbits to establish cyclic temperature profiles and then, after instantaneously

acquiring the XIOP/ZLV attitude, four or more additional orbits are flown. Each orbit begins and ends when leaving earth shadow so the XIOP/ZLV attitude is attained before passing the target area.

G. Cases Analyzed

Even with the simplified mission, considerable effort is required to calculate the space thermal environment and considerable computer time is required to simulate CBRM thermal response. Therefore, only five cases were run to establish CBRM thermal limitations in the earth resources mission. These five cases, described in Table 2, adequately cover the effects of β angle, operating power level P , and absorptance α , which are the three variables ultimately controlling CBRM thermal behavior.

TABLE 2

Case 1 - Panel 7 (+X axis), $\beta = 0^\circ$, $P=200$ watts, $\alpha=.5$
Case 2 - Panel 1 (-Y axis), $\beta=60^\circ$, $P=200$ watts, $\alpha=.5$
Case 3 - Panel 1 (-Y axis), $\beta=60^\circ$, $P=150$ watts, $\alpha=.5$
Case 4 - Panel 1 (-Y axis), $\beta=60^\circ$, $P=200$ watts, $\alpha=.2$
Case 5 - Panel 1 (-Y axis), $\beta=60^\circ$, $P=122$ watts, $\alpha=.5$

IV. RESULTS

Case 1 represents the hottest case in the $0^\circ < \beta < 30^\circ$ range for the XIOP/ZLV attitude. Panel 7 is the hottest CBRM location in this range, and it is hottest at $\beta=0^\circ$. With $\alpha=.5$, the fully degraded value, the orbit averaged absorbed heat

rate is 87.5 BTU/HR FT^2 . In addition, an operating level of 200 watts is imposed, which is probably a higher value than can be sustained by the solar arrays in an XIOP/ZLV attitude. Since, for this hot case, the calculated cell temperature as plotted in Figure 5 does not rise significantly above the 86°F normal limit and remains well below the 105°F maximum limit, no other cases were studied for $0^\circ < \beta < 30^\circ$.

For $\beta > 30^\circ$, the hottest CBRM location is panel 1 instead of panel 7. As β increases above 30° , the heat absorbed at panel 1 increases rapidly. At $\beta=60^\circ$, the highest

angle considered, the orbit average rate is $172.3 \text{ BTU/HR FT}^2$ for $\alpha=.5$. This is almost twice the rate used in case 1. Thus, case 2 with $\beta=60^\circ$, $\alpha=.5$, and $P = 200$ watts represents the extreme hot case. This is indicated in Figure 6 which shows a rapid increase in cell temperature after the XIOP/ZLV attitude is acquired. The strong effect of direct solar heating is evident. The number of sunlit passes that can be completed under these conditions is approximately 1.6.

Case 3 is identical to case 2 except a more realistic operating level of 150 watts is used. Again, as indicated in Figure 6, battery cell temperature increases rapidly during solar exposure in the XIOP/ZLV attitude. An extra XIOP/ZLV orbit is permissible at this reduced power level primarily because of lower cell temperatures in the solar inertial portion of the mission. The number of sunlit passes that can be completed for these conditions is approximately 2.6.

Case 4 is identical to case 2 except an undergraded absorptance ($\alpha=.2$) is used. This has a marked effect. The average heat rate is reduced to only 84.2 BTU/HR FT², or approximately half the rate used in case 2. As indicated in Figure 6, the battery cell temperature for case 4 does not exceed the 86°F specified limit after 5 sunlit passes in the XIOP/ZLV attitude.

A lower CBRM operating level is of interest. In one of the parallel studies it was determined that the ATM electrical power system is sufficient for three successive XIOP/ZLV passes at a reduced average load of 2200 watts, $\beta=60^\circ$, and a 70% battery depth of discharge. The equivalent CBRM operating level is 122 watts and the corresponding temperatures are shown in Figure 6, case 5.

V. CONCLUSIONS

CBRM battery cell temperatures are increased significantly at high β angles by direct solar heating in the XIOP/ZLV earth-oriented attitude. Several factors determine the number of successive sunlit passes that can be completed in this attitude before reaching the maximum allowable cell temperature of 105°F. For the conditions studies, i.e., the XIOP/ZLV attitude is preceded by four orbits in the solar inertial attitude and the shear panel temperature is 37.2°F, it was found that the number of successive sunlit passes is determined by further conditions, as follows:

1. For an undegraded coating value of $\alpha=.2$, $\beta<60^\circ$, and a CBRM operating level of 200 watts, at least 3 sunlit passes can be completed.
2. For a degraded coating value of $\alpha=.5$, $\beta<60^\circ$, and a CBRM operating level of 122 watts, at least 3 sunlit passes can be completed.
3. For a fully degraded coating value of $\alpha=.5$, $\beta<60^\circ$, and a CBRM operating level of 150 watts, at least 2 sunlit passes can be completed.

4. For a fully degraded coating value of $\alpha=.5$, $\beta \leq 60^\circ$, and a CBRM operating level of 200 watts, at least 1 sunlit pass can be completed.

J. E. Waldo

J. E. Waldo

D. P. Woodard

D. P. Woodard

George Yanizeski

G. M. Yanizeski

JEW
1022-DPW-bw
GMY

Attachments

BELLCOMM. INC.

References

1. L. H. Usher and W. E. Schultz, "Thermal Analysis of the Charger/Battery/Regulator/Module," Sperry Space Support Division report prepared for S&E-ASTR-MA under TD 216-808, August 11, 1969.
2. John P. Millard, "Results from the Thermal Control Coatings Experiment on OSO-III," Progress in Astronautics and Aeronautics, Volume 21, page 769 or presented as AIAA paper 68-794, June 24, 1968.
3. "Cluster Systems Description Document," prepared by the Martin Marietta Corporation for MSFC under NAS8-24000, May, 1969.

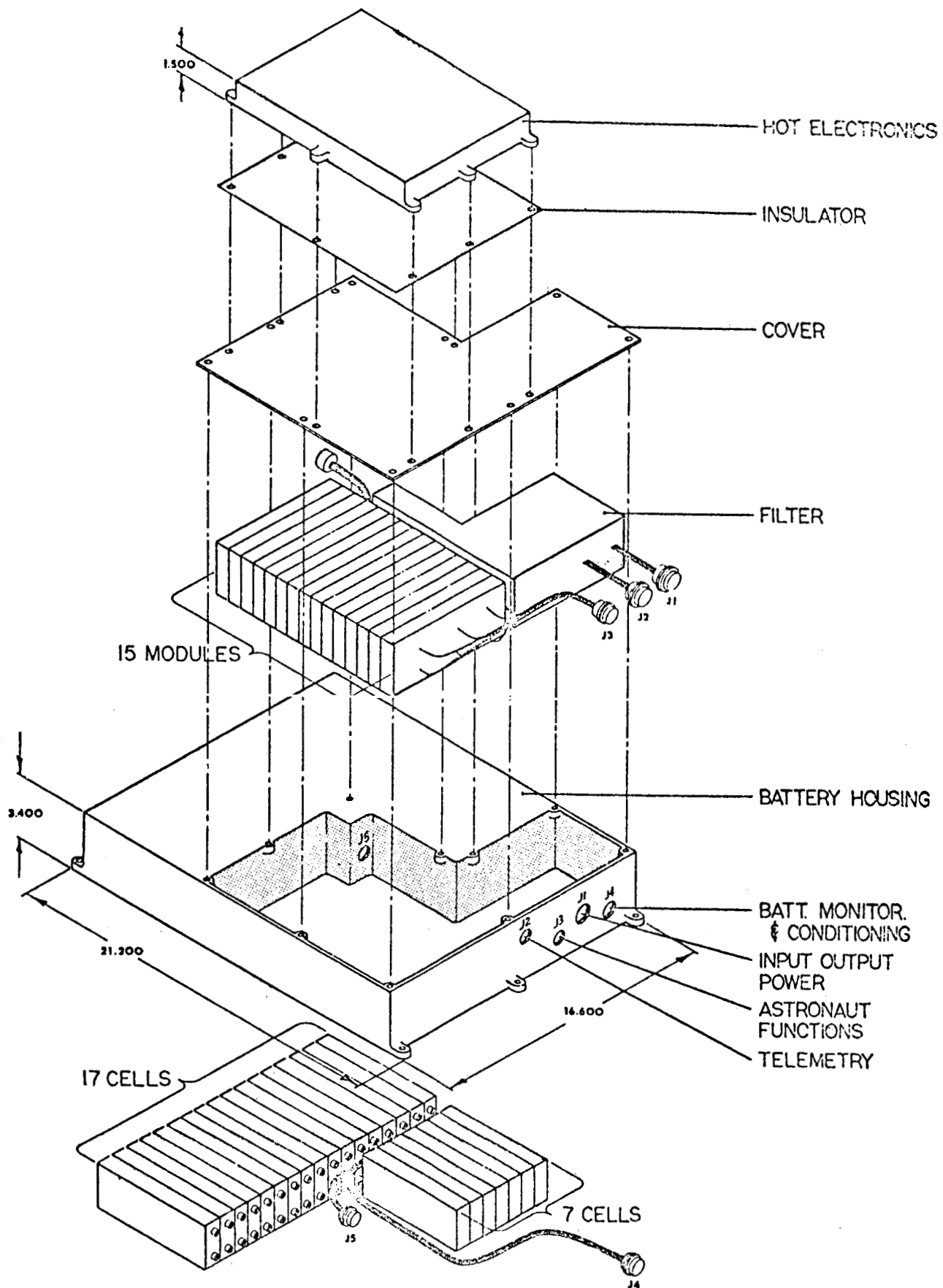


FIGURE 1 - CHARGER-BATTERY-REGULATOR MODULE
 (REF. 1)

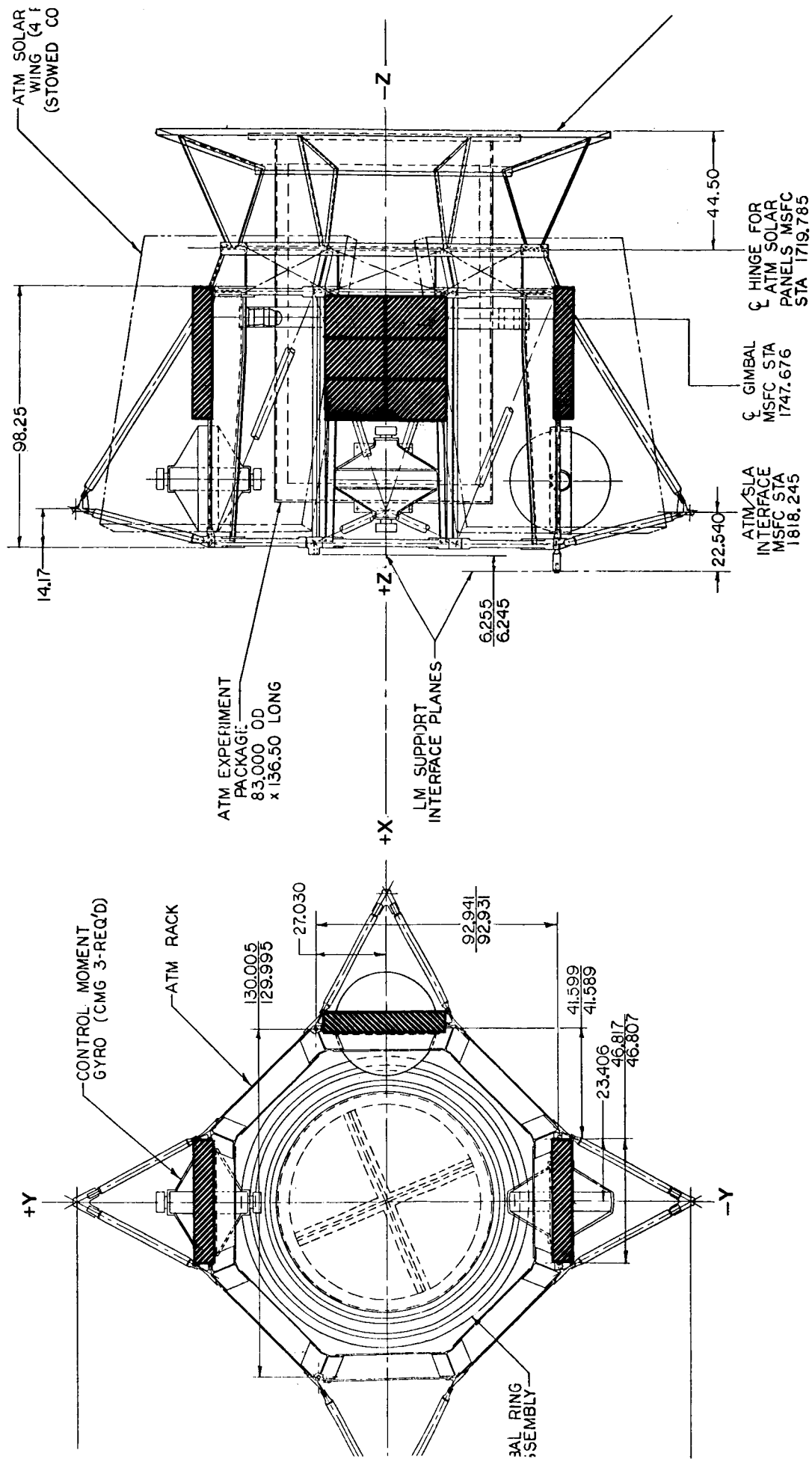


FIGURE 2 - LOCATION OF CRBM ARRAYS
(CROSS HATCHED AREAS)
(MODIFIED FROM REF. 3)

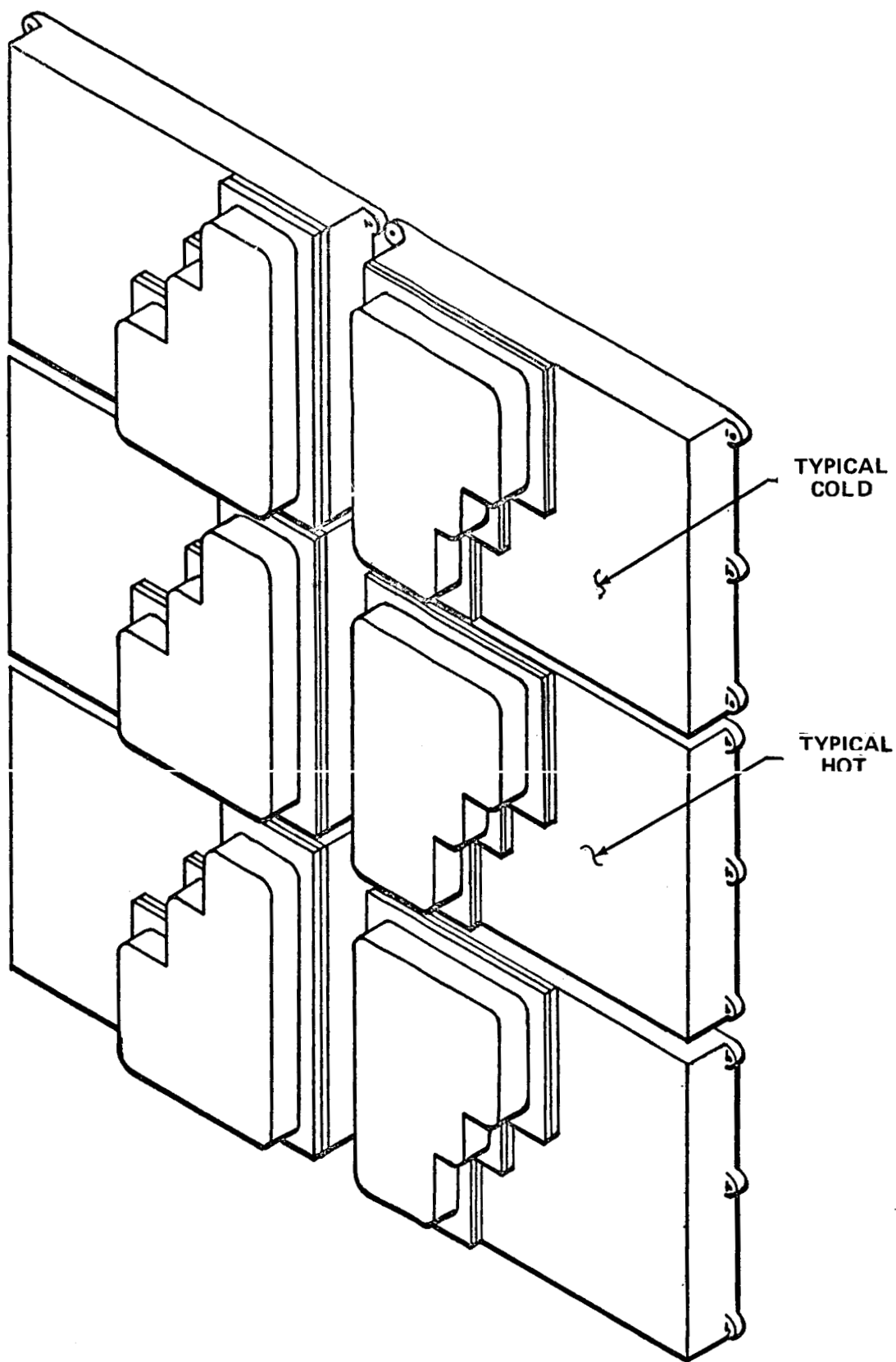


FIGURE 3 - TYPICAL CBRM ARRAY CONFIGURATION
(FIG. 1 FROM SPERRY RAND REPORT)
(REF. 1)

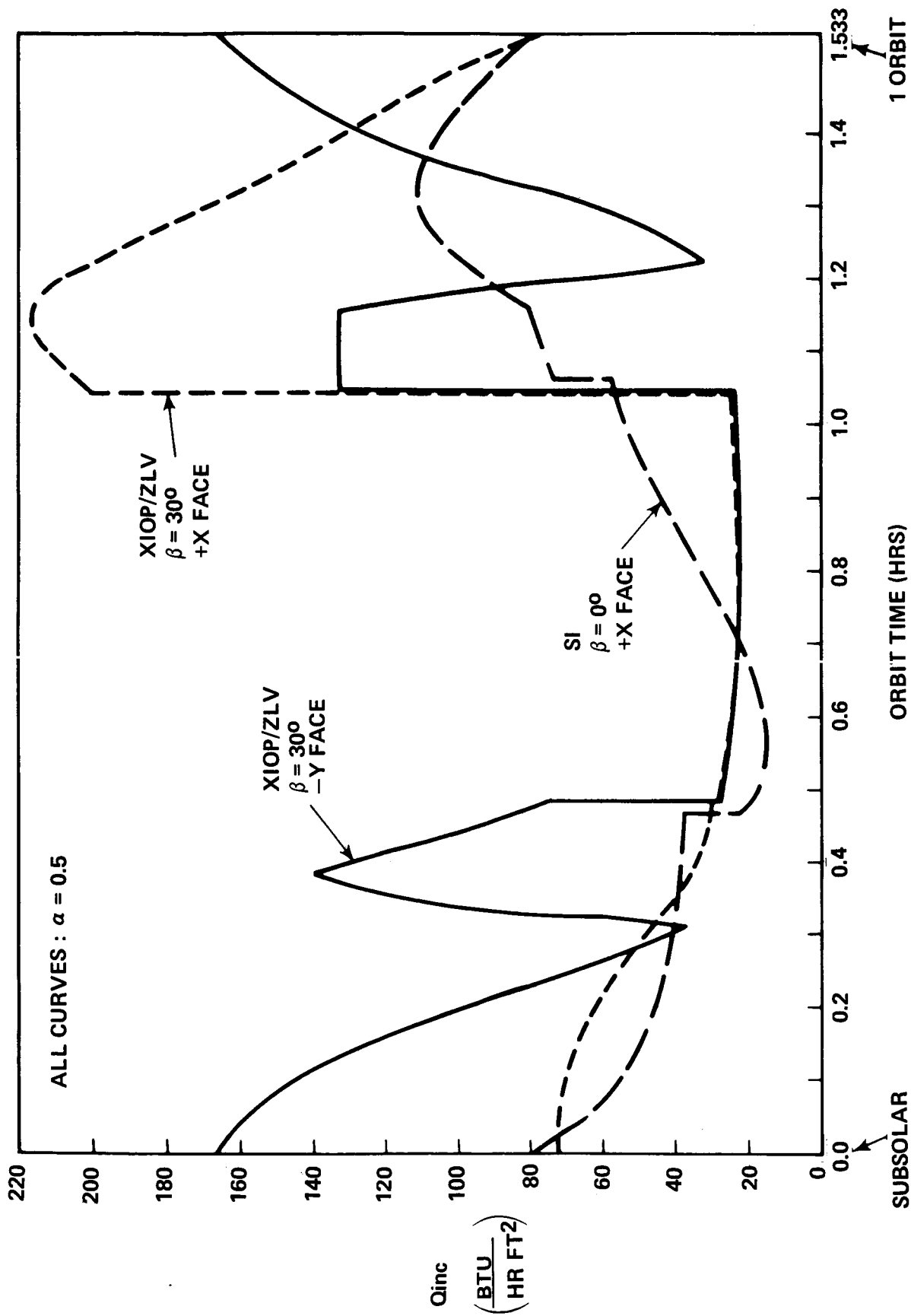


FIGURE 4 - THREE ABSORBED HEATING PROFILES

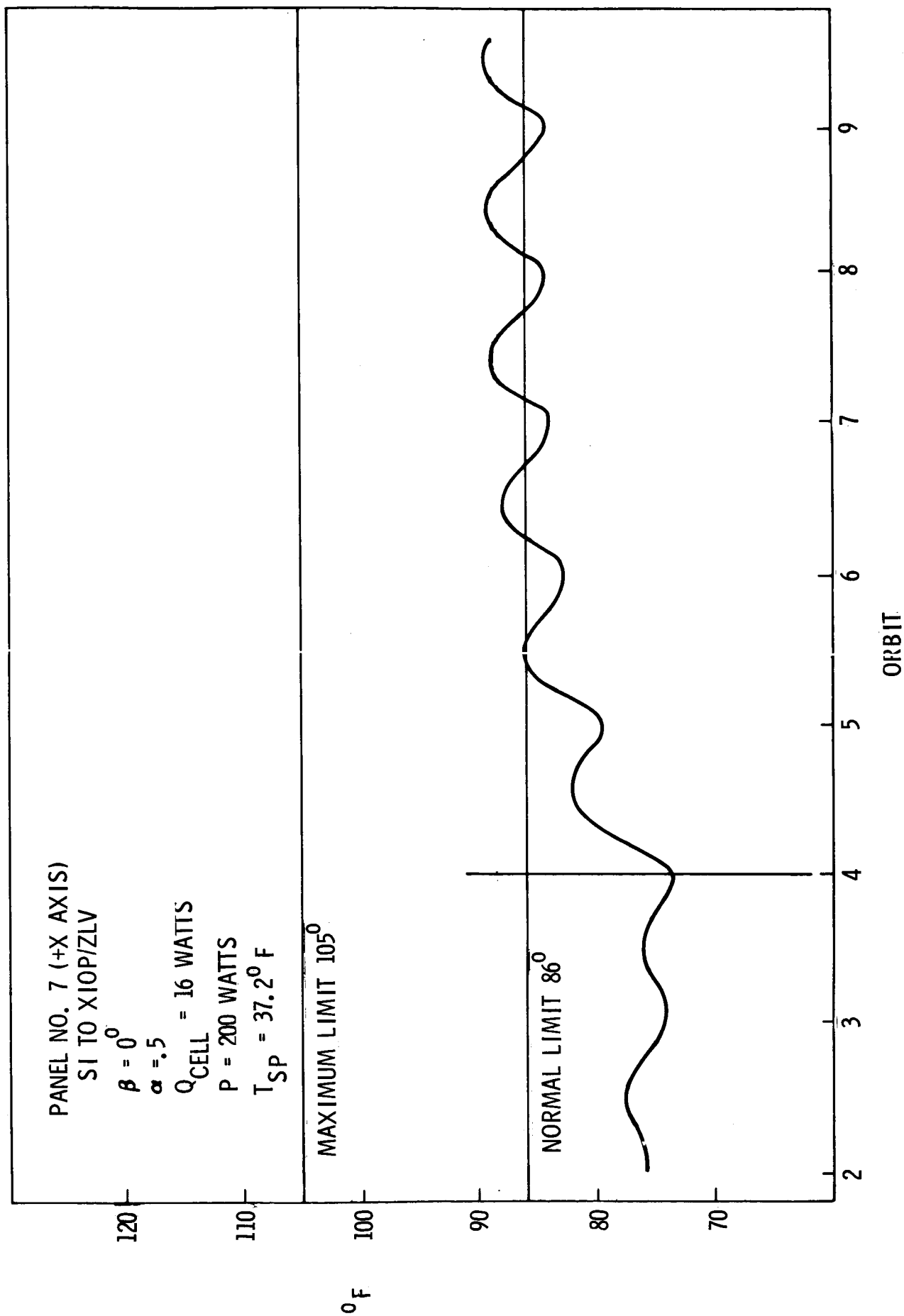


FIGURE 5 - TRANSIENT BATTERY CELL TEMPERATURE FOR CASE 1

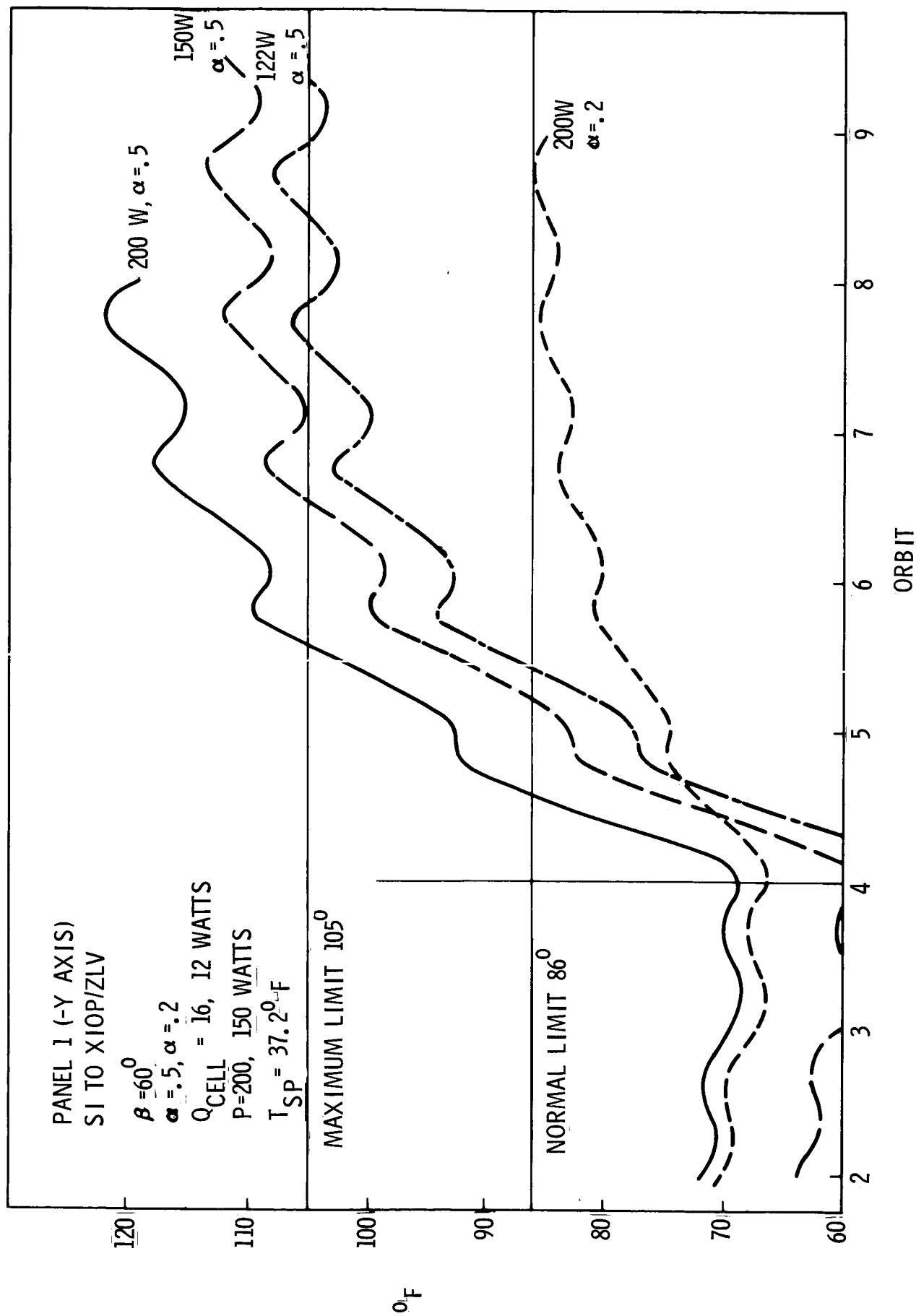


FIGURE 6 - TRANSIENT BATTERY CELL TEMPERATURE FOR CASE 2-5

BELLCOMM, INC.

Subject: Thermal Response of the ATM
Charger/Battery/Regulator
Modules During the Proposed
SL Earth Oriented Missions
Case 620

From: J. E. Waldo
D. P. Woodard
G. M. Yanizeski

Distribution List

NASA Headquarters

H. Cohen/MLR
J. H. Disher/MLD
W. B. Evans/MLO
L. K. Fero/MLV
J. P. Field, Jr./MLP
W. H. Hamby/MLO
T. E. Hanes/MLA
T. A. Keegan/MA-2
M. Savage/MLT
W. C. Schneider/ML

GSFC

J. T. Skladany/713

Langley Research Center

P. R. Kurzhals/AMPD

MSC

R. G. Brown/ES-16
C. N. Crews/KS
W. R. Cunningham/CB
R. E. Durkee/ES-5
R. L. Frost/KS
O. K. Garriott/CB
F. C. Littleton/KM
R. M. Machell/KF
P. S. Miglicco/KS
O. G. Smith/KF
H. E. Whitacre/KM

MSFC

R. M. Aden/S&E-ASTR-E
W. B. Chubb/S&E-ASTR-SGD
J. C. Cody/S&E-ASTN-PLA
D. N. Counter/S&E-ASTR-MA
C. B. Graff/S&E-ASTR-EP

MSFC (continued)

G. B. Hardy/PM-AA-EI
G. D. Hopson/S&E-ASTN-PL
E. H. Hyde/S&E-ASTN-PF
H. F. Kennel/S&E-ASTR-A
G. F. McDonough/S&E-CSE-A
E. F. Noel/S&E-ASTR-SI
W. C. Patterson/S&E-ASTN-PLA
J. W. Sims/S&E-ASTN-PTA
J. D. Stroud/S&E-ASTR-SE
J. W. Thomas/PM-AA
H. F. Trucks/S&E-ASTN-PTA
J. L. Vaniman/S&E-ASTN-PT
R. D. Wegrich/S&E-CSE-AA
A. P. Woosley/S&E-ASTR-SEC
H. E. Worley/S&E-AERO-DOI

Martin-Marietta

H. S. Nassen/Denver
E. F. Bjoro/Washington
M. S. Imamura/Denver
R. W. Wilson/Denver

McDonnell-Douglas

G. Weber/Eastern Division

Bellcomm

A. P. Boysen
D. R. Hagner
W. G. Heffron
B. T. Howard
J. Z. Menard
J. M. Nervik
I. M. Ross
P. F. Sennewald
J. W. Timko
R. L. Wagner
M. P. Wilson
Departments 2031, 2034 Supervision
Department 1024 File
Division 102
Central Files
Library

BELLCOMM, INC.

955 L'ENFANT PLAZA NORTH, S.W.

WASHINGTON, D. C. 20024

B70 01059

SUBJECT: Solar Array Temperatures During
the AAP-SWS Earth Pointing
Experiments Mission Mode
Case 620

DATE: January 28, 1970

FROM: J. W. Powers

ABSTRACT

An accurate prediction of the electrical power available from the solar array of a spacecraft must consider the panel time-temperature profile. Solar array time-temperature data are presented for three flight attitudes being studied for the earth pointing experiments of the AAP-SWS 1 mission. These attitudes are earth pointing for the total orbit; solar inertial for the two mission segments of a single orbit before and after earth pointing; an earth oriented attitude which maximizes the array power output for the two mission segments of a single orbit before and after earth pointing.

SUBJECT: Solar Array Temperatures During
the AAP-SWS Earth Pointing
Experiments Mission Mode
Case 620

DATE: January 28, 1970

FROM: J. W. Powers

MEMORANDUM FOR FILE

I. INTRODUCTION

To make an accurate prediction of electrical power available from a spacecraft's solar array the temperature-time profile of the panel must be known. This temperature profile will be a function of the following parameters: materials, proportions and coating properties of the panel; orbit characteristics; panel attitude; sun angle inclination; reflective, radiative and geometric characteristics of other vehicle components which shadow and/or emit thermal flux to the panel.

If the earth pointing attitude required for the earth resources experiments of AAP-SWS 1 is maintained for the total sunlight portion of the orbit, a major reduction of solar array electrical power from decreasing incident solar flux will occur. Different flight profiles which increase the orbit averaged electrical power output are under study for the earth pointing experiments portion of the mission. These profiles consider flight attitudes other than earth pointing for the sunlight portions of a single orbit before and after the earth pointing mission segment.

Approximate solar array temperatures as functions of orbital position have been obtained for missions in which the panel orientation changes during a single orbit. This analysis uses the CINDA and GSFC Thermal Flux¹ Computer Programs.

In Reference 2 OWS solar array panel temperatures for an inertial spacecraft attitude have been developed without use of the flux program.

II. EARTH RESOURCES EXPERIMENT SUN CONSTRAINT

The S-101 experiment sun illumination constraint is some maximum angle relative to the sun-earth line. The geometry of this constraint may be visualized as a right circular cone of vertex angle Δ whose axis is the sun-earth line with the

vertex at the earth center. For circular orbits the experiment pointing zone is that spherical surface area contained within the intersection of the sun constraint cone and orbital sphere. If β is the angle between the orbital plane and sun-line, and η_{sc} is the total noon centered angle in the orbital plane during which the experiment may operate, the relationship between angles is $\cos(\Delta/2) = \cos\beta \cos(\eta_{sc}/2)$.

Maximum earth pointing time occurs at $\beta=0$, and the limiting case of zero earth pointing time occurs at $|\beta| = \Delta/2$. The sun constraint angle used in this analysis is $\Delta = 120^\circ$. Figure 1 shows the earth pointing time for a 235 NM circular orbit as a function of β angle.

III. FLIGHT ATTITUDES

The earth resources experiment viewing axis(z) is normal to the SWS-axis (x) and 180° away from the ATM-axis. During earth pointing the vehicle is positioned in the orbit with the SWS-axis in the orbital plane and the z-axis in the direction of the local vertical. This earth pointing attitude is defined X-IOP/Z-LV and is maintained for full sunlight travel during one of the modes. In this attitude the orbit averaged solar array electrical power is reduced by the following effects as compared with the solar inertial attitude (SI): The cosine loss experienced for positions away from orbital noon; the cosine loss experienced when $|\beta| > 0$; the reduced sunlight travel time of the panels which is limited to $\pm 90^\circ$ from the orbital noon position.

The second flight mode is SI outside the earth pointing zone. The transition period between the earth pointing attitude and other flight attitudes in a single orbit is discussed in Section IV.

In the third flight mode the SWS solar array panels are not normal to the orbital plane during the two segments of a single orbit before and after earth pointing. This optimum roll (OR) attitude is like X-IOP/Z-LV except that the solar array plane is rotated so that maximum orbit averaged panel area normal to the solar vector occurs outside the earth pointing zone. This maximization is a consequence of the longer sunlight angular travel ($>90^\circ$ and $<270^\circ$) with canted array panels and $|\beta| > 0$. If β is defined as positive for noon positions of the orbital plane below the ecliptic plane, the corresponding array plane optimum rotation direction is about the minus X-axis considering the right hand rotation rule. If ϕ is the angle of the array plane rotation measured from the normal to the orbital plane and η is the vehicle position angle in the orbit measured from noon, the angle (γ) between the array plane normal vector and the solar vector is obtained from

$$\cos \gamma = \cos \phi \cos \eta \cos \beta + \sin \beta \sin \phi$$

For $\beta < \sin^{-1}[R/(R+h)]$ there is some orbital position angle ($>90^\circ$ and $<180^\circ$ measured from noon) at which the panel will either enter the zone of the earth's shadow (η_{es}) or will be self shadowed (η_{ss}). If $\beta \geq \sin^{-1}[R/(R+h)]$ no earth shadowing of the panel will occur. Self shadowing begins at the position where the array normal and solar pointing vectors are perpendicular. These angles are

$$\eta_{es} = \cos^{-1} \left[\frac{\sqrt{2Rh+h^2}}{(R+h) \cos \beta} \right]^*$$

$$\eta_{ss} = \cos^{-1}(-\tan \beta \tan \phi)**$$

where h and R are the circular orbit altitude and earth radius.

Optimum ϕ is the roll angle about the X-axis which maximizes the integral $\int_{\eta_{sc}}^{\eta_j} \cos \lambda d\eta$, where η_j is the minimum

value of either η_{es} or η_{ss} . The optimum roll angle is thus a function of β angle and may be a function of orbital altitude. For a 235 NM circular orbit the following data are from a computer program developed by Mrs. P.R. Dowling:

Sun Angle, β°	Optimum Roll Angle, ϕ°
0	0
5	19.93
10	46.13
15	72.86
30	80.73
45	83.00
60	80.10

*This angle is an output of the flux program

**This angle can be determined from the flux program to within the accuracy of the orbital angular increment selected by observing the position at which the direct solar flux becomes zero.

IV. TRANSITION FROM EARTH POINTING TO OTHER FLIGHT ATTITUDE

The S/C transition in the orbital plane from earth pointing to either the SI or the OR attitude will require RCS induced rotations in some finite time. Achieving the SI attitude requires a rotation $\eta_{sc} + \xi$ about the y-axis, where ξ is the orbital angle traveled during the maneuver execution time. A β angle rotation about the SWS X-axis must also be performed during the transition maneuver to the SI mode. After the SI position has been achieved an angular velocity equal to the orbital angular velocity must be impressed about the S/C y-axis to maintain the attitude. Achieving the OR attitude requires only a vehicle roll thru an angle ϕ about the X-axis. From electrical power considerations, the transition maneuver should be quickly executed for maximum array illumination time; but for minimum RCS propellant expenditure, the maneuver should be as long as possible.

Rotation about the y-axis to achieve the SI attitude from the earth pointing attitude during sunlight orbital travel must be at a rate greater than the orbital rate (0.0644 deg/sec for a 235 NM circular orbit). If $\dot{\eta}$ and ω_y are the respective orbital and vehicle y-axis turning rates, the time equality to rotate the vehicle to the SI attitude in a transition angle ξ is

$$\xi/\dot{\eta} = (\xi + \eta_{sc})/\omega_y$$

The total angle η_{si} that the vehicle spends in the SI attitude during an orbit is

$$\begin{aligned} \eta_{si} &= 360-2 (\eta_{es} + \eta_{sc} + \xi) \\ &= 360-2 \left\{ \cos^{-1} \left[\frac{\sqrt{2 Rh+h^2}}{(R+h) \cos \beta} \right] + \left(\frac{\omega_y}{\omega_y - \dot{\eta}} \right) \cos^{-1} \left(\frac{\cos \Delta/2}{\cos \beta} \right) \right\} \end{aligned}$$

Figure 1 shows the times in the SI attitude as a function of β for different vehicle y-axis rotational rates.

Although the details of the earth pointing to SI transition maneuver have not been defined, it must be formulated considering both the limits of the x and y axis vehicle rotational rates and the β angle effects tabulated below. For a 235 NM circular orbit altitude and sun constraint angle of 120° the β effects are

	<u>$\beta=0^\circ$</u>	<u>$\beta =60^\circ$</u>
Earth pointing angle	Maximum (120°)	Minimum (0°)
Illuminated orbital arc	Minimum (221.24°)	Maximum (269.54°)
Transition angle for y-axis rot.	Maximum*	Minimum (0°)
Transition angle for x-axis rot.	Minimum (0°)	Maximum (60°)

If the vehicle angular velocities about the x and y axes are not equal the respective times to achieve the SI attitude with respect to rotational axes are β/ω_x and $\cos^{-1}(\frac{\cos\Delta/2}{\cos\beta})/(\omega_y - \dot{\eta})$.

For the numerical analysis the ω_x and ω_y angular velocities were assumed to be capable of attaining the SI mode in a 30° transition angle for $\beta=20^\circ$, 40° and a 45° transition angle was assumed for $\beta=0^\circ$, 60° .

V. SOLAR ARRAY THERMAL MODEL

A single two surface node with the appropriate absorptivity (α) and emissivity (ϵ) on each face was used as the solar array thermal model. The array planer surfaces receive time varying direct solar, earth reflected solar, and earth emitted IR thermal fluxes as functions of altitude, attitude and orbital position relative to the sun. Deep space is a boundary node at -460°F . No thermal gradients are assumed in the array (infinite isotropic thermal conductivity). The energy balance on the array panel is as given by Equation (1) of Reference 2 and will not be repeated here. Although a SWS geometry model exists for use in the GSFC shadowing program¹, shadowing of the SWS arrays by other workshop components was not considered in this study. No thermal interchange between radiation reflected and emitted by vehicle components adjacent to the arrays was considered.

*Dependent upon y-axis vehicle rotational rate

Surface coating properties and physical properties of the array from Reference 2 are

Front surface $\alpha/\epsilon = 0.7/0.8$

Back surface $\alpha/\epsilon = 0.9/0.9$

Composite Mass Density = 1.527 lb/ft²

Composite Specific Heat = 0.2 Btu/lb - °F

Incident thermal fluxes as functions of orbital position for a 235 NM circular orbit and different β angles were obtained by use of the GSFC flux program. These fluxes were determined at 15° orbital increments and at entry to and exit from the earth shadow zone. In the transition zones from the earth pointing to the SI and OR attitudes and vice versa linear interpolation between the flux values at the beginning and end of the transition segment was used.

Figure 2 shows array steady-state temperature vs orbit position for the earth pointing attitude during the complete orbit at the optimum (0°) and worst (60°) β angle conditions relative to available earth pointing time.

Figure 3 shows the array temperatures for β angles of 0° and 60° and includes the transition sections to the SI attitude outside of the earth pointing zone. Figure 3 also shows the limiting upper temperature curve for this altitude which occurs at $\beta=0$ with the solar array in the SI attitude for the complete orbit. Reduced darkside travel occurs with increasing β . The maximum temperature occurs at $\beta=0$ from the higher albedo and IR fluxes on the panel back face. Figure 4 shows the earth pointing-OR attitude with included transition sections for β angles of 20° and 60°. For $\beta=0$ this attitude is identical to earth pointing for the complete orbit (Figure 2). The anticipated maximum and minimum time-temperature profiles for the three earth pointing modes considered are seen in the earth pointing-SI mode (Figure 3) and earth pointing mode (Figure 4). These data were obtained by use of the CINDA Program with an assumed initial solar array temperature of 130°F at noon and all examples show the third complete orbit.

In a 235 NM circular orbit the spacecraft is 100% in the sun for $|\beta| > 69.4^\circ$. For $|\beta| = 69.4^\circ$, 235 NM, and the SI mode for the complete orbit, the array temperature profile is approximately constant with a 135°F maximum occurring shortly after orbital noon. A minimum array temperature of 125°F for this case occurs after about 180° of orbital travel from the maximum position. For this high inclination SI case the maximum array temperature is approximately 36°F below the maximum temperature for the $\beta = 0$ SI case. A lower maximum array temperature for the high β angle 100% sunlight orbit as compared with the minimum sunlight orbit is caused by the reduced incident albedo and IR thermal fluxes.

J.W. Powers
J. W. Powers

1022-JWP-mef

Attachments
References
Figures 1-4

BELLCOMM, INC.

REFERENCES

1. J. W. Powers, "Spacecraft Shadowing and Thermal Flux Computer Programs with Sample Problems", Bellcomm Memorandum for File, July 8, 1968.
2. J. Gillespie, "OWS Solar Array Temperature", Bellcomm Memorandum for File, March 18, 1969.

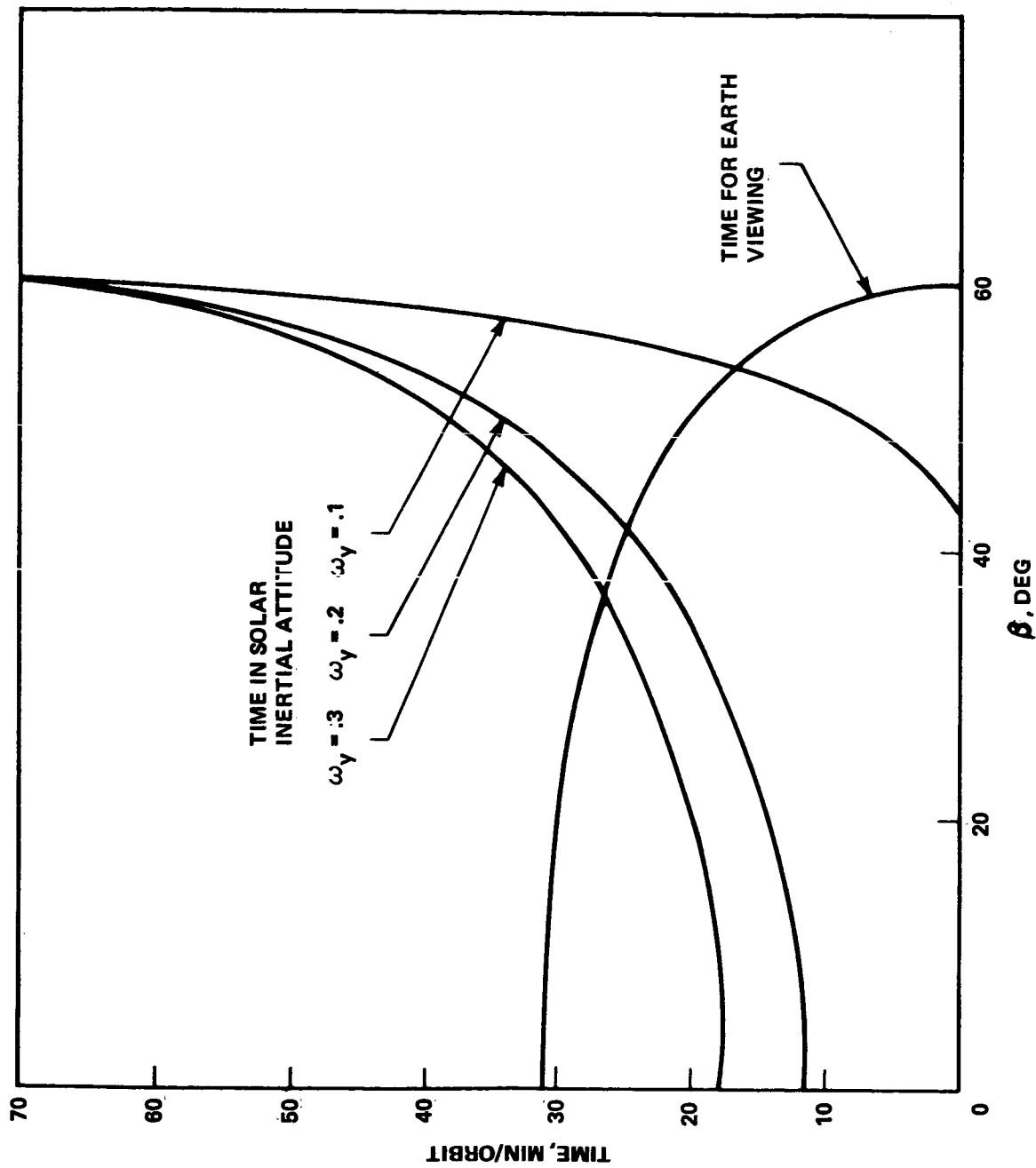


FIGURE 1 - EARTH-VIEWING-SOLAR INERTIAL ATTITUDE, EARTH-VIEWING & SOLAR INERTIAL TIMES
235 NM CIRCULAR ORBIT AND DIFFERENT VEHICLE ROLL RATES (ω_y = DEG/SEC)

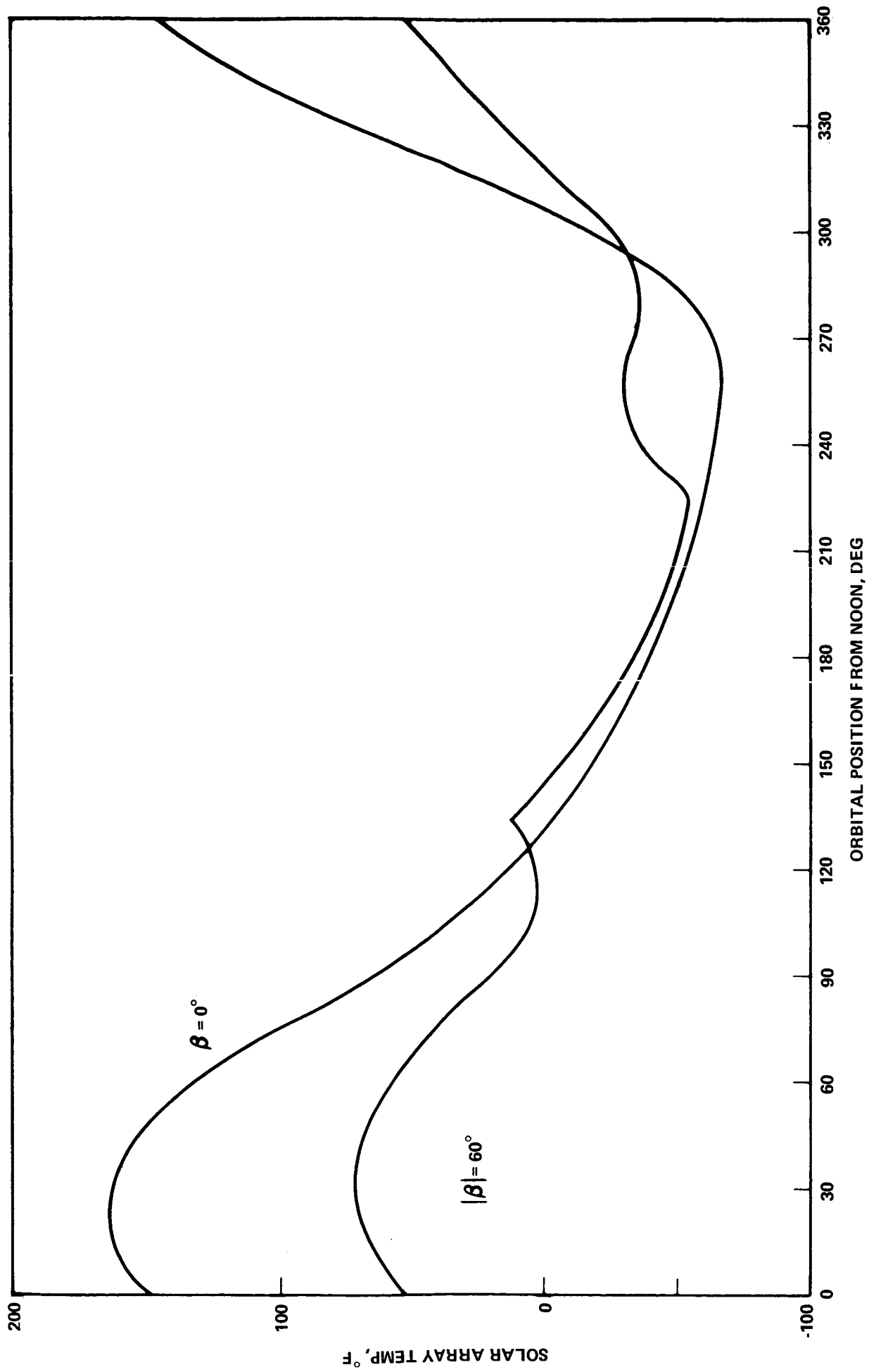


FIGURE 2 - SWS SOLAR ARRAY TEMPERATURE VS ORBITAL POSITION, EARTH-VIEWING ATTITUDE FOR COMPLETE ORBIT, 235 NM CIRCULAR ORBIT

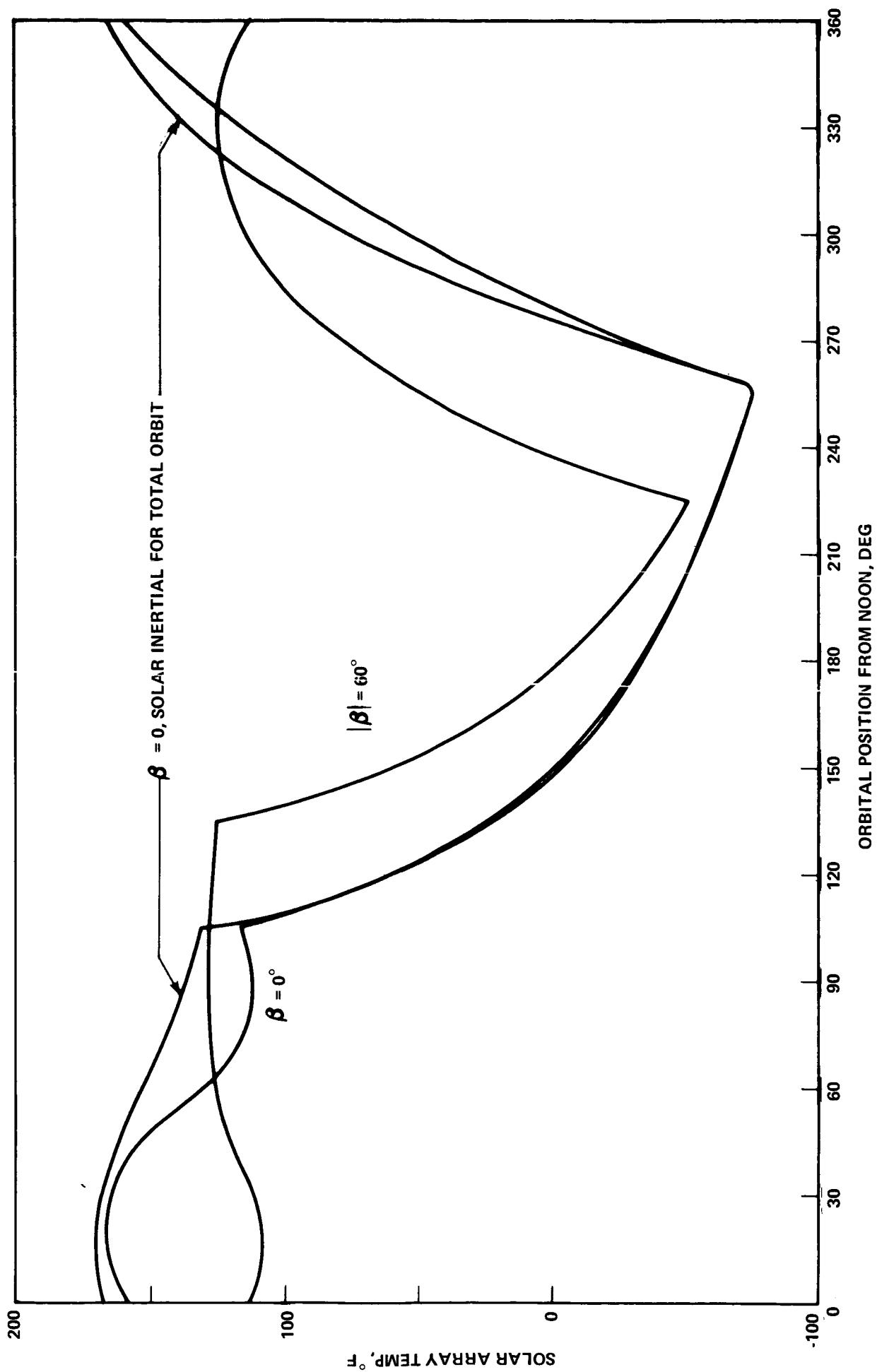


FIGURE 3 - SWS SOLAR ARRAY TEMPERATURE VS ORBITAL POSITION, EARTH-VIEWING-SOLAR INERTIAL ATTITUDE IN SINGLE ORBIT, 235 NM CIRCULAR ORBIT

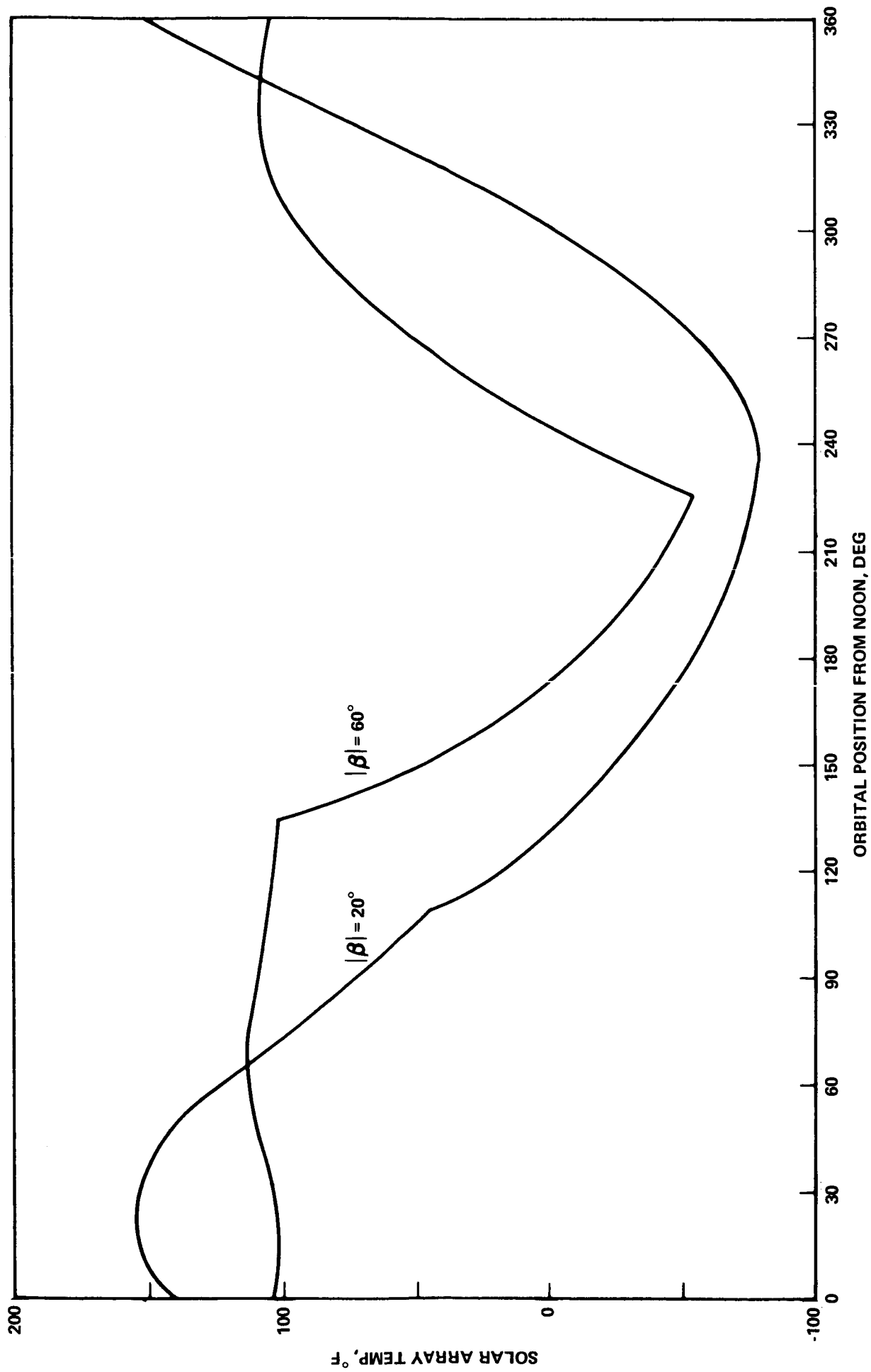


FIGURE 4 - SWS SOLAR ARRAY TEMPERATURE VS ORBITAL POSITION EARTH-VIEWING-OPTIMUM ROLL ATTITUDE IN SINGLE ORBIT, 235 NM CIRCULAR ORBIT

BELLCOMM, INC.

Subject: Solar Array Temperatures During
the AAP-SWS Earth Pointing
Experiments Mission Segment
Case 620

From: J. W. Powers

Distribution List

NASA Headquarters

H. Cohen/MLR
J. H. Disher/MLD
W. B. Evans/MLO
L. K. Fero/MLV
J. P. Field, Jr./MLP
W. H. Hamby/MLO
T. E. Hanes/MLA
T. A. Keegan/MA-2
M. Savage/MLT
W. C. Schneider/ML

GSFC

J. T. Skladany/713

Langley Research Center

P. R. Kurzhals/AMPD

MSC

R. G. Brown/ES-16
C. N. Crews/KS
W. R. Cunningham/CB
H. W. Dotts/KS
R. E. Durkee/ES-5
R. L. Frost/KS
O. K. Garriott/CB
F. C. Littleton/KM
R. M. Machell/KF
P. S. Miglicco/KS
O. G. Smith/KF
R. E. Thompson/KA
H. E. Whitacre/KM

MSFC

R. M. Aden/S&E-ASTR-E
W. B. Chubb/S&E-ASTR-SGD
J. C. Cody/S&E-ASTN-PLA
D. N. Counter/S&E-ASTR-MA
C. B. Graff/S&E-ASTR-EP
G. B. Hardy/PM-AA-EI

MSFC (continued)

G. D. Hopson/S&E-ASTN-PL
E. H. Hyde/S&E-ASTN-PF
H. F. Kennel/S&E-ASTR-A
E. F. Noel/S&E-ASTR-SI
W. C. Patterson/S&E-ASTN-PLA
J. W. Sims/S&E-ASTN-PTA
J. D. Stroud/S&E-ASTR-SE
J. W. Thomas/PM-AA
H. F. Trucks/S&E-ASTN-PTA
J. L. Vaniman/S&E-ASTN-PT
R. D. Wegrich/S&E-CSE-AA
A. P. Woosley/S&E-ASTR-SEC
H. E. Worley/S&E-AERO-DOI

Martin-Marietta

H. S. Nassen/Denver
E. F. Bjoro/Washington
M. S. Imamura/Denver
R. W. Wilson/Denver

McDonnell-Douglas

G. Weber/Eastern Division

Bellcomm, Inc.

A. P. Boysen
D. R. Hagner
W. G. Heffron
B. T. Howard
J. Z. Menard
J. M. Nervik
I. M. Ross
J. W. Timko
R. L. Wagner
M. P. Wilson
Departments 2031, 2034 Supervision
Department 1024 File
Division 102
Central File
Library